Contract Report S-68-1

INVESTIGATION OF GROUND SHOCK EFFECTS
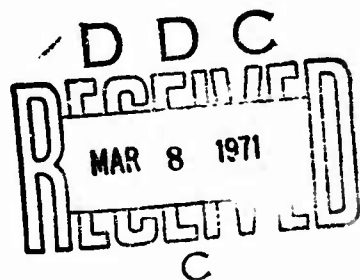
IN NONLINEAR HYS⁻⁻RETIC MEDIA

Report 2

MODELING THE BEHAVIOR OF A REAL SOIL

by

I. Nelson

July 1970

Sponsored by Defense Atomic Support Agency

Conducted for

U.S. Army Engineer Waterways Experiment Station

Vicksburg, Mississippi

Under Contract No. DACA39-67-C-0048

By Paul Weidlinger, Consulting Engineer, New York, New York

FOREWORD

The work on variable moduli models was conducted for the U.S. Army Engineer Waterways Experiment Station (WES) under sponsorship of the Defense Atomic Support Agency (DASA) as part of NWER Subtask SB209, "Propagation of Ground Shock Through Earth Media".

The contract was monitored by Dr. J.S. Zelasko, Impulse Loads Section, Soil Dynamics Branch, under the general supervision of Mr. J.P. Sale, Chief, Soils Division, WES. COL Ernest D. Peixotto, CE, was the contracting officer.

ABSTRACT

The present report extends the combined variable moduli
model introduced in the previous report, Ref. [1]. This more
general model is defined, conditions are set on the various
parameters, and the model behavior in uniaxial strain,
triaxial compression and proportional loading tests is dis-
cussed.

The major portion of the present report deals with the
procedures used to fit the current model, including the
loading and unloading, to a rather complete set of laboratory
data for McCormick Ranch Sand. Actually, four different fits
are described, one of them, Uniax-Triax I, in some detail.
The theoretical and experimental results are compared and
with one fit, Uniax-Triax II, excellent agreement is found
for uniaxial strain, triaxial compression and proportional
loading tests.

Finally, recommendations are made concerning reloading
in shear. User's guides and FORTRAN listings of the two
programs, UNAX2 and PROP, used to compute uniaxial strain and
proportional loading (including triaxial compression) tests
are given in an appendix.

PREFACE

The objectives of the work reported herein were to (a) evaluate the capability of variable moduli type models, Ref. [1], to quantitatively match typical load-unload-reload soil property test data obtained with different laboratory test devices, and (b) document procedures for determining the model coefficients from a given set of data. This work forms part of a broad theoretical and experimental research program being conducted at WES under DASA NWER Subtask SB209, "Propagation of Ground Shock Through Earth Media," aimed at defining, describing and evaluating those characteristics of earth media which govern the propagation and attenuation cf ground shock.

All laboratory data utilized for this report were furnished by WES. Representative uniaxial strain stress-strain relations were determined based on analyses of a series of tests conducted at WES in support of a DASA-sponsored HEST test at the McCormick Ranch test site, Ref. [2]. The standard triaxial compression test data, proportional loading shear data and hydrostatic compression data were obtained from the Georgia Institute of Technology, under contract to WES, as part of a research study on the behavior of soils under high pressure, Ref. [3].

The vertical deformation measurement of triaxial test specimens is generally considered a routine operation. Ref. [3] describes the development and pplication of an innovative device for measuring the lateral deformations of cylindrical soil specimens inside the triaxial test chamber. These additional measurements allowed for the computation

of the complete strain tensor for each triaxial test. However, as pointed out in Ref. [3], and more recently in Ref. [4], interpretation of these deformation measurements is still a matter of major concern and the subject of intense additional research. Thus, the triaxial test data utilized in this report, though generally self-consistent and assuredly of the correct order of magnitude, cannot be considered surgically precise.

Finally, as pointed out by the author in Section III of this report, there is some disagreement between the virgin loading stress-strain relations obtained with the triaxial test device and the virgin loading uniaxial strain relation. Considering the facts that the two types of data were obtained with totally different objectives in mind, that two different pieces of test apparatus were used, each located in a different laboratory and each using specimens of different size prepared by slightly different techniques, some data disagreement should be no surprise. Indeed, the fact that the data agree as well as they do is considered remarkable at WES.

Vicksburg, Miss.   J. S. ZELASKO
November 1970   Contracting Officer's Representative

MODELING THE BEHAVIOR OF A REAL SOIL

Table of Contents

LIST OF SYMBOLS

a_1 , a_0 , ... , a_3	Coefficients in polynomial fits.
E	Young's modulus.
E_0	Stress free value of E.
E_{UN}	Young's modulus during unloading.
e	Mean strain.
e_0 , e^* , e^{**}	Values of e, see Fig. (1).
e_1	Axial strain deviator.
$e_1^{(0)}$, e_1^* , e_1^{**}	Values of e_1 , see Fig. (2).
e_{ij}	Deviatoric strain tensor.
F	A measure of state of stress defined by Eq. (79).
F_m	Maximum previous value of F.
G	Shear modulus.
G_{LD} , G_{UN} , G_{RE}	Shear moduli in loading, unloading, reloading.
G_0 , G_{0U} , G_1 , G_{1U}	Constants in expressions for the shear modulus.
$\bar{G}_0$, $\bar{G}_1$, $\bar{G}_2$	Constants in shear modulus during proportional loading.
J_2'	Second invariant of the deviatoric stresses.
K	Bulk modulus.
K_{LD} , K_{UN}	Bulk modulus in loading, unloading.
K_0 , K_1 , K_2	Constants in expression for K_{LD} .
K_{0U} , K_{1U}	Constants in expression for K_{UN} .
L, L_0	Length, initial length.

M	Constrained modulus.
M_o , M_{LD}	Initial value of constrained modulus, Constrained modulus during loading.
N	Number of data points.
n	Constant, exponent appearing in Eqs. (76) and (81).
p	Pressure.
P_c	Critical pressure at which the transition between the two expressions for G takes place.
P_o , p^* , p^{**}	Values of p, see Fig. (1).
P_{lim}	Limiting value of p in proportional loading.
P_1 , P_2 , P_3	Limiting values of p in triaxial compression, given by Eqs. (27), (28), (34).
q	Stress rate ratio $\dot{\sigma}_3/\dot{\sigma}_1$ in proportional loading.
s_{ij}	Deviatoric stress tensor.
s_1	Axial deviatoric stress.
s_1^* , s_1^{**}	Values of s_1 corresponding to e_1^* and e_1^{**}, see Fig. (2).
V, V_o	Volume, initial volume.
y, y^*	Measured value of a function, value of the least squares fit at the same point.
α, β	Constants in Eq. (76).
γ_1 , γ_2 , $\bar{\gamma}_1$	Constants in expression for G_{LD} .
γ_{1U} , γ_{2U} , $\bar{\gamma}_{1U}$	Constants in expression for G_{UN} .

Δ	Change.
ε_{kk}	Volumetric strain.
ε_1 , ε_3	Axial and radial strains.
ν, ν_o	Poisson's ratio, initial value of Poisson's ratio.
ρ, ρ_o	Density, initial value of the density.
σ_1 , σ_2 , σ_3	Principal stresses.
$\sigma_1^{(o)}$, $\sigma_2^{(o)}$	Initial values of stress in proportional loading.
σ_{3c}	Critical value of σ_3 in triaxial tests, see Eq. (37).

MODELING THE BEHAVIOR OF A REAL SOIL

List of Tables

MODELING THE BEHAVIOR OF A REAL SOIL

List of Figures

List of Figures (Continued)

I   INTRODUCTION.

The advances in the design of hardened underground structures have led to increased demands for accurate predictions of ground shock effects from nuclear explosions. These demands, in turn, have led to the requirement of more realistic mathematical models of the behavior of the in situ material, namely, highly nonlinear and hysteretic soils.

The models, ideally, should reproduce real soil behavior for both laboratory tests and the complex geometries of real nuclear and high explosive field events. Of course, little field data exists for nuclear events. The approach therefore, is to make the model conform to material property data obtained from a variety of dynamic laboratory tests and to evaluate the model in calculations of existing high explosive field tests. Although this does not guarantee the correct behavior in a nuclear event, it is the most physically meaningful means of obtaining confidence in code predictions.

Up to now, all computations have been performed with elastic-plastic models. The historic development of advanced elastic-plastic models is given in Ref. [1]. Although, as indicated in Ref. [1], elastic-plastic models do reproduce soil uniaxial strain test data quite well, and contain the measured failure envelope, they do not correctly model material behavior approaching failure in triaxial compression tests. This deficiency led to the development of the variable moduli models in which both the bulk and shear moduli are functions of the stress and/or strain invariants, and in which there is no

explicit yield condition. The early models discussed in Ref. [1] do give qualitative agreement with the results of the usual laboratory tests, namely, the uniaxial strain and triaxial compression tests; in this report, a more advanced model is described which agrees qualitatively and quantitatively with laboratory test data for a real soil, McCormick Ranch Sand.

In Section II, the mathematical model is described, as are analytic results for the various test configurations and allowable ranges of the material parameters. The available laboratory data and the method used to pick parameters for loading and unloading are discussed in Section III. In Section IV, results are given for the McCormick Ranch Sand and the question of reloading is reexamined. Finally, in Section V, recommendations are given for future work.

II MODEL DESCRIPTION.

The present mathematical model, Combined Variable
Moduli Model II, is an extension of the combined variable
moduli model described in Ref. [1]. As before, the material
is described by incremental stress-strain relations

$$\dot{s}_{ij} = 2G\dot{e}_{ij} \tag{1}$$

$$\dot{p} = 3K\dot{e} \tag{2}$$

The bulk modulus on virgin loading is retained

$$K_{LD} = K_o + K_1 e + K_2 e^2 \tag{3}$$

However, in order to allow for more general pressure-volume
relations in unloading, a linear expression in pressure is
used as the bulk modulus for unloading and reloading

$$K_{UN} = K_{oU} + K_{1U}p \tag{4}$$

The major change, however, is in the shear modulus.
Whereas the failure envelope for the combined variable
moduli model described in Ref. [1] is a straight line
corresponding to a Prager-Drucker type yield condition,
the failure envelope of most partially saturated soils
starts as a straight line, but then flattens out and
reaches a maximum with increasing pressure. Advanced
plastic models such as the one described in Ref. [1]
mirror this behavior with a yield condition in which $\sqrt{J_2'}$
is taken as a more general function of pressure. Here,
two different expressions are used for the shear modulus.

For small pressure, i.e., for p less than some critical pressure p_c

$$G = \begin{cases} G_{LD} = G_o + \bar{\gamma}_1 \sqrt{J_2'} + \gamma_1 p + \gamma_2 p^2 & , \quad J_2' > 0 \quad (5) \\ \\ G_{UN} = G_{oU} + \bar{\gamma}_{1U} \sqrt{J_2'} + \gamma_{1U} p + \gamma_{2U} p^2 & , \quad J_2' \leq 0 \quad (6) \end{cases}$$

If in Eq. (5) $\gamma_1 > 0$ and $\gamma_2 < 0$, then G_{LD} at constant J_2' will increase with increasing pressure until a maximum is reached at

$$p_c = - \frac{\gamma_1}{2\gamma_2} \tag{7}$$

If it is assumed that the same transition pressure p_c applies in both loading and unloading, then necessarily

$$\frac{\gamma_{1U}}{\gamma_{2U}} = \frac{\gamma_1}{\gamma_2} \tag{8}$$

For larger pressures, i.e., $p \gtrsim p_c$

$$G = \begin{cases} G_{LD} = G_1 + \bar{\gamma}_1 \sqrt{J_2'} & , \quad J_2' > 0 \quad (9) \\ \\ G_{UN} = G_{1U} + \bar{\gamma}_{1U} \sqrt{J_2'} & , \quad J_2' \leq 0 \quad (10) \end{cases}$$

where

$$G_1 = G_o - \frac{1}{4} \frac{\gamma_1^2}{\gamma_2} \tag{11}$$

$$G_{1U} = G_{oU} - \frac{1}{4} \frac{\gamma_1^2}{\gamma_2} \tag{12}$$

Of course, at $p = p_c$, the expressions for G_{LD} and G_{UN} are continuous. It is seen that the present model has almost

as much flexibility in unloading as in initial loading, something not true of previous models. The special case of $\dot{J}_2 = 0$ is included with $\dot{J}_2 < 0$ by analogy with the neutral plastic state in plasticity. At present, the model makes no distinction between initial loading in shear and subsequent reloading. The ramifications of this and an alternative choice are discussed later.

Conditions on the Parameters.

In order for there to be no energy generated during infinitesimal stress cycles, two necessary conditions are

$$K_{UN} \geq K_{LD} \tag{13}$$

$$G_{UN} \geq G_{LD} \tag{14}$$

During initial loading the pressure may be found in terms of the mean strain by direct integration of Eqs. (2) and (3)

$$p = 3K_o e + \frac{3}{2} K_1 e^2 + K_2 e^3 \tag{15}$$

Along the initial loading curve, by substituting Eq. (15) into Eq. (4)

$$K_{UN} = K_{oU} + K_{1U}(3K_o e + \frac{3}{2} K_1 e^2 + K_2 e^3) \tag{16}$$

so that the condition $K_{UN} \geq K_{LD}$ becomes

$$(K_{oU} - K_o) + (3K_{1U}K_o - K_1)e + (\frac{3}{2} K_{1U}K_1 - K_2)e^2 + (K_{1U}K_2)e^3 \geq 0 \tag{17}$$

A sufficient condition for the inequality Eq. (17) to be satisfied for all positive values of e is for each of the

coefficients to be positive. The first and second terms
lead to

$$K_{oU} \geq K_o \tag{18}$$

$$K_{1U} \geq \frac{K_1}{3K_o} \tag{19}$$

If $K_1 < 0$ and $K_2 > 0$, the third term would not be satisfied,
but since e is small this case need not be considered.

The condition on the shear moduli, Eq. (14), leads to

$$(G_{oU} - G_o) + (\bar{\gamma}_{1U} - \bar{\gamma}_1)\sqrt{J_2'} + (\gamma_{1U} - \gamma_1)p + (\gamma_{2U} - \gamma_2)p^2 \geq 0 \tag{20}$$

The initial shear modulus is, of course, positive, so that

$$G_{oU} \geq G_o > 0 \tag{21}$$

Since in loading the material softens with increasing load
$\bar{\gamma}_1 < 0$ and the second term will be positive whenever

$$\bar{\gamma}_{1U} > \bar{\gamma}_1 < 0 \tag{22}$$

so that $\bar{\gamma}_{1U} > 0$ is certainly possible. Using Eqs. (7) and
(8) the pressure terms in Eq. (20) reduce to

$$p(\gamma_{1U} - \gamma_1)(1 - \frac{p}{2p_c}) \geq 0 \tag{23}$$

which being valid only for $p < p_c$ leads to

$$\gamma_{1U} > \gamma_1 > 0 \tag{24}$$

Looking at the loading and unloading shear moduli for $p > p_c$
leads again to Eqs. (21) and (22) and gives no new information.

Uniaxial Strain Test.

As was done for the simpler combined variable moduli model in Ref. [1], the expression for the constrained modulus during initial loading, $M_{LD} = K_{LD} + \frac{4}{3} G_{LD}$, may be integrated to obtain the stress-strain curve, $\sigma_1(e)$, in closed form. The solution for the stress is an exponential plus a sixth degree polynomial in e with the coefficients in terms of the material parameters. The result is not given here (it would take a whole page to write!) since the program which computed the uniaxial strain test actually used numerical integration rather than the closed form expressions. The other stress quantities, such as s_1 and σ_3 , may be obtained from $\sigma_1(e)$ and $p(e)$, Eq. (15). All strain quantities are proportional to e.

Triaxial Compression Test.

In the triaxial compression test all the stress rates are proportional and since $\sigma_2 = \sigma_3$

$$\sqrt{J_2'} = \frac{\sqrt{3}}{2} s_1 = \frac{1}{\sqrt{3}} (\sigma_1 - \sigma_3) \qquad (25)$$

The shear modulus for $p \leq p_c$, Eq. (5), becomes

$$G_{LD} = G_o + \gamma_1 p + \sqrt{3}\, \bar{\gamma}_1(p - \sigma_3) + \gamma_2 p^2 = \gamma_2(p - p_1)(p - p_2) \qquad (26)$$

where with $\gamma_1 > 0$, $\bar{\gamma}_1$ and $\gamma_2 < 0$, and $(\gamma_1 + \sqrt{3}\, \bar{\gamma}_1) < 0$ as in

Ref. [1]

$$p_1 = \frac{[-(\gamma_1 + \sqrt{3}\,\bar{\gamma}_1) + \sqrt{(\gamma_1 + \sqrt{3}\,\bar{\gamma}_1)^2 - 4\gamma_2(G_o - \sqrt{3}\,\bar{\gamma}_1\sigma_3)}\,]}{2\gamma_2} < 0 \tag{27}$$

and

$$p_2 = \frac{[-(\gamma_1 + \sqrt{3}\,\bar{\gamma}_1) - \sqrt{(\gamma_1 + \sqrt{3}\,\bar{\gamma}_1)^2 - 4\gamma_2(G_o - \sqrt{3}\,\bar{\gamma}_1\sigma_3)}\,]}{2\gamma_2} > 0 \tag{28}$$

By integrating $\dot{e}_1 = \dot{s}_1/2G = \dot{p}/G$ with G given by Eq. (26), the strain deviator e_1 is obtained in closed form

$$e_1 = \int_{\sigma_3}^{p} \frac{d\bar{p}}{G(\bar{p})} = \frac{\ln\left(\frac{p - p_1}{\sigma_3 - p_1}\right) - \ln\left(\frac{p - p_2}{\sigma_3 - p_2}\right)}{\sqrt{(\gamma_1 + \sqrt{3}\,\bar{\gamma}_1)^2 - 4\gamma_2(G_o - \sqrt{3}\,\bar{\gamma}_1\sigma_3)}} \tag{29}$$

which is positive and finite as long as $p_1 < 0 < \sigma_3 < p < p_2$. However, as p approaches p_2 the strain becomes infinite so that p_2 represents the pressure at failure. The stress difference at failure as a function of σ_3 may be obtained from Eq. (28)

$$(\sigma_1 - \sigma_3)_{max} = -3\sigma_3 - \frac{3}{2\gamma_2} \left[(\gamma_1 + \sqrt{3}\,\bar{\gamma}_1) + \right.$$
$$\left. + \sqrt{(\gamma_1 + \sqrt{3}\,\bar{\gamma}_1)^2 - 4\gamma_2(G_o - \sqrt{3}\,\bar{\gamma}_1\sigma_3)}\,\right] \tag{30}$$

If the limit of Eq. (30) is taken as $\gamma_2 \to 0$, the result corresponds to that of the simpler model in Ref. [1] where γ_2 does not appear, namely,

$$(\sigma_1 - \sigma_3)_{max}\Big|_{\gamma_2 = 0} = -\frac{3(G_0 + \gamma_1\sigma_3)}{\gamma_1 + \sqrt{3}\,\bar{\gamma}_1} \tag{31}$$

The expression for e_1^-, Eq. (29), also reduces to that given previously.

When $\sigma_3 < p_c < p$, since the expression for G changes, one integrates first from σ_3 to p_c and then from p_c to p. The resulting expression for e_1 is

$$e_1 = \frac{\ln\left(\dfrac{p_c - p_1}{\sigma_3 - p_1}\right) - \ln\left(\dfrac{p_c - p_2}{\sigma_3 - p_2}\right)}{\sqrt{(\gamma_1 + \sqrt{3}\,\bar{\gamma}_1)^2 - 4\gamma_2(G_0 - \sqrt{3}\,\bar{\gamma}_1\sigma_3)}} +$$

$$+ \frac{1}{\sqrt{3}\,\bar{\gamma}_1} \ln\left[\frac{G_0 - \dfrac{1}{4}\dfrac{\gamma_1^2}{\gamma_2} + \sqrt{3}\,\bar{\gamma}_1(p - \sigma_3)}{G_0 - \dfrac{1}{4}\dfrac{\gamma_1^2}{\gamma_2} + \sqrt{3}\,\bar{\gamma}_1(p_c - \sigma_3)}\right] \tag{32}$$

for $\sigma_3 < p_c < p$.

Finally, when both σ_3 and p are greater than p_c

$$e_1 = \frac{1}{\sqrt{3}\,\bar{\gamma}_1} \ln\left[\frac{G_0 - \dfrac{1}{4}\dfrac{\gamma_1^2}{\gamma_2} + \sqrt{3}\,\bar{\gamma}_1(p - \sigma_3)}{G_0 - \dfrac{1}{4}\dfrac{\gamma_1^2}{\gamma_2}}\right] \tag{33}$$

Both Eqs. (32) and (33) become infinite when

$$p = p_3 = \sigma_3 - \frac{1}{\sqrt{3}\,\bar{\gamma}_1}\left(G_0 - \frac{1}{4}\frac{\gamma_1^2}{\gamma_2}\right) \tag{34}$$

The various expressions for e_1 , Eqs. (29), (32) and (33), are continuous as either p or σ_3 crosses p_c .

From Eq. (30) for the stress difference at failure one obtains the intercept

$$(\sigma_1 - \sigma_3)_{max}\bigg|_{\sigma_3 = 0} = - \frac{3}{2\gamma_2} \left[(\gamma_1 + \sqrt{3}\,\bar{\gamma}_1) + \right.$$
$$\left. + \sqrt{(\gamma_1 + \sqrt{3}\,\bar{\gamma}_1)^2 - 4\gamma_2 G_o} \right] \tag{35}$$

and the initial slope

$$\frac{d(\sigma_1 - \sigma_3)_{max}}{d\sigma_3}\bigg|_{\sigma_3 = 0} = -3 - \frac{3\sqrt{3}\,\bar{\gamma}_1}{\sqrt{(\gamma_1 + \sqrt{3}\,\bar{\gamma}_1)^2 - 4\gamma_2 G_o}} \tag{36}$$

of the failure envelope. One may also find the chamber pressure σ_{3c} at which the failure envelope flattens out, i.e., $\dfrac{d(\sigma_1 - \sigma_3)_{max}}{d\sigma_3} = 0$

$$\sigma_{3c} = \frac{-\gamma_1(\gamma_1 + 2\sqrt{3}\,\bar{\gamma}_1) + 4\gamma_2 G_o}{4\gamma_2\,\bar{\gamma}_1\,\sqrt{3}} \tag{37}$$

It should be noted that when $\sigma_3 = \sigma_{3c}$, Eqs. (28) and (34) lead to $p_2 = p_3 = p_c$. It is thus seen that in the present model there is a unique pressure p_c which represents the pressure at which the failure surface flattens out, an observed phenomenon in partially saturated soils. The present model is therefore a strong candidate for representing real soils. The actual fitting to laboratory data is described in the next section.

Proportional Load Test.[*]

In a so-called "proportional load" test the stresses are constrained according to the relation

$$\dot{\sigma}_2 = \dot{\sigma}_3 = q\dot{\sigma}_1 \tag{38}$$

where q is a constant. The two limiting conditions are

$$\left.\begin{array}{ll} q = 0 & \text{producing triaxial loading} \\[2mm] q = 1 & \text{producing hydrostatic loading} \end{array}\right\} \tag{39}$$

The constitutive relations are those of Eqs. (1) and (2), the bulk moduli are given by Eqs. (3) and (4), and the shear moduli by Eqs. (5), (6), (9) and (10). For pressure reloading up to a previous peak $K = K_{UN}$, but for reloading of deviators $G = G_{LD}$. Figures (1) and (2) show typical paths of loading-unloading-reloading which have been considered.

(1) Solutions for the Volumetric Portion.

Initial prestressing of the system has been introduced through the quantities $\sigma_1^{(o)}$ and $\sigma_2^{(o)}$ such that the initial pressure is

$$P_o = \frac{1}{3} (\sigma_1^{(o)} + 2\sigma_2^{(o)}) \tag{40}$$

and initial mean strain e_o may be found from the appropriate root of the Eq. (15) at $p = P_o$

$$K_2 e_o^3 + 1.5K_1 e_o^2 + 3K_o e_o - P_o = 0 \tag{41}$$

[*]   This section contributed by A. Matthews.

The loading portion of the volumetric curve, Fig. (1), from p_o to p^* is fully described by Eq. (15). An unloading portion of the volumetric curve, from p^* to p^{**}, is described by the integral of Eq. (2) when K_{UN} of Eq. (4) is used. The expression is

$$e = \frac{1}{3K_{1U}} \ell n \; [\frac{K_{oU} + K_{1U}p}{K_{oU} + K_{1U}p^*}] + e^* \qquad (42)$$

for $K_{1U} \neq 0$, or

$$e = \frac{1}{3K_{oU}} (p - p^*) + e^* \qquad (43)$$

for $K_{1U} = 0$. The reload portion from p^{**} to p^* is established from the same equations, except that p^{**} and e^{**} replace p^* and e^*, respectively, in Eqs. (42) and (43). For further reloading above p^*, Eq. (15) is again used to describe the curve.

(2) Solutions for the Deviatoric Portion.

Initial deviatoric strain, $e_1^{(o)}$ is considered to be zero. With this condition, the deviatoric constitutive relation, Eq. (1), which uses G_{LD} given by Eq. (5) may be integrated in closed form for proportional loading. In particular, for this case the invariant J_2' may be written as

$$\sqrt{J_2'} = \sqrt{3} \; (\frac{1 - q}{1 + 2q})p + \frac{\sqrt{3}}{1 + 2q} \; (q\sigma_1^{(o)} - \sigma_2^{(o)}) \qquad (44)$$

It is therefore convenient to rewrite the shear modulus G in the form

$$G = \bar{G}_o + \bar{G}_1 p + \bar{G}_2 p^2 \qquad (45)$$

where, for loading

$$\bar{G}_o = G_o + \frac{\sqrt{3}\ \bar{\gamma}_1}{1 + 2q}\ (q\sigma_1^{(o)} - \sigma_2^{(o)})$$

$$\bar{G}_1 = \frac{1 - q}{1 + 2q}\ \sqrt{3}\ \bar{\gamma}_1 + \gamma_1 \qquad\qquad \left.\begin{array}{c} \\ \\ \\ \end{array}\right\}\qquad (46)$$

$$\bar{G}_2 = \gamma_2$$

while, for unloading

$$\bar{G}_o = G_{oU} + \frac{\sqrt{3}\ \bar{\gamma}_{1U}}{1 + 2q}\ (q\sigma_1^{(o)} - \sigma_2^{(o)})$$

$$\bar{G}_1 = \frac{1 - q}{1 + 2q}\ \sqrt{3}\ \bar{\gamma}_{1U} + \gamma_{1U} \qquad \left.\begin{array}{c} \\ \\ \\ \end{array}\right\}\qquad (47)$$

$$\bar{G}_2 = \gamma_{2U}$$

Therefore, for $p < p_c$ the integral of combined Eqs. (1) and (45) is

$$e_1 - e_1^{(o)} = \frac{(1-q)/(1+2q)}{\sqrt{\bar{G}_1^2 - 4\bar{G}_o\bar{G}_2}}\ \ell n\left[\left(\frac{2\bar{G}_2 p + \bar{G}_1 - \sqrt{\bar{G}_1^2 - 4\bar{G}_o\bar{G}_2}}{2\bar{G}_2 p + \bar{G}_1 + \sqrt{\bar{G}_1^2 - 4\bar{G}_o\bar{G}_2}}\right)\right.$$

$$\left.\left(\frac{2\bar{G}_2 p_o + \bar{G}_1 + \sqrt{\bar{G}_1^2 - 4\bar{G}_o\bar{G}_2}}{2\bar{G}_2 p_o + \bar{G}_1 - \sqrt{\bar{G}_1^2 - 4\bar{G}_o\bar{G}_2}}\right)\right] \qquad (48)$$

providing $\bar{G}_2 \neq 0$. If $\bar{G}_2 = 0$, then

$$e_1 - e_1^{(o)} = \frac{(1-q)/(1+2q)}{\bar{G}_1}\ \ell n\left[\frac{\bar{G}_o + \bar{G}_1 p}{\bar{G}_o + \bar{G}_1 p_o}\right] \qquad (49)$$

When $q=0$ (triaxial case) Eq. (48) is equivalent to Eq. (29).

It may be noted in Eq. (48) that the deviatoric strain increases without limit as p approaches a value p_{lim} determined by setting the denominator of the ℓn term equal

to zero. The resulting expression defining p_{1lm} reduces
to the expression p_2 , Eq. (28) when q=0. [Alternatively,
setting the numerator of the log term equal to zero produces
an expression for a p_{1lm} of negative sign. When q=0 this
is equivalent to p_1 of Eq. (27).] Note also that for q=1,
as in a case of hydrostatic loading, all deviatoric strains
are zero and no p_{1lm} can be computed. When $\bar{G}_2$ = 0, p_{1lm}
comes from setting the numerator of the log term equal to
zero. In that case a valid p_{1lm} is obtained providing

$$q < \frac{\sqrt{3} \left|\bar{\gamma}_1\right| - \gamma_1}{\sqrt{3} \left|\bar{\gamma}_1\right| + 2\gamma_1} \tag{50}$$

For the initial loading portion of the deviatoric curve,
up to s_1^* (see Fig. 2), Eq. (48) or (49) holds with $e_1^{(o)}$ = 0
and $\bar{G}$ quantities given by Eqs. (46). In the unloading stage
from s_1^* to s_1^{**} Eq. (48) or (49) again holds but $e_1^{(o)}$ is
replaced by e_1^* , p_o is the pressure corresponding to s_1^* and
the expressions for $\bar{G}$ are given by Eqs. (47). Reloading
the stresses above s_1^{**} may also be computed from the
appropriate one of the above two equations providing $\bar{G}$
expressions again come from Eqs. (46), and $e_1^{(o)}$ = e_1^{**} and
p_o is replaced by the pressure corresponding to s_1^{**} .

In the special case where pressure p exceeds the
critical pressure of Eq. (7) the $\bar{G}$ quantities of Eqs. (46)
and (47) must be redefined as

$$\left.\begin{array}{l} \bar{G}_o = G_o - \frac{1}{4} \frac{\gamma_1^2}{\gamma_2} + \frac{\sqrt{3} \, \bar{\gamma}_1}{1 + 2q} \, (q\sigma_1^{(o)} - \sigma_2^{(o)}) \\[3mm] \bar{G}_1 = \frac{1 - q}{1 + 2q} \sqrt{3} \, \bar{\gamma}_1 \\[3mm] \bar{G}_2 = 0 \end{array}\right\} \qquad (51)$$

for loading, while

$$\left.\begin{array}{l} \bar{G}_o = G_{oU} - \frac{1}{4} \frac{\gamma_1^2}{\gamma_2} + \frac{\sqrt{3} \, \bar{\gamma}_{1U}}{1 + 2q} \, (q\sigma_1^{(o)} - \sigma_2^{(o)}) \\[3mm] \bar{G}_1 = \frac{1 - q}{1 + 2q} \sqrt{3} \, \bar{\gamma}_{1U} \\[3mm] \bar{G}_2 = 0 \end{array}\right\} \qquad (52)$$

for unloading. In either case, since $\bar{G}_2 = 0$ the appropriate
solution equation is Eq. (49) for both loading and unloading
when $p > p_c$.

III MATCHING LABORATORY DATA.

The true test of any mathematical model is its ability
to match experimental data for a real material. The process
used to choose the parameters such that the model described
in the previous section fits the experimental curves for a
real soil, namely McCormick Ranch Sand, is discussed in the
present section. The results for various tests are compared
with typical experimental data in Section IV.

Description of the Available Experimental Data.

The laboratory data, available at the time the models
were fit, consisted of the following:

(a) A series of static triaxial compression tests in which
     stress difference was plotted against axial strain.
     The tests were in three groups. In the first group the
     load was increased monotonically to failure. In the
     second and third groups, the specimens were loaded to
     approximately 35% and 75% of failure, respectively, then
     unloaded and reloaded for several cycles and finally
     loaded to failure.

(b) A composite static uniaxial strain test: A series of
     both static and dynamic tests were run in which the
     axial stress and axial strain were measured. The
     radial stress was not measured. A single uniaxial
     strain curve was estimated by W.E.S. as the most
     representative static curve for the soil with the

water content and density typical of the triaxial tests.
An idea of the possible variation of the uniaxial stress-
strain curve may be seen in Fig. (3) where dynamic curves
for three different samples, as well as the W.E.S. con-
structed dynamic composite curve, are shown.

(c) Three static hydrostats: The actual measured values of
pressure and volumetric strain and the W.E.S. constructed
average curve are shown in Fig. (4). No unloading or
reloading was measured.

(d) Three composite static proportional loading tests: The
tests were run with the ratios of the radial stress to
axial stress maintained at 0.4, 0.6 and 0.8, respectively.
The only data available were the three composite plots
of vertical stress versus vertical strain. This data
was used only as a check.

(e) Stress difference versus strain difference in triaxial
compression. This information was received after the
original initial loading models were already constructed.
As a result, for these models the loading data was only
used as a check, however, the unloading data was used
in constructing the unloading portion of the model.
The loading data was used in the improved models discussed
in Section IV.

A few comments are in order to qualify the data. The
model described in Section II is assumed to apply to a single
homogeneous isotropic (albeit nonlinear) material. Obviously,

soil is not homogeneous, although in a macroscopic sense it may behave as if it were. However, different samples have somewhat different properties. Thus, at least as far as initial loading is concerned, each test destroys the sample so that different samples must be used in different tests. It is therefore difficult in comparing results for different test configurations to decide whether the model is in error, or whether the data for the various tests simply apply to different materials. An example of this uncertainty may be seen by comparing the initial bulk modulus $K_o \simeq 20$ ksi from Fig. (4) and the initial constrained modulus $M_o \approx K_o +$
$+ \frac{4}{3} G_o < 20$ ksi from Fig. (3). The only way the two results could be compatible would be for $G_o < 0$, an obvious absurdity.

Another difficulty was that the data was incomplete. For example, in the uniaxial strain test the lateral stress σ_3 required to maintain zero lateral strain was not measured[*]. If σ_3 had been measured, an independent pressure-volume relation for the sample in the uniaxial strain configuration could have been constructed.

Finally, it should be noted that the data came from two different laboratories. The uniaxial strain tests were run at W.E.S. All other tests, the hydrostats, the triaxial tests and the proportional loading tests, were performed at Georgia Tech under W.E.S. contract. All the Georgia Tech samples were

---

[*] At the time the tests were conducted such measurements could not be made. Presently, however, they are made as a matter of course at W.E.S.

prepared the same way and tested on the same apparatus. The
uniaxial samples were prepared at W.E.S. in a different
fashion and were tested on a different type of apparatus.
A more complete qualification of the data is given by
J.S. Zelasko of W.E.S. in the preface. One more fact worth
mentioning is that the lateral deformation measurements obtained
for specimens tested in the triaxial device were part of an ex-
perimental research and development project Strain computations
based on these measurements were found to be highly sensitive to
interpretation of the raw data, Ref. [3].

Hydrostat-Triaxial Fit.

The problem of choosing material parameters to fit the
data is greatly simplified when there are tests available in
which as few of the independent variables as possible are
varied simultaneously. The hydrostat, in which the pressure
and volumetric strain are measured, is therefore a likely
candidate for computing the various K's which appear in
Eq. (15). A series of pure shear tests in which shear stress
and shear strain were measured and in which the pressure was
kept constant during each test would be desirable tests from
which to determine the various γ's in the shear moduli.
However, such tests were not available.

Of the available data, the stress difference at failure
in the various triaxial tests may be used to obtain all but
one constant in the expression for G_{LD} , Eqs. (5) and (9).
At failure $G_{LD} = 0$, so that by dividing Eq. (5) by $-\bar{\gamma}_1 > 0$,

one has $\sqrt{J_2'}$ as a quadratic function of pressure valid for $p \leq p_c$, or

$$\sqrt{J_2'} = a_0 + a_1 p + a_2 p^2 = \frac{G_0}{-\bar{\gamma}_1} + \frac{\gamma_1}{-\bar{\gamma}_1} p + \frac{\gamma_2}{-\bar{\gamma}_1} p^2 \tag{53}$$

The raw data of σ_3 and $(\sigma_1 - \sigma_3)_{max}$ for each test were transformed into p and $\sqrt{J_2'}$. A least-squares second degree polynomial was then fit through the resulting data.

The results for the various early trials are shown in Table I cases 1 to 9. The second column "N" refers to the number of tests included in the trial, while the mean square residual is a measure of the width of the scatter band. After the three coefficients a_i the ratio of $a_1/a_0 = \gamma_1/G_0$ and the cut-off pressure $p_c = -a_1/2a_2$ are given. Finally, the maximum value of $\sqrt{J_2'}$ for the particular fit, the value at $p = p_c$, is given. Upon examination of the output of the first four cases it was evident that (a) systematic errors appeared in the fit by trying to include both high chamber pressure (σ_3 up to 10 ksi) and low chamber pressure tests, and (b) there appeared to be significant differences between the noncyclic and the cyclic tests.

It was therefore decided to base the failure fit upon the low chamber pressure tests which were loaded straight to failure. Although the mathematical model, described in Section II, in which failure would occur at the same stress level in both the cycled and uncycled triaxial tests, ran

(to a certain extent) counter to the evidence in this regard,
no attempt was made to alter the model so that the failure
stress state would depend upon the previous load history.
Sample 16 was eliminated from further consideration since
its water content was significantly lower than that of the
other samples and its strength correspondingly higher. Tests
at lower and lower chamber pressures were eliminated (cases
5-7) until all tests included in the group failed at pressures
lower than the computed p_c for the group. Case 8 which included
thirteen tests all at chamber pressures less than or equal to
0.8 ksi was this final result. The pressure at maximum shear
strength p_c was 1.166 ksi and the corresponding value of $\sqrt{J_2'}_{max}$
was 0.2303 ksi. As a check, the best constant through the
remaining uncycled triaxial data, case 9, was found to be
0.2323 ksi, which was within 1% of the above value.

The triaxial tests were also used to obtain an estimate
of one of the two "elastic constants" E_o . This was accomplished
by extrapolating backward to zero chamber pressure the best fit
of initial slope as a function of σ_3 . The value obtained
using a least squares procedure was $E_o = 14.14$ ksi. The details
of the procedure will be discussed later when the second fit
based upon the triaxial and uniaxial test results is described.

The hydrostat, Fig. (4), was used in this early fit to
obtain the values of the various K's. The best least squares
cubic was fit through the various groups of data points. The
results are shown in Table II. The use of all points simul-
taneously, case 1, leads to nonsense since $\Sigma(y - y^*)^2$, rather

than the distance to the curve, is what is minimized. Although there are small differences in strain at a given (high) pressure, the large differences in pressure at a given strain drive the entire computation. Including the high pressures even for a single sample is still inaccurate for the same reason. Terms higher than cubic should be included if high pressure data is to be taken into account. The last three cases, each limited to a single sample at lower pressures, give meaningful results. The last two cases, in fact, are very good as shown by the mean square residual. The quantity a_o should be zero for $p=0$ when $\varepsilon_{kk} = 0$. For the last two cases it is less than 2 psi and was neglected. For this early fit the values of a_1 to a_3 for case 7 were used since the sample 48 data falls between that of the other two samples. Using $e = \varepsilon_{kk}/3$ and Eq. (15) the following values were obtained:

$$
\left.
\begin{aligned}
K_o &= a_1 = 20.6 \text{ ksi} \\
K_1 &= 6a_2 = -3800 \text{ ksi} \\
K_2 &= 27a_3 = 965000 \text{ ksi}
\end{aligned}
\right\} \qquad (54)
$$

Based upon the value $K_o = 20.6$ ksi and $E_o = 14.14$ ksi obtained from the triaxial test initial slopes, the initial Poisson's ratio and shear modulus

$$
\left.
\begin{aligned}
\nu_o &= 0.385 \\
G_o &= 5.11 \text{ ksi}
\end{aligned}
\right\} \qquad (55)
$$

are obtained. From G_o and the coefficients of the triaxial failure fit given in Table I the various γ's are computed,

i.e.,

$$\bar{\gamma}_{\hat{1}} = -G_o/a_o = -62.9$$
$$\gamma_1 = -\bar{\gamma}_1 a_1 = 16.05$$
$$\gamma_2 = -\bar{\gamma}_1 a_2 = -6.89/ksi$$

(56)

The model during initial loading is completely defined by the values given in Eqs. (54) to (56). The behavior of the model in the various test configurations was computed using specialized codes[*] PROP and UNAX2 and compared with the experimental data.

There was fairly good agreement of the computed behavior using the present model and the measured results of the triaxial tests. This was true of both the stress difference versus axial strain plots and the stress difference versus strain difference plots, which were received after the model (and the later Uniaxial-Triaxial Model I) was already constructed. The results, not shown, are generally comparable, as far as agreement with the triaxial test experimental curves is concerned, with those obtained with the later Uniaxial-Triaxial Model I, discussed later. The model results are too soft, especially at higher chamber pressures, but have the proper failure stress. Of course, the present model, which was based on the hydrostat, agrees with that test. The results are discussed more completely in Section IV.

Unfortunately, but not unexpectedly, the present Hydrostat-

---

[*] Short descriptions and FORTRAN listings of PROP and UNAX2 are found in the Appendix.

Triaxial model produced a stress-strain curve in uniaxial strain, Fig. (8), which was stiffer than the suggested experimental curve by more than a factor of two. This is partially explained by just the computed initial constrained modulus M_o = 27.4 ksi versus a value certainly less than 20 ksi suggested by Fig. (8).

Since the uniaxial strain geometry is closer to that occurring during real events, and since W.E.S. had much greater confidence in the uniaxial data than in the hydro-static data, it was decided to forego the hydrostat entirely and base a fit on the uniaxial and triaxial data exclusively. The description of the later model follows.

Triaxial-Uniaxial Fit.

The present approach utilized the failure envelope from the triaxial tests to obtain the ratio of the γ's, the initial slopes of the triaxial tests to estimate E_o and the initial slope of the uniaxial test M_o as the other "elastic" constant. Finally, K_1 and K_2 were found by a trial and error routine to obtain the properly shaped uni-axial strain curve. This later approach was done in a more systematic fashion since experience had already been gained during the earlier fit.

Moreover, the data was somewhat refined from what was used previously. For example, whereas before one had to select which triaxial failure data to use, presently all the test samples which had water contents and chamber pressures

in the appropriate range were used. In addition, the
numerical values were slightly more accurate. The data
used to compute the new failure envelope is shown in
Table III. The raw data, σ_3 and $(\sigma_1 - \sigma_3)_{max}$, which came
from W.E.S. were used to compute p and $\sqrt{J_2'}$. The uppermost
section of the table are the uncycled tests: the middle and
bottom sections are the tests in which unloading took place
at 35% and 75% of the failure stress, respectively.

The results of the various least squares fits are given
in Table I, cases 10 to 13. The data from the uncycled tests,
case 10, contain much less scatter than the tests with un-
loading as can be seen from the mean square residual. This
is also apparent from Figs. (5) and (6). In Fig. (5) the
failure fit ($\sqrt{J_2'}$ versus p) is plotted for the uncycled
tests together with the data points. The scatter band is
quite small; Fig. (6), on the other hand, which is the same
plot for each of the cyclic loading sets, shows a large
scatter band, particularly at higher pressure. It is noted,
however, that the maximum value of $\sqrt{J_2'}$ is approximately the
same for all the groups of tests. The model was based on
case 10, the uncycled triaxial tests because of the small
scatter band. It is seen that the coefficients a_i did not
change drastically from the previous model, case 8.

As in the earlier Hydrostat-Triaxial fit, one of the
"elastic constants" was obtained from the initial slopes of
the triaxial tests. The results are summarized in Table IV.

Various degree polynomial fits were tried on various segments
of the data. The emphasis was placed on the lower pressure
($\sigma_3 \leq 400$ psi) tests since the primary interest was an
accurate estimate of $E_o = a_o$. There was less scatter in
the cyclic test data than in the noncyclic tests, as
witnessed by comparing the mean square residual of cases 5
and 6 with case 4. However, since there was no reason why
the initial slope, prior to any unloading, should depend on
the subsequent loading history, all tests were included.
The result used, case 10, a linear fit through all the tests
with $\sigma_3 \leq 400$ psi, was $E_o = 12.2$ ksi. The last column in
Table IV shows the computed value of E at $\sigma_3 = 100$ psi. The
computed value for case 10, 30 ksi, fails within the raw data.
The measured values of initial slope together with the fit
used are plotted against chamber pressure in Fig. (7). The
computed curve is dashed above 0.4 ksi since it is not
applicable. The wide scatter in the initial slope data is
immediately apparent from Fig. (7).

The remaining "elastic" constant was the initial slope
of the uniaxial strain test M_o. This was taken as 16.5 ksi
based on the experimental curve, Fig. (8), suggested by W.E.S.
Using the relations between the elastic constants

$$M = K + \frac{4}{3} G \tag{57}$$

and

$$E = \frac{9KG}{3K + G} \tag{58}$$

one may solve for G and K in terms of E and M as

$$G = \frac{(3M + E) - \sqrt{(9M - E)(M - E)}}{8}$$ (59)

and

$$K = M - \frac{4}{3} G$$ (60)

With $E_o = 12.2$ ksi and $M_o = 16.5$ ksi, Eqs. (59) and (60) give

$$\left.\begin{array}{l} G_o = 4.69 \text{ ksi} \\[6pt] K_o = 10.24 \text{ ksi} \end{array}\right\}$$ (61)

The initial value of Poisson's ratio ν_o turned out to be 0.30.

From the values of a_1 of the failure envelope (case 10 in Table I) and G_o the various γ's were computed.

$$\left.\begin{array}{l} \bar{\gamma}_1 = -G_o/a_o = -64.2 \\[6pt] \gamma_1 = -\bar{\gamma}_1 a_1 = 18.9 \\[6pt] \gamma_2 = -\bar{\gamma}_1 a_2 = -8.76/\text{ksi} \end{array}\right\}$$ (62)

The remaining two constants required to complete the material description for initial loading, K_1 and K_2 , were obtained by a trial and error scheme which was continued until a suitable fit to the experimental uniaxial test was obtained. First, with some trial value of K_2 held constant, K_1 was varied so that the influence of a change in K_1 on the stress-strain curve could be ascertained. Then K_1 was adjusted to make the computed curve agree with the experimental one in the middle stress range (σ_1 between 300 and

500 psi). Next, with K_1 held constant, K_2 was varied and adjusted to make the curves coincide in the high stress range. With this value of K_2, the cycle was repeated to "fine tune" K_1. The final values

$$\left. \begin{aligned} K_1 &= -1,250 \text{ ksi} \\ K_2 &= 97,000 \text{ ksi} \end{aligned} \right\} \quad (63)$$

were obtained in a few iterations. The computed curve is superimposed on the experimental curve in Fig. (8).

After all the material parameters for initial loading were determined, plots of stress difference versus strain difference for some of the triaxial tests were received. These plots would have enabled one to obtain G_o, γ_1 and γ_2 directly from the initial slope as a function of σ_3. The resulting shear modulus would have been significantly stiffer than the one obtained from the failure envelope and E_o. This is shown clearly in Table V where the computed values labeled Uniax-Triax I are all smaller than the lower bounds of the measured values. (The computed values of $2G_{initial}$ for the improved models discussed in Section IV, also given in Table V, agree much better with the measured values.)

It is not clear whether this discrepancy is in the model formulation or in the measurement of lateral strain. In any case, this discrepancy shows up in the results which will be discussed later.

Although the plots of stress difference versus strain difference were not used at all in determining the present

loading model[*]), they were the basis upon which the unloading
shear modulus parameters were determined.

Unloading.

The values of the various material parameters which
describe the model in unloading were determined completely
from the cycled triaxial tests. Where there were several
unload-reload cycles, the initial unloading segment was used.
Since values of the shear modulus were directly obtainable
from the slopes of the $\sigma_1 - \sigma_3$ versus $\varepsilon_1 - \varepsilon_3$ curves, which
had just become available, these slopes were the basis of the
parameters in G_{UN} . After G_{UN} was determined, the measured
slopes of the conventional triaxial plots E were used to
calculate K_{UN} . The unloading portion of the uniaxial
strain test was used only as a check.

The slope of the stress difference versus strain
difference plots were measured at the top and bottom of the
initial unloading portion of each of the cyclic triaxial tests
available, i.e., at the points (s_1^*, e_1^*) and (s_1^{**}, e_1^{**}),
respectively, in Fig. (2). The stress difference $(\sigma_1 - \sigma_3)$
at each end and the chamber pressure σ_3 were noted. From
$(\sigma_1 - \sigma_3)$ and σ_3 values of p and $\sqrt{J_2'}$ were computed. The
results are summarized for the tests unloaded from 75% and
35% of failure in Tables VI and VII, respectively. At the
bottom the dominant effect is due to p since $\sqrt{J_2'}$ is small.
The most self-consistent values of $2G_{Bottom}$ occur in the

---

[*]   They were used in formulating the improved models
     Uniax-Triax II and Hydro-Triax II discussed in Section IV.

samples unloaded from 75% of failure with σ_3 of 200 and
400 psi. These values are boxed-in in Table VI. By
assuming $\sqrt{J_2'}$ is negligible and using Eq. (8) to relate
γ_{1U} and γ_{2U}, the expression for G_{UN}, Eq. (6), is reduced
to one involving two independent parameters G_{oU} and γ_{1U}.
Using the average value of p and the average value of
$2G_{UN}$ for the two boxed cases, one has two simultaneous
equations for G_{oU} and γ_{1U}.

At the top of the unloading portion $\sqrt{J_2'}$ is clearly
important. The most self-consistent values of $2G_{Top}$ occur
in the 35% group with $\sigma_3 = 100$ psi. Only samples 112 and
115 are boxed-in in Table VII, since sample 108 obviously
belongs in the 75% cyclic group even though it is labeled
35%. Using the average $2G_{Top}$ of samples 112 and 115, and
the known values of p and $\sqrt{J_2'}$ together with the previously
determined values G_{oU} and γ_{1U} (and γ_{2U}) leads to the
determination of $\bar{\gamma}_{1U}$.

The tentative values of the unloading shear parameters
so determined are

$$
\left.
\begin{aligned}
G_{oU} &= \quad 7.0 \text{ ksi} \\
\gamma_{1U} &= \quad 51.1 \\
\gamma_{2U} &= -23.7/\text{ksi} \\
\bar{\gamma}_{1U} &= \quad 172
\end{aligned}
\right\} \qquad (64)
$$

The values of the unloading shear modulus computed with the
constants, Eqs. (64), (slightly rounded off) are compared
with the range and average measured values for each case

in Tables VIII and IX. Fairly good agreement is seen for $2G_{UN}$ at the bottom of the unloading segment, Table VIII, with only three cases falling slightly outside the scatterband. At the top of the unloading segment, Table IX, however, agreement is found only for a single case, namely, the 35% - 100 psi group used to compute $\bar{\gamma}_{1U}$ in the first place. All other computed values of $2G_{UN}$ fall significantly below the bottom of the scatterband, indicating a choice of $\bar{\gamma}_{1U}$ which was far too low.

New higher values of $\bar{\gamma}_{1U}$ were used to compute new calculated values in Tables VIII and IX. Better agreement was obtained at the top, but the higher values of $\bar{\gamma}_{1U}$ also caused higher calculated values of $2G_{UN}$ at the bottom. As a result, slight modifications were made in G_{oU} and γ_{1U} (and γ_{2U}) to improve the agreement at the bottom. The final values of the unloading shear parameters used

$$\left.\begin{array}{rl} G_{oU} &= 6.0 \text{ ksi} \\ \gamma_{1U} &= 40.0 \\ \gamma_{2U} &= -18.5/\text{ksi} \\ \bar{\gamma}_{1U} &= 500 \end{array}\right\} \quad (65)$$

represent a reasonable attempt to stay within the scatter. The choice is not claimed to be unique. The values of $2G_{UN}$ computed with the parameters, Eqs. (65), are compared with the measured values in Tables VIII and IX. At the bottom, Table VIII, three cases fall outside the range of measured values, the same as for the tentative values, Eqs. (64). However, at the top of the unloading segment, Table IX, the calculated values fall outside the range of measured values for only two cases (including the 35% - 100 psi case which agreed previously!).

In order to compute the parameters K_{oU} and K_{1U} in the unloading bulk modulus the slopes of the conventional triaxial plots E were used in conjunction with the values Eqs. (65). The slopes $d(\sigma_1 - \sigma_3)/d\varepsilon_1 = E$ were measured near the bottom of the initial unloading segment of representative samples. The results are summarized in Table X. From the chamber pressure σ_3 and the value of $(\sigma_1 - \sigma_3)$ at which E_{UN} is measured, p and $\sqrt{J_2'}$ may be computed, and with the help of values, Eqs. (65), G_{UN} as well. Finally, from Eq. (58)

$$K = \frac{EG}{9G - 3E} \tag{66}$$

so that K_{UN} may be computed for each sample listed in Table X. It is apparent that the two values of K_{UN} at p $=$ 0.112 ksi are inconsistent, whereas the pair of values of K_{UN} at p $\simeq$ 0.22 ksi and at p $\simeq$ 0.42 ksi agree quite well. Taking the average pressure and corresponding values of K for those two cases, the two constants appearing in Eq. (4), K_{oU} and K_{1U}, are found by solving two simultaneous equations to be

$$\left. \begin{array}{l} K_{oU} = 32.0 \text{ ksi} \\ K_{1U} = 143 \end{array} \right\} \tag{67}$$

The values Eqs. (65) and (67) completely define the model in unloading. It should be noted that the inequalities Eqs. (18), (19), (21), (22) and (24) are satisfied by the unloading values Eqs. (65) and (67) and either the Hydrostat-Triaxial fit [Eqs. (54), (55) and (56)] or the Uniaxial-Triaxial fit [Eqs. (61), (62) and (63)].

IV DISCUSSION OF RESULTS.

Initial Loading.

The behavior of the model, in particular the Uniaxial-
Triaxial fit, in initial loading is illustrated in Figs.
(8)-(20). The stress-strain relation in uniaxial strain,
Fig. (8), closely follows the typical experimental curve
suggested by W.E.S. The maximum deviation is less than
15 psi for stresses less than 500 psi and about 25 psi at
$\sigma_1 \simeq 700$ psi. This is not surprising since the experimental
curve was not used to construct the model. Also shown in
Fig. (8) is the stress-strain curve predicted by the
earlier Hydrostat-Triaxial fit. As mentioned previously,
the Hydrostat-Triaxial fit results in a uniaxial strain
stress-strain relation which is far stiffer than any observed.

The stress difference versus axial strain results in
triaxial compression tests, loaded to failure, are given
in Figs. (9)-(12) for chamber pressures of σ_3 = 0.1, 0.2,
0.4 and 0.8 ksi. The plots of stress difference versus
strain difference for the same configuration and the same
chamber pressures are shown in Figs. (13)-(16). The various
experimental curves, several for each figure, are the light
solid lines. All the available experimental curves are
included, the cycled tests as well as the uncycled ones.
The unloading-reloading cycles have been left out in Figs.
(9)-(12) for clarity. The single cycle of unloading-reloading
was included in Figs. (13)-(15) to give some idea of the
spread in cyclic data. No such data is shown in Fig. (16),

again for clarity. It should be noted that the exact values
of initial slopes and (to a much lesser extent) stress
differences at failure differ from those given in Fig. (7)
and Table III. The actual fit was constructed from uncorrected
raw test data, while the experimental curves shown represent
processed data. The scatter in the initial modulus $E_{initial}$
is reduced significantly in Figs. (9)-(12) as compared with
Fig. (7).

The heavy solid curve, labeled "Uniax-Triax 1", is the
curve computed using the Uniaxial-Triaxial fit discussed in
Section III. The earlier Hydrostat-Triaxial fit, not shown,
gave results which were very similar. The computed stress
difference at failure is shown as a horizontal asymptote.
The other heavy curves labeled "Uniax-Triax 2" and "Hydro-
Triax 2" are improved fits which are discussed below.

With the exception of Figs. (9) and (13) which correspond
to the tests run at σ_3 = 100 psi, all computed curves approach
the correct stress at failure. The reason for the computed
$(\sigma_1 - \sigma_3)_{max}$ being high at σ_3 = 100 psi is evident from
Figs. (5) and (6) where all the data points at 100 psi fall
below the failure fit. Although, in general, the computed
curves on the Uniax-Triax 1 fit approach the proper value at
failure, they are too soft at stresses significantly below
failure. The discrepancy appears to increase with chamber
pressure in both the conventional triaxial and stress
difference - strain difference plots. The similar trend in
both sets of plots suggests that the shear modulus $G_{LD}(p, \sqrt{J_2'})$

is at fault and that altering the values of the parameters G_o, γ_1, γ_2 and $\bar{\gamma}_1$ may lead to significant improvements.

The proportional loading tests are shown in Figs. (17), (18) and (19) for stress ratios q of 0.4, 0.6 and 0.8, respectively. Since these tests were in no way used to construct the model, they serve as a check on its validity in a different loading geometry. For q = 0.4, Fig. (17), the computed axial stress at failure agrees well with the peak stress in the experimental curves. As q increases, the computed peak axial stress becomes larger than that which is measured. At a stress ratio of q = 0.8, Fig. (19), the discrepancy is quite pronounced, the computed value of $\sigma_{1_{max}}$ being 2.01 ksi while the measured peak stress ranges from 1.22 to 1.62 ksi.

It turns out that the axial stress at failure is quite sensitive to uncertainties in the stress ratio q. Since these stress levels correspond to the horizontal (or nearly so) portion of the failure surface, Fig. (5),

$$\sigma_{1_{max}} = \frac{(\sigma_1 - \sigma_3)_{max}}{1 - q} = \frac{0.403}{1 - q} \text{ ksi} \tag{68}$$

If when the test was run q had been 0.75 rather than 0.80, (a not unreasonable error of 6%), according to Eq. (68) $\sigma_{1_{max}}$ would have been 1.61 ksi, a value very close to one actually measured. Even the lowest value $\sigma_{1_{max}}$ = 1.22 ksi, corresponds to a value q = 0.67, only 16% below the nominal value. Of course, the present discussion applies to a fixed value $(\sigma_1 - \sigma_3)_{max}$. As an example of the possible scatter

from sample to sample in the stress difference at failure
at stress levels of $\sigma_1 \simeq 1.2$ ksi refer to Fig. (12). The
shape of the curves, labeled "Uniax-Triax 1" in Figs.
(17)-(19) agrees reasonably well with those measured.

Finally, the hydrostatic test results are shown in
Fig. (20). The curve marked "Hydro-Triax Fit" agrees well
with the data, at least up to 800 psi. This is no surprise
since it was constructed to do so, see Section III. The
curves based upon the uniaxial test, on the other hand,
both the present Uniax-Triax 1 fit and the improved Uniax-
Triax 2 discussed below, are considerably softer than the
measured results.

Unloading-Reloading.

The behavior of the model in unloading and reloading
is illustrated in Fig. (8) in the uniaxial strain test and
in Figs. (21)-(28) in the triaxial configuration. In the
uniaxial test only unloading was measured, while in the
triaxial case complete cyclic data was available.

The computed unloading curve in uniaxial strain, Fig.
(8), agrees reasonably well with the measured curve, except
for the sharp tail at the bottom. Of course, the scale,
chosen to portray the loading portion well, more or less
obscures small differences in the nearly vertical unloading
portion. The tail at the bottom of the unloading stroke has
been impossible to reproduce exactly with any of a variety
of mathematical models with which the author has had

experience. Upon reloading, a hysteresis loop, albeit a small one is formed and the reloading portion then crosses the unloading portion and approaches the extended initial loading curve.

The results of the cyclic triaxial tests, unloaded from 75% of the failure load are shown in Figs. (21)-(24); the 35% cyclic tests are shown in Figs. (25)-(28). The conventional plots, stress difference versus axial strain are in part (a), while the stress difference versus strain difference plots are in part (b). To avoid confusion, only a single experimental curve is shown in each figure.

The curve chosen, in each case, is typical of the better data. It should be noted that the starting point for unloading is determined by the (initial) loading model and not the unloading fit.

The unloading behavior in the triaxial test agrees reasonably well with the experimental results, especially when the wide scatter, c.f. Tables VI and VII, in the latter is considered. On reloading, however, the model is clearly too soft. Upon multiple cycles of loading-unloading, the stress difference versus strain difference plots predicted by Eqs. (5) and (6) [or Eqs. (9) and (10) where applicable] would consist of multiple reproductions of the first cycle, each displaced in the strain direction. In the corresponding stress difference versus axial strain plots, some difference would exist between the first (initial) loading and subsequent reloading since, while $G = G_{LD}$, $K = K_{UN}$ during reloading.

Nevertheless, the model predicts much more "walking", i.e., excessive strain, than is observed.

Suggested Modifications.

The Uniax-Triax Fit 1 model described above adequately predicts the behavior of McCormick Ranch Sand in the various available laboratory tests with three exceptions. (1) The hydrostat is too soft; (2) the initial loading behavior in triaxial tests is somewhat too soft; and (3) on reloading the model predicts excessive "walking". As far as (1) is concerned, the experimental data is simply inconsistent and no modification of the existing theory can eliminate the discrepancy between the measured uniaxial strain and hydrostatic behavior. The remaining discrepancies can be largely eliminated by the modification suggested below.

The general trend is for the bulk modulus to increase with increasing stress level (beyond some low stress) and for the shear modulus to increase with pressure and decrease with increasing stress deviators. In a strain controlled test, such as the uniaxial strain test, the pressure volume relation dominates, since the deviatoric strains are con- strained by geometry. The bulk modulus increases much faster than the shear modulus so that K/G becomes much larger than unity. The slope, or constrained modulus

$$M = K(1 + \frac{4}{3} \frac{G}{K}) \simeq K \tag{69}$$

so that at moderately high stresses the stress-strain relation is insensitive to G.

In a stress controlled test, such as the triaxial compression test, where the deviatoric stress increases faster than the pressure, the ratio G/K becomes small since G approaches zero. The slope at higher stress differences

$$E = \frac{9G}{3 + \frac{G}{K}} \approx 3G \tag{70}$$

is thus insensitive to K. Of course, the slope of the stress difference versus strain difference curves are exactly 2G and are independent of K. The slope $d\sigma_1/d\varepsilon_1$ in a proportional loading test is intermediate between Eqs. (69) and (70)

$$\frac{d\sigma_1}{d\varepsilon_1} = \frac{9G}{3(1-q) + \frac{G}{K}(1 + 2q)} \tag{71}$$

and depends on the stress ratio q. The bulk modulus becomes more important as q approaches one.

In view of the discussion above, the fact that the $(\sigma_1 - \sigma_3)$ versus both ε_1 and $(\varepsilon_1 - \varepsilon_3)$ triaxial test plots are too soft clearly suggests that the values of G_o, $\bar{\gamma}_1$, γ_1 and γ_2 given by Eqs. (61) and (62) are in error.

In Fig. (29), the measured values of initial slopes $2G_{LD}$ are plotted against chamber pressure. A fit through the data, also shown, intersects the 2G axis at approximately 16 ksi. Using $G_o = 8.0$ ksi and the original failure fit (Case 10, Table I), the modified shear modulus parameters become

$$
\left.
\begin{array}{l}
G_o = 8.0 \text{ ksi} \\[4pt]
\bar{\gamma}_1 = -110.0 \\[4pt]
\gamma_1 = 32.4 \\[4pt]
\gamma_2 = -15.0/\text{ksi}
\end{array}
\right\} \tag{72}
$$

The function $2G_{LD}(p,C)$ based on Eqs. (72) is shown in Fig. (29), as is that based on Eqs. (61) and (62). The stiffer shear modulus comes much closer to the measured values.

Two modified complete initial loading models were used to recompute the various tests for which measurements were available, Figs (9) to (20); both used Eqs. (72) to define the shear modulus. The "Hydro-Triax Fit 2" used the bulk constants, Eqs. (54), found previously based on the hydrostatic test. The second model, the "Uniax-Triax Fit 2", used the initial constrained modulus $M_o = 16.5$ ksi and repeated the trial and error procedure used previously to fir. K_1 and K_2 so that the uniaxial strain test was adequately reproduced. The final values of the bulk constants were

$$
\left.
\begin{array}{l}
K_o = 5.83 \text{ ksi} \\[4pt]
K_1 = 80 \text{ ksi} \\[4pt]
K_2 = 30,000 \text{ ksi}
\end{array}
\right\} \tag{73}
$$

The computed uniaxial strain curve for the Uniax-Triax Fit 2 is compared with the experimental curve in Fig. (30). The agreement is at least as good as that in Fig. (8), the original uniaxial-triaxial fit. Also shown are the uniaxial

curves produced by both Hydrostat-Triaxial fits. The
closeness of the two clearly validates the contention,
Eq. (69), that the uniaxial strain curve is insensitive
to the shear modulus. The unloading model used to compute
the unloading-reloading portion of Fig. (30) was that given
earlier by Eqs. (65) and (67) with the exception that G_{oU}
was increased

$$G_{oU} = 8.0 \text{ ksi} \qquad (74)$$

so that inequality, Eq. (21), is not violated.

It is worth noting that, although the two Uniaxial-
Triaxial fits give substantially the same stress-strain
curve in uniaxial strain, the corresponding stress paths
differ appreciably, see Fig. (31). In fact, the initial
Poisson's ratio in the Uniax-Triax Fit 2 is only 0.029
(perhaps unrealistically low) although by an axial stress
of 100 psi it is already 0.23. The radial stress was not
measured so that the actual stress path remains unknown.

The stress difference versus axial strain curves in
triaxial compression produced by both modified fits are
shown in Figs. (9)-(12). As suggested by Eq. (70), the
curves are close together and thus insensitive to the bulk
relation. Of course, the curves in Figs. (13)-(16) depend
only on G and the two modified fits are identical. It is
seen from Figs. (9)-(16) that the shear modulus parameters,
Eqs. (72) produce results which are in excellent agreement
with the data.

In the proportional loading tests, Figs. (17)-(19), the two modified fits grow further apart as q increases, as suggested by Eq. (71). The Hydro-Triax Fit 2 becomes much too stiff when q = 0.8. The Uniax-Triax Fit 2 agrees slightly less well with the data than the softer Uniax-Triax Fit 1; nevertheless, the agreement with the data is not unreasonable. Finally, the hydrostats based on all fits are shown in Fig. (20). Both uniaxial fits are much softer than the measured results, a discrepancy discussed earlier.

The present model, which makes no distinction between initial loading in shear and subsequent reloading in shear, results in excessive strains during cyclic loading. One possibility, analogous to the bulk modulus treatment, would be to use

$$
G = \begin{cases} G_{LD}(p, \sqrt{J_2'}) & \text{when } \dot{J}_2' > 0 \text{ and } J_2' = J_{2\,max}' \\[2em] G_{UN}(p, \sqrt{J_2'}) & \text{when } \dot{J}_2' \leq 0 \text{ or } J_2' < J_{2\,max}' \end{cases} \tag{75}
$$

where $J_{2\,max}'$ is the maximum previous value of J_2'. Use of Eqs. (75) would eliminate all additional hysteresis and additional permanent strain after the first cycle of cyclic loading. Another possibility is the introduction of a new function G_{RE} which would be a linear combination of the two independent shear moduli G_{LD} and G_{UN}, namely

$$
G_{RE} = \alpha\{(\tfrac{F}{F_m})^n\}\, G_{LD}(p,J_2') + \{1-\beta\,(\tfrac{F}{F_m})^n\}\, G_{UN}(p,J_2') \tag{76}
$$

where α, β and n are constants, and where F/F_m is a measure of the present state of stress relative to the maximum (in some sense) previous state of stress. When $F/F_m = 0$, for the behavior to be continuous when J_2' (or F) $= 0$, $G_{RE} = G_{UN}$, while when $F/F_m = 1$ one sets

$$G_{RE} = \alpha \; G_{LD} + (1-\beta) \; G_{UN} = G_{LD} \qquad (77)$$

This produces the relation between α and β

$$(1-\alpha) \; G_{LD}(F_m) = (1-\beta) \; G_{UN}(F_m) \qquad (78)$$

which varies with the loading history of each point. However, Eq. (78) is satisfied identically for all loading histories if $\alpha = \beta = 1$.

The measure of the state of stress will be related to $G_{LD}(p,J_2') \geq 0$

$$F = 1 - \frac{G_{LD}(p,J_2')}{G_{LD}(p,0)} \qquad (79)$$

When $J_2' = 0$, $F = 0$, while if J_2' is such that $G_{LD} = 0$, $F = 1$. The function F is thus restricted to the range

$$0 \leq F \leq 1 \qquad (80)$$

The final form of G_{RE} is

$$G_{RE} = \left(\frac{F}{F_m}\right)^n G_{LD}(p,J_2') + \left[1 - \left(\frac{F}{F_m}\right)^n\right] G_{UN}(p,J_2') \qquad (81)$$

with F given by Eq. (79) and F_m its maximum previous value at the point.

The reloading curve will start out with the unloading slope. For small (relative to the previous maximum) cyclic loading the hysteresis and "walking" will be small. Since $G_{UN} \geq G_{LD}$, G_{RE} is restricted to the range

$$G_{LD} \leq G_{RE} \leq G_{UN} \tag{82}$$

As the load is increased towards its maximum previous value, there is a smooth transition to the virgin loading curve. The suddenness of the transition is controlled by the parameter n; for $F/F_m < 1$ as $n \to \infty$, $G_{RE} \to G_{UN}$, while as $n \to 0$, $G_{RE} \to G_{LD}$ for $F > 0$. The value of n could be chosen so that the reloading shear stress - shear strain curve is always concave downward, thereby eliminating the possibility of any shear shocks. Work on reloading is continuing.

V CONCLUSIONS AND RECOMMENDATIONS.

A model has been developed, namely the Uniax-Triax Fit 2, which agrees excellently with the available initial loading uniaxial strain and triaxial compression data. The agreement with the proportional loading data and the unloading triaxial data is adequate. The questions of the hydrostat and reloading in shear are discussed in Section IV.

On the basis of the present study, the essential in- gredients for fitting a variable modulus model of the type described in Section II to a given soil are (a) the stress strain relation in uniaxial strain, (b) the failure envelope and (c) the stress difference - strain difference relation in a test where shear effects predominate, such as a triaxial compression test. The measurement of the lateral stress in a uniaxial strain test is highly desirable. Also desirable is a hydrostatic test which contains unloading-reloading and which is compatible with the uniaxial results.

The question of reloading in shear, e.g., finding a reasonable value for the parameter n in Eq. (81), is presently left unanswered.

REFERENCES

[1] "Investigation of Ground Shock Effects in Nonlinear Hysteretic Media - Report 1 - Development of Mathematical Material Models", by I. Nelson and M.L. Baron, U.S. Army Engineer Waterways Experiment Station, Vicksburg, Mississippi, Contract DACA39-67-C-0048, Report S-68-1, March 1968.

[2] "Study of Soil Behavior under High Pressure - Report 1 - Response of Two Recompacted Soils to Various States of Stress", by B.B. Mazanti and C.N. Holland, U.S. Army Engineer Waterways Experiment Station, Vicksburg, Mississippi, Contract DACA39-67-C-0051, Report S-70-2, Volumes 1, 2 and 3, February 1970.

[3] "Soil Property Investigation and Free-Field Ground Motion Measurements", by J.S. Zelasko and J.K. Ingram, U.S. Army Engineer Waterways Experiment Station, Vicksburg, Mississippi, Project BACKFILL, Preliminary Data Report, December 1967.

[4] "Calculation of Stress and Strain from Triaxial Test Data on Undrained Soil Specimens", by J.Q. Ehrgott, U.S. Army Engineer Waterways Experiment Station, Vicksburg, Mississippi, Miscellaneous Paper (in process of publication), 1970.

TABLE I - Least Squares Polynomial Fit to Triaxial Failure Data

For "Failure" G=0, or $\sqrt{J_2'} = a_o + a_1 p + a_2 p^2 = \frac{G_u}{-\bar{\gamma}_1} + \frac{\gamma_1}{-\bar{\gamma}_1} p + \frac{\gamma_2}{-\bar{\gamma}_1} p^2$

Case	N	MEAN SQ. RESIDUAL	a_o	a_1	a_2	$\frac{a_1}{a_o} = \frac{\gamma_1}{G_o}$	$P_c = \frac{-a_1}{2a_2}$	$\sqrt{J_2'}_{max}$
1. All tests	53	0.00178	0.1642	0.01704	-0.00088	0.1037	9.638	0.2463
2. N.C.	31	0.00143	0.1730	0.01755	-0.00087	0.1014	10.040	0.2611
3. Cycled @ 35%	9	0.00275	0.1341	0.02817	-0.00150	0.2100	.9390	0.2663
4. Cycled @ 75%	13	0.00188	0.1673	0.00540	-0.00008	0.0322	30.751	0.2503
5. N.C. No #16 $\sigma_3 \leq 3.2$	22	0.00042	0.1189	0.11190	-0.02380	0.9411	2.350	0.2504
6. N.C. No #16 $\sigma_3 \leq 1.6$	19	0.00033	0.0960	0.19460	-0.07010	2.0270	1.388	0.2310
7. N.C. No #16 $\sigma_3 \leq 1.2$	16	0.00025	0.0781	0.27330	-0.12780	3.4993	1.069	0.2242
8. N.C. No #16 $\sigma_3 \leq 0.8$	13	0.00019	0.0813	0.25560	-0.10960	3.1439	1.166	0.2303
9. N.C. $\sigma_3 \geq 1.2$	17		0.2323					0.2323

10. N.C.	14	0.00016	0.0731	0.29490	-0.13620	4.0308	1.082	0.2327
11. All tests	41	0.00100	0.0462	0.44190	-0.27620	9.5545	0.799	0.2230
12. Cycled @ 35%	14	0.00189	0.0135	0.65330	-0.47770	48.2496	0.683	0.2369
13. Cycled @ 75%	13	0.00111	0.0532	0.37000	-0.20890	6.9496	0.885	.

TABLE II

LEAST SQUARES FIT TO HYDROSTAT DATA

Case	N	Mean Sq. Residual	a_o	a_1	a_2	a_3
1. All points	21	0.0898	0.0062	0.732	2498.0	-37403.0
2. Sample 35, all points	7	0.0284	-0.0241	64.60	-6355.0	180578.0
3. Sample 44, all points	7	0.0535	-0.0227	73.09	-8950.0	369563.0
4. Sample 48, all points	7	0.0508	-0.0249	58.55	-5555.0	178973.0
5. Sample 35, $p \leq 0.8$ ksi	5	0.0020	-0.0117	47.47	-4071.0	117848.0
6. Sample 44, $p \leq 0.8$ ksi	5	0.00013	-0.0014	22.625	-684.92	65137.0
7. Sample 48, $p \leq 0.8$ ksi	5	0.00019	-0.0019	20.619	-631.0	35785.0

$$p = a_1 \epsilon_{kk} + a_2 \epsilon_{kk}^2 + a_3 \epsilon_{kk}^3$$

$$= K_o \epsilon_{kk} + \frac{1}{6} K_1 \epsilon_{kk}^2 + \frac{1}{27} K_2 \epsilon_{kk}^3$$

TABLE III

McCORMICK RANCH SAND - TRIAXIAL TEST FAILURE DATA

	SAMPLE	σ_3	$\sigma_1 - \sigma_3$	p	J_2'
NONCYCLIC	88	0.100	0.202	0.167	0.116
	76	0.100	0.191	0.163	0.110
	91	0.100	0.198	0.166	0.114
	97	0.100	0.197	0.165	0.113
	75	0.200	0.252	0.284	0.145
	77	0.200	0.282	0.294	0.162
	22	0.200	0.295	0.298	0.170
	85	0.400	0.335	0.511	0.193
	87	0.400	0.320	0.506	0.184
	89	0.400	0.285	0.495	0.164
	15	0.800	0.415	0.938	0.239
	49	0.800	0.422	0.940	0.243
	70	0.800	0.380	0.926	0.219
	71	0.800	0.377	0.925	0.217
CYCLED AT 35%	108	0.100	0.187	0.162	0.107
	112	0.100	0.155	0.151	0.089
	115	0.100	0.180	0.159	0.103
	114	0.200	0.253	0.264	0.146
	132	0.200	0.300	0.300	0.173
	137	0.200	0.311	0.303	0.179
	133	0.400	0.412	0.537	0.237
	136	0.400	0.425	0.541	0.245
	137	0.400	0.425	0.541	0.245
	130	0.800	0.390	0.930	0.225
	134	0.800	0.440	0.946	0.254
	135	0.800	0.451	0.950	0.260
	138	0.800	0.250	0.883	0.144
	139	0.800	0.225	0.875	0.129
CYCLED AT 75%	107	0.100	0.170	0.156	0.098
	109	0.100	0.190	0.163	0.109
	113	0.100	0.165	0.155	0.095
	105	0.200	0.280	0.293	0.161
	110	0.200	0.230	0.276	0.132
	123	0.200	0.270	0.290	0.155
	118	0.400	0.267	0.489	0.154
	120	0.400	0.365	0.521	0.210
	121	0.400	0.363	0.521	0.209
	111	0.800	0.245	0.881	0.141
	126	0.800	0.360	0.919	0.207
	128	0.800	0.410	0.936	0.236
	131	0.800	0.460	0.953	0.265

TABLE IV

TRIAXIAL INITIAL SLOPE

CASE	N	MEAN SQ. RESID.	a_0	a_1	a_2	COMMENTS	E @ 100 PSI
#1 3rd POLY, 800, ALL	39	879	11.8	175.0	55.3	SYS. ERROR	29.78
#2 2nd POLY, 800, ALL	39	855	7.49	228.0	-100.0	SYS. ERROR	25.30
#3 2nd POLY, 400, ALL	26	299	10.8	192.0	-29.3		29.78
#4 2nd POLY, 400, N.C.	9	467	29.2	116.8	29.4		41.26
#5 2nd POLY, 400, 35%	9	103	3.99	261.0	-256.0		27.59
#6 2nd POLY, 400, 75%	8	184	2.83	153.0	229.0		20.49
#7 3rd POLY, 800, N.C.	13	2021	29.3	116.0	32.6		41.26
#8 2nd POLY, 800, N.C.	13	1819	29.1	118.0	26.9		41.24
#9 LINEAR, 800, ALL	39	856	21.2	133.0	-	NO GOOD	34.65
#10 LINEAR, 400, ALL	26	286	12.2	177.0	-	GOOD	30.02

TABLE V

INITIAL SHEAR MODULI
(All Stresses in KSI)

σ_3	Measured Initial Slope	Computed $2G_{initial}$	
		Uniax-Triax I	Hydro-Triax II Uniax-Triax II
0.100	25.0 - 29.0	13.0	22.2
0.200	27.5 - 41.0	16.3	27.8
0.400	40.0 - 51.5	21.8	37.1
0.800	52.5 - 70.0	28.5	48.6

TABLE VI

MEASURED SHEAR MODULUS ON UNLOADING
Samples Unloaded from 75% of Failure
(All Stresses in KSI)

σ_3	Sample No.	$(\sigma_1 - \sigma_3)$ Top	P Top	$\sqrt{J_2'}$ Top	2G Top	$(\sigma_1 - \sigma_3)$ Bottom	P Bottom	$\sqrt{J_2'}$ Bottom	2G Bottom
.100	107	.126	.142	.073	100	.025	.108	.014	30.0
	109	.135	.145	.078	125	.024	.108	.014	25.6
	113	.122	.141	.070	59	.018	.106	.010	34.5
.200	105	.226	.275	.131	250	.020	.207	.012	33.3
	110	.205	.268	.118	100	.025	.208	.014	35.7
	123	.216	.272	.125	91	.025	.208	.014	30.4
.400	118	.190	.463	.110	250	.010	.403	.006	45.5
	120	.248	.483	.143	500	.016	.405	.009	50.0
	121	.250	.483	.144	500	.016	.405	.009	47.6
.800	111	.215	.872	.124	200	.023	.808	.013	46.0
	126	.225	.875	.130	133	.010	.803	.006	62.0
	128	.305	.902	.176	400	.008	.803	.005	89.0
	131	.325	.908	.188	250	.050	.817	.029	73.2

TABLE VII

MEASURED SHEAR MODULUS ON UNLOADING
Samples Unloaded from 35% of Failure
(All Stresses in KSI)

σ_3	Sample No.	$(\sigma_1 - \sigma_3)$ Top	p Top	$\sqrt{J_2'}$ Top	2G Top	$(\sigma_1 - \sigma_3)$ Bottom	p Bottom	$\sqrt{J_2'}$ Bottom	2G Bottom
.100	108*	.127	.142	.073	54.0	.022	.107	.013	25.0
	112	.062	.121	.036	33.0	.028	.109	.016	33.0
	115	.062	.121	.036	43.0	.024	.108	.014	40.0
.200	114	.107	.236	.062	105.0	.031	.210	.018	33.0
	132	.111	.237	.064	200.0	.020	.207	.012	50.0
	137	.109	.236	.063	77.0	.033	.211	.019	32.0
.400	133	.114	.438	.066	143.0	.026	.409	.015	36.0
	136	.120	.440	.069	200.0	.030	.410	.017	42.0
	137	.111	.437	.064	91.0	.026	.409	.015	50.0
.800	130	.160	.853	.092	131.0	.020	.807	.012	82.0
	134	.152	.851	.088	104.0	.032	.811	.018	81.0
	135	.164	.855	.095	550.0	.040	.813	.023	89.0
	139	.160	.853	.092	103.0	.056	.819	.032	91.0

* Sample 108, although labeled "35%", is obviously part of the 75% group.

TABLE VIII

Comparison of Measured and Computed Unloading Shear Moduli
Bottom of the Initial Unloading Cycle

Tentative Parameters: $G_{oU} = 7.0$ ksi, $Y_{1U} = 50$, $Y_{2U} = -23.15/ksi$, $\bar{Y}_{1U} = 170$

Final Parameters : $G_{oU} = 6.0$ ksi, $Y_{1U} = 40$, $Y_{2U} = -18.5/ksi$, $\bar{Y}_{1U} = 500$

σ_3	P_{ave}	$\sqrt{J'_{2\,ave}}$	Measured $2G_{UN}$		Computed $2G_{UN}$	
			Range	Average	Tentative	Final
Cycled @ 35%						
0.100	0.1080	0.0143	25.0 - 40.0	32.67	29.12	34.50
0.200	0.2093	0.0163	32.0 - 50.0	38.33	38.44	43.42
0.400	0.4093	0.0157	36.0 - 50.0	42.67	52.51	54.24
0.800	0.8125	0.0213	81.0 - 91.0	85.75	71.92	73.87
Cycled @ 75%						
0.100	0.1073	0.0127	25.6 - 34.5	30.03	28.51	32.85
0.200	0.2077	0.0133	30.4 - 35.7	33.13	37.29	40.31
0.400	0.4043	0.0080	45.5 - 50.0	47.70	49.58	46.29
0.800	0.8077	0.0133	46.0 - 89.0	67.55	69.08	65.77

TABLE IX

Comparison of Measured and Computed Unloading Shear Moduli
Top of the initial Unloading Cycle

Tentative Parameters: $G_{oU} = 7.0$ ksi, $Y_{1U} = 50$, $Y_{2U} = -23.15$/ksi, $\bar{Y}_{1U} = 170$

Final Parameters : $G_{oU} = 6.0$ ksi, $Y_{1U} = 40$, $Y_{2U} = -18.5$/ksi, $\bar{Y}_{1U} = 500$

	σ_3	P_{ave}	$\sqrt{J_2'}_{ave}$	Measured $2G_{UN}$		Computed $2G_{UN}$	
				Range	Average	Tentative	Final
Cycled @ 35%	0.100	0.1280	0.0483	33. - 54.	43.33	42.46	69.93
	0.200	0.2363	0.0630	77. - 200.	127.33	56.46	91.83
	0.400	0.4383	0.0663	91. - 200.	144.67	71.47	106.25
	0.800	0.8530	0.0918	103. - 550.	222.00	96.82	145.11
Cycled @ 75%	0.100	0.1427	0.0737	59. - 125.	94.67	52.38	96.36
	0.200	0.2717	0.1247	91. - 250.	147.00	80.15	155.70
	0.400	0.4763	0.1323	250. - 500.	416.67	96.10	174.01
	0.800	0.8890	0.1545	133. - 400.	244.75	118.83	208.37

TABLE X

UNLOADING MODULI

Sample	σ_3	E_{UN}	G_{UN}	p	K_{UN}
35%					
115	.100	50.0	21.7	0.112	24.0
132	.200	80.0	31.2	0.220	62.5
136	.400	111.0	42.7	0.427	92.0
75%					
113	.100	55.6	21.7	0.112	43.2
110	.200	74.0	28.3	0.217	64.0
121	.400	105.0	40.0	0.423	93.5
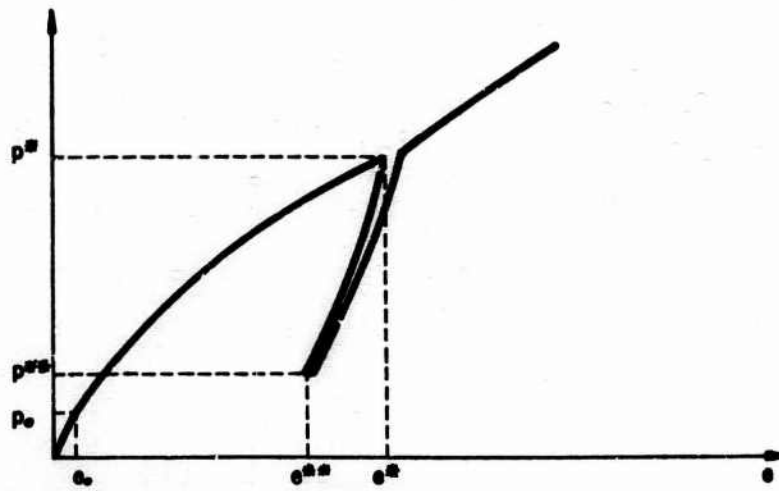
FIG. I   TYPICAL   VOLUMETRIC   STRESS -
STRAIN PATH
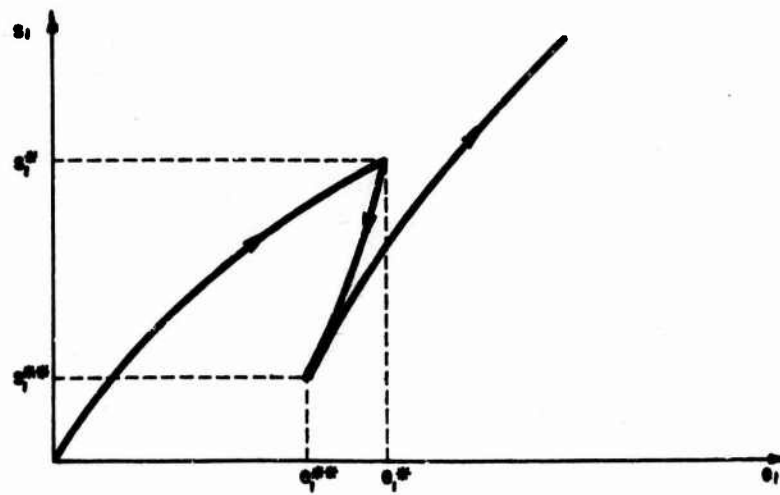
FIG. 2   TYPICAL   DEVIATORIC   STRESS -
STRAIN PATH
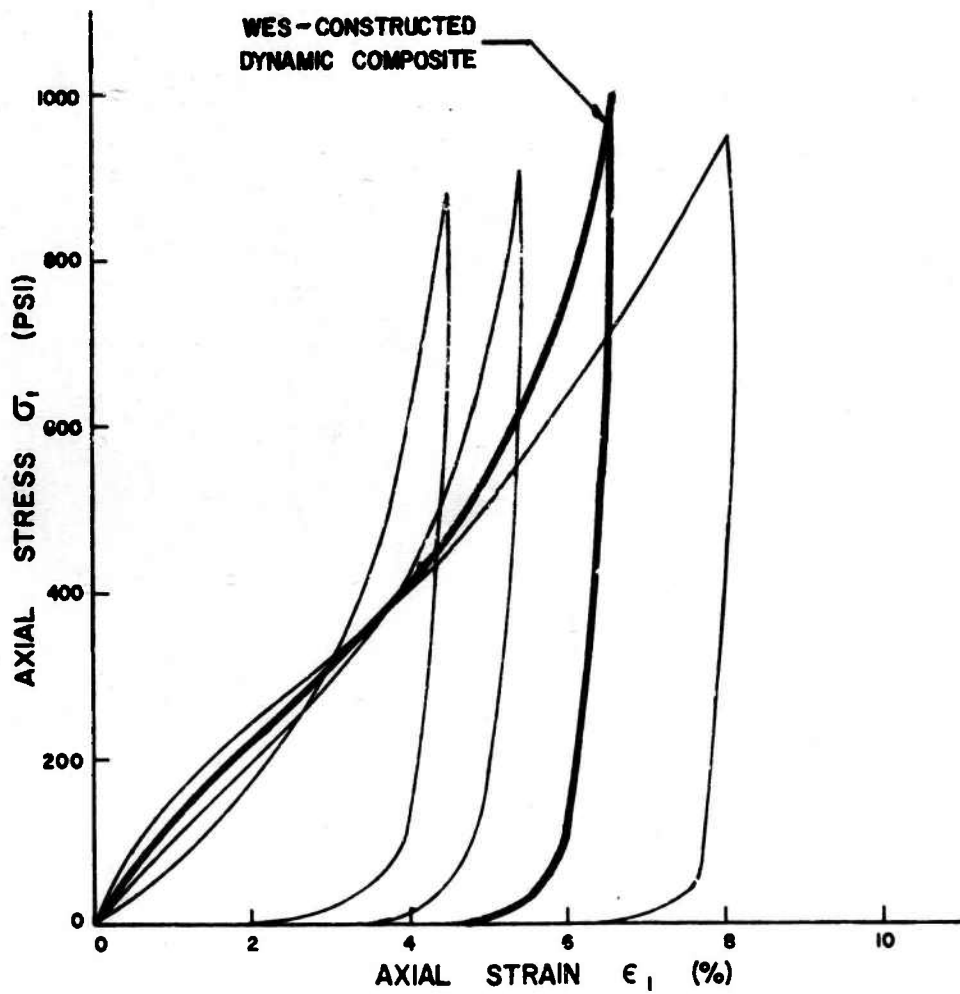
FIG. 3   Mc CORMICK RANCH SAND
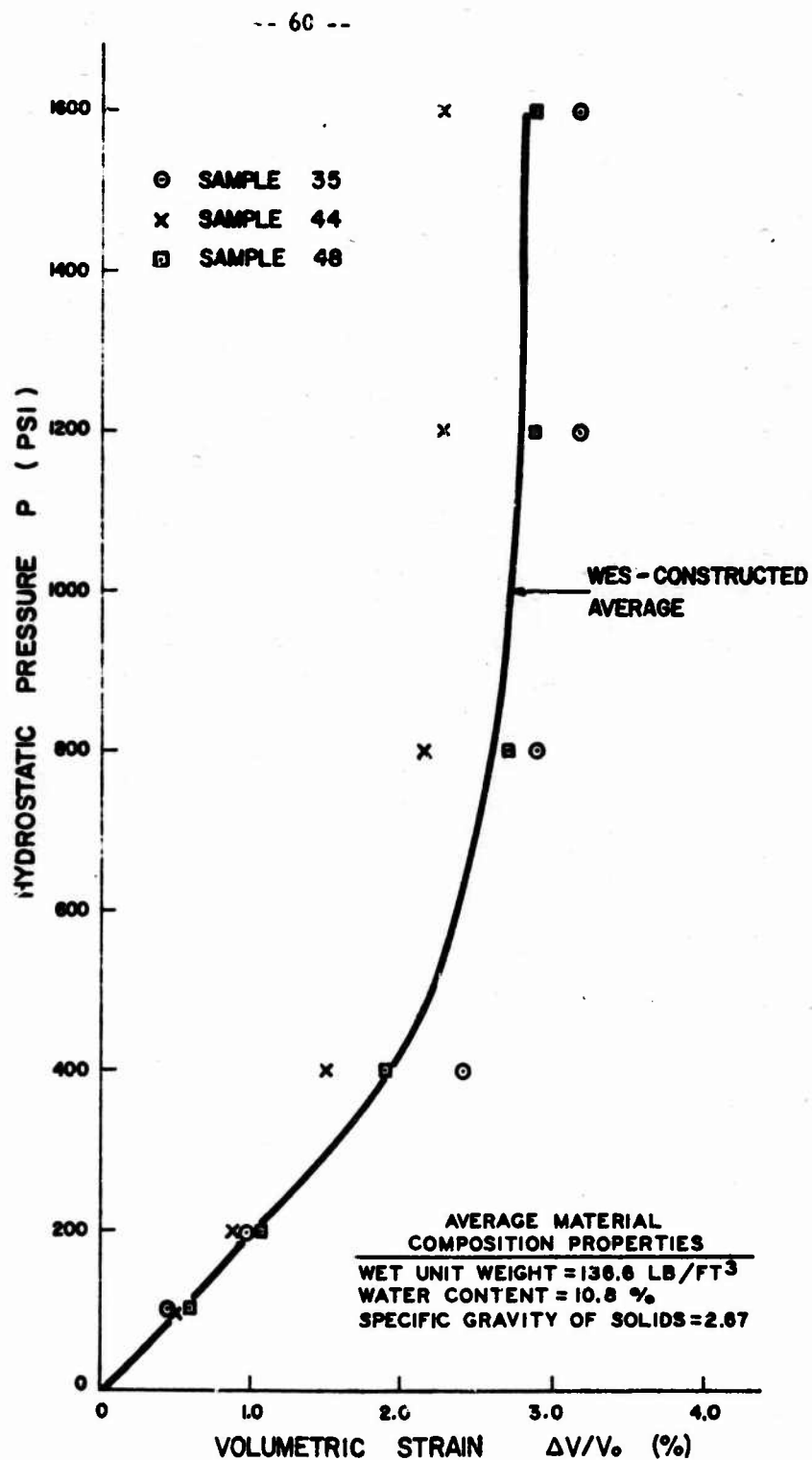   UNIAXIAL STRAIN TESTS
          POSSIBLE VARIATION

FIG. 4   Mc CORMICK   RANCH   SAND
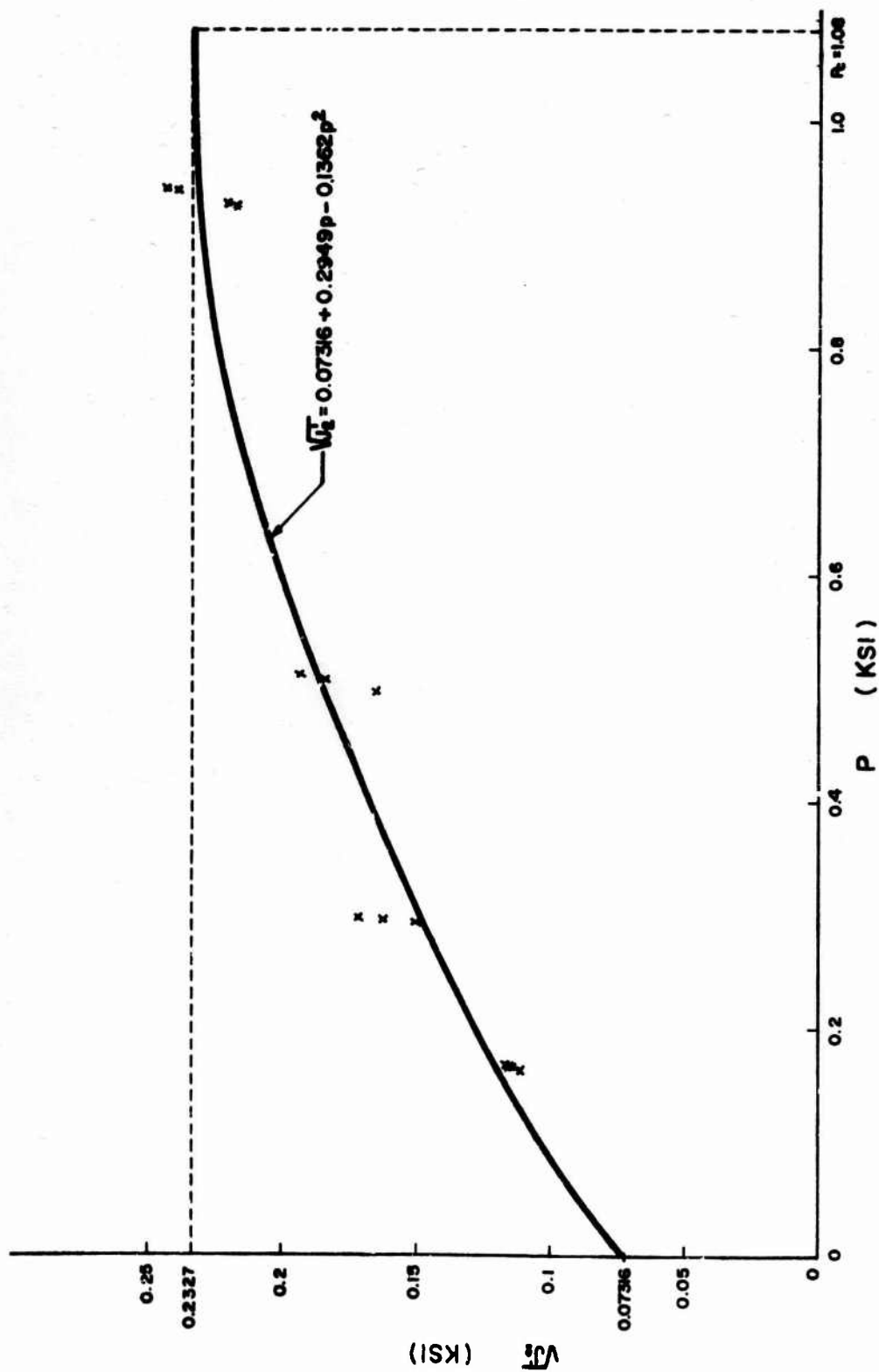STATIC   HYDROSTAT, LOADING   ONLY

$$\sqrt{J_2} = 0.07316 + 0.2949p - 0.1362p^2$$

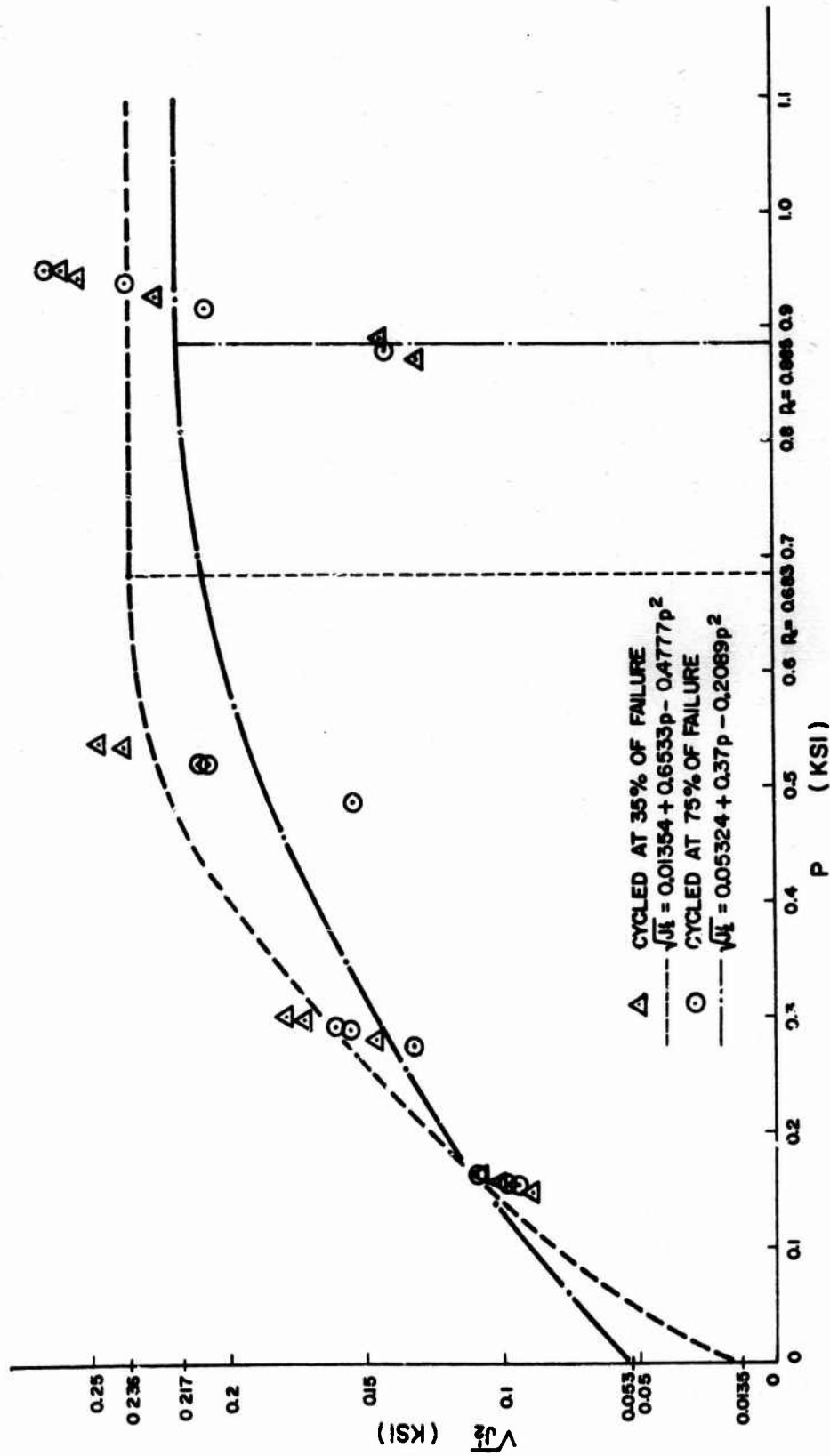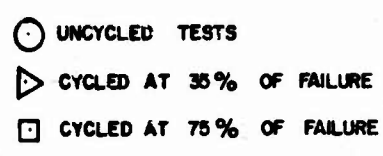FIG. 5   FAILURE FIT BASED ON UNCYCLED TRIAXIAL TESTS

FIG 6 FAILURE FITS BASED ON CYCLED TRIAXIAL TESTS

FIG.7 TRIAXIAL INITIAL SLOPE VE.SUS
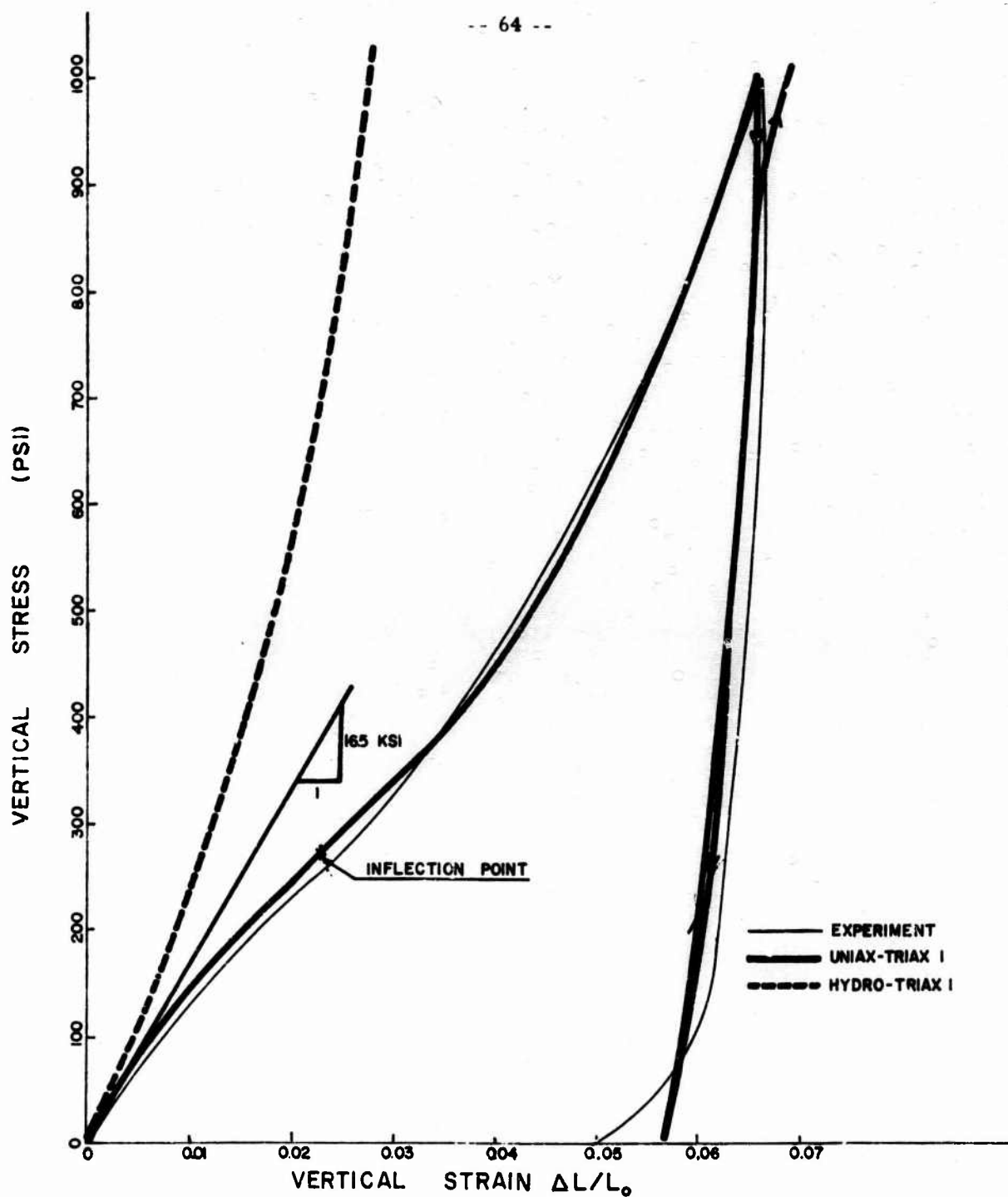CHAMBER PRESSURE

FIG. 8   UNIAXIAL   STRAIN   TEST
McCORMICK   RANCH   SAND

FIG. 9   TRIAXIAL   COMPRESSION   TEST
STRESS   DIFFERENCE   VERSUS   AXIAL   STRAIN
$\sigma_3 = 100$ PSI
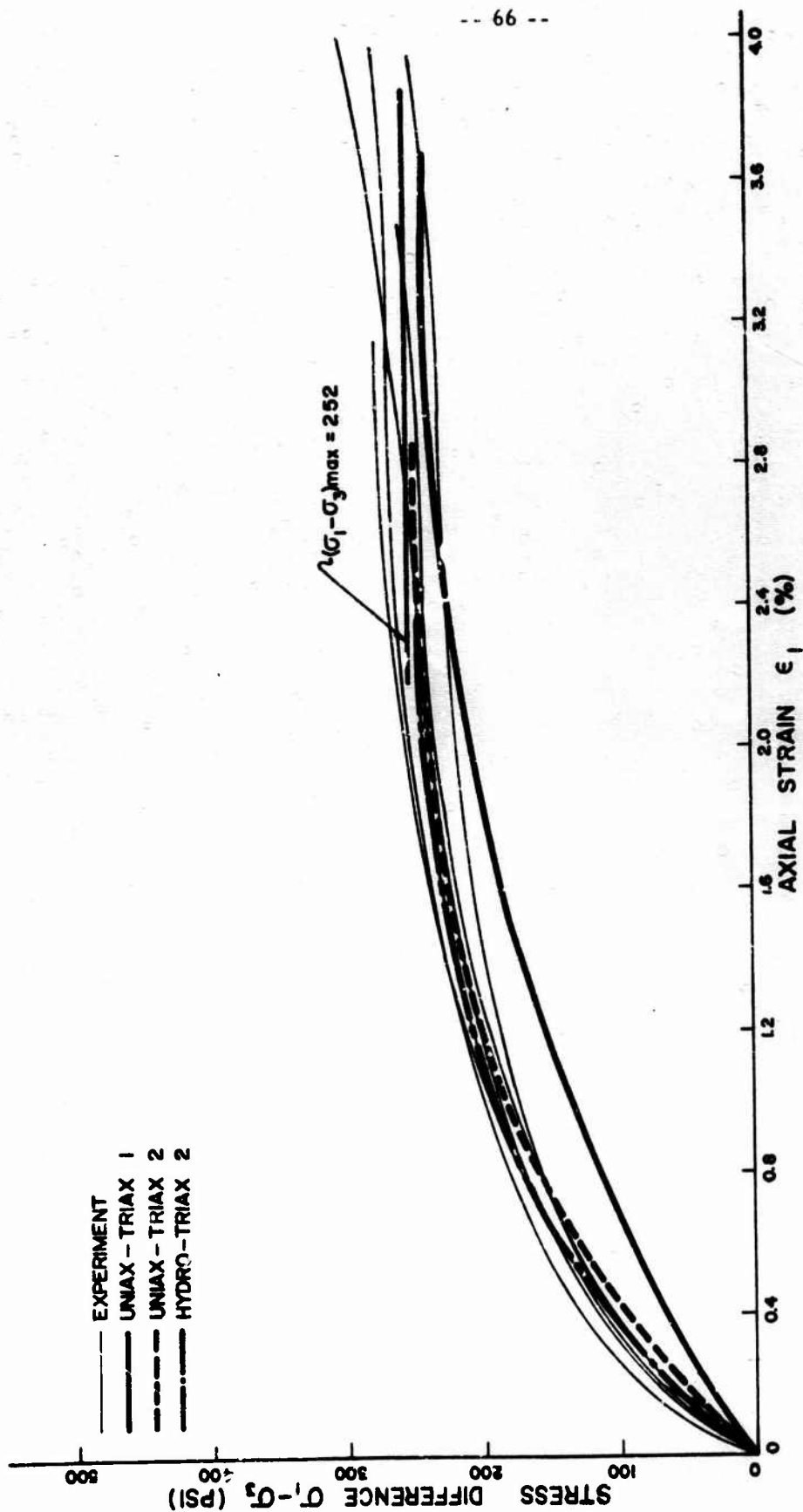
FIG.10   TRIAXIAL   COMPRESSION   TEST
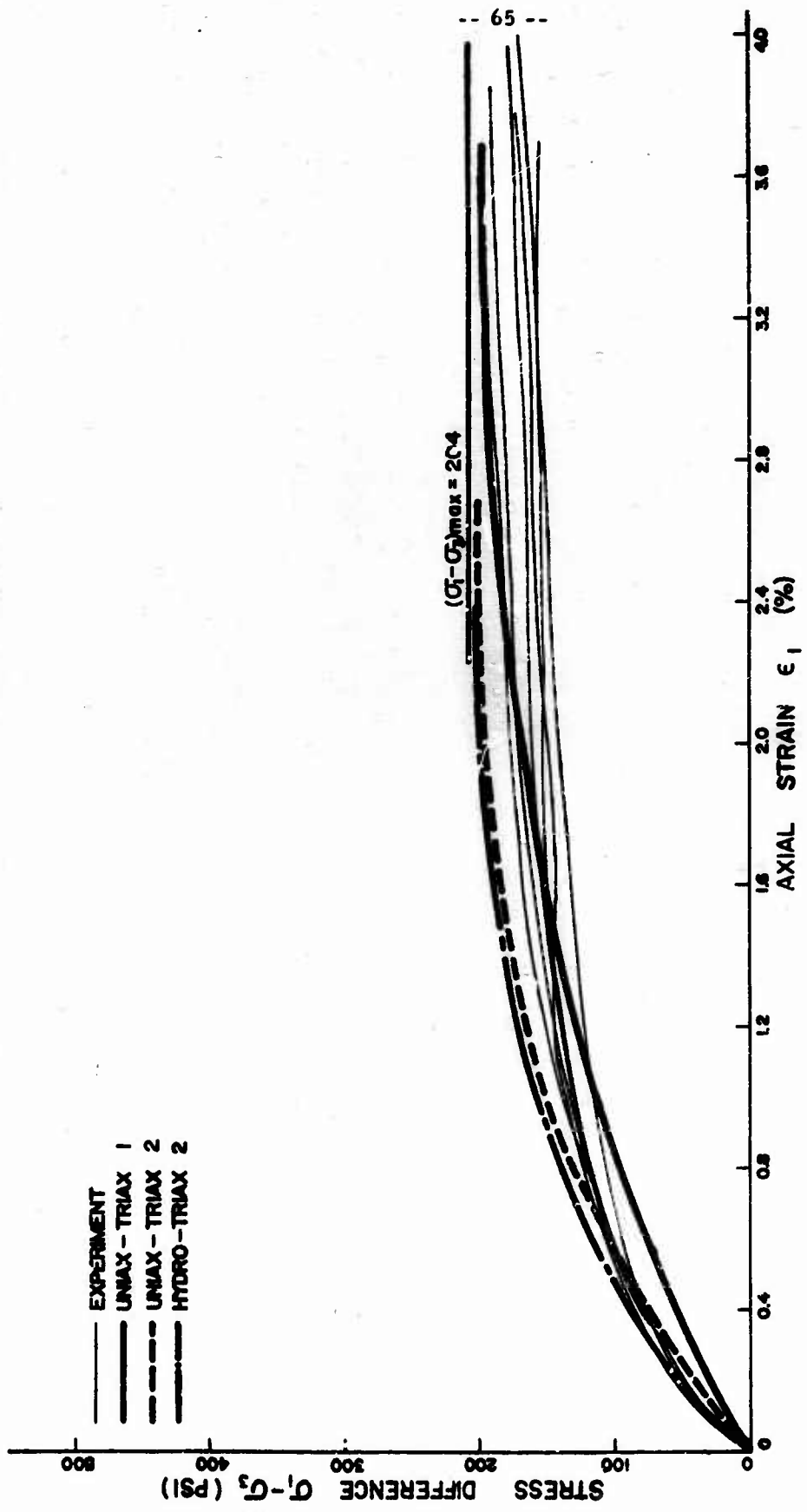STRESS   DIFFERENCE   VERSUS   AXIAL   STRAIN
$\sigma_3 = 200$ PSI
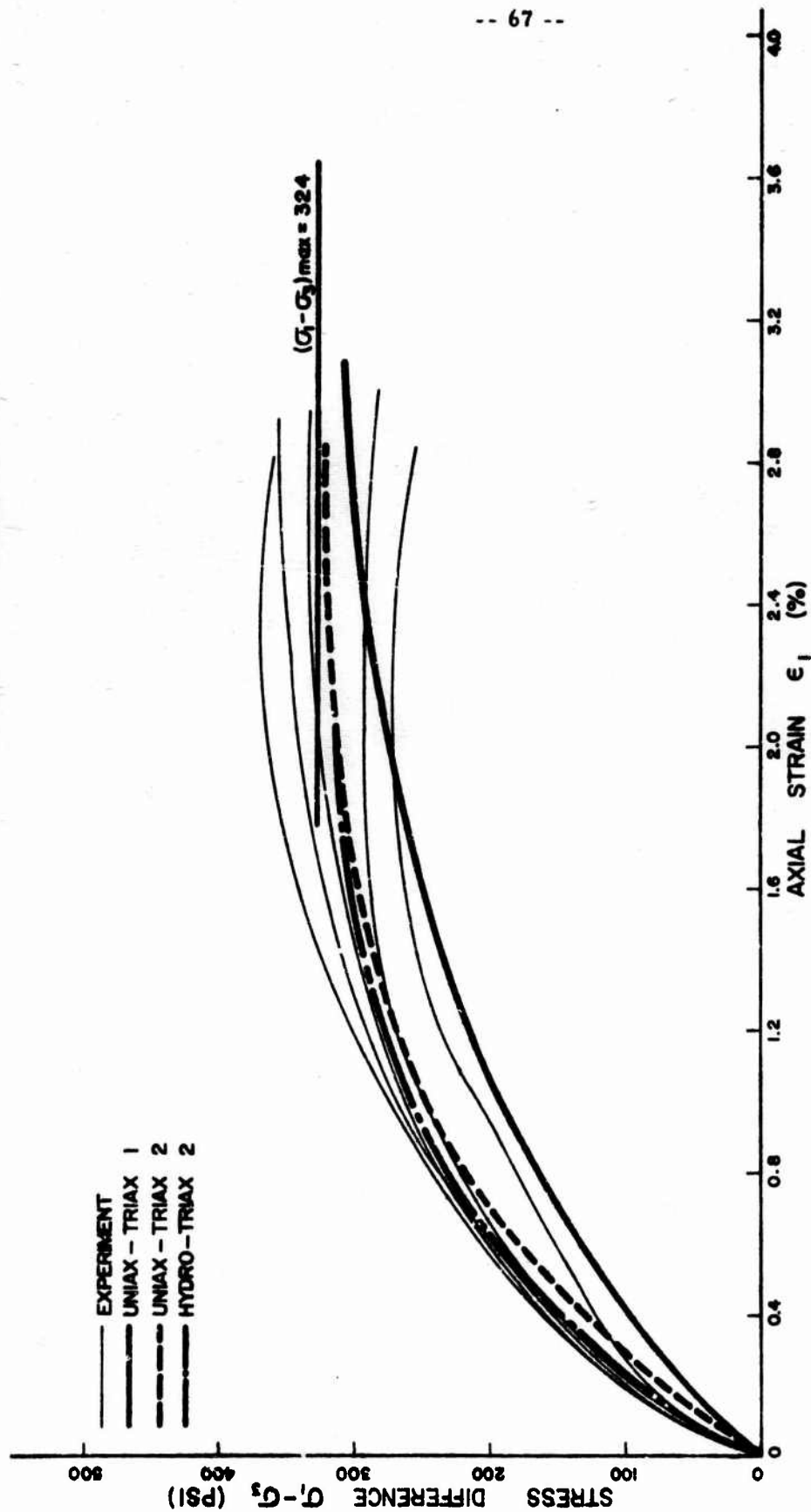
FIG M TRIAXIAL COMPRESSION TEST STRESS DIFFERENCE VERSUS AXIAL STRAIN $\sigma_3 = 400$ PSI

FIG.12   TRIAXIAL   COMPRESSION   TEST
STRESS   DIFFERENCE   VERSUS   AXIAL   STRAIN
$\sigma_3 = 800$ PSI

-- 69 --

$(\sigma_1-\sigma_3)$ max = 204

EXPERIMENT
UNIAX – TRIAX 1
{UNIAX – TRIAX 2
{HYDRO – TRIAX 2

STRESS DIFFERENCE $\sigma_1-\sigma_3$ (PSI)

STRAIN DIFFERENCE $\epsilon_1-\epsilon_3$ (%)

FIG.13 TRIAXIAL COMPRESSION TEST
STRESS DIFFERENCE VERSUS
STRAIN DIFFERENCE
$\sigma_3 = 100$ PSI
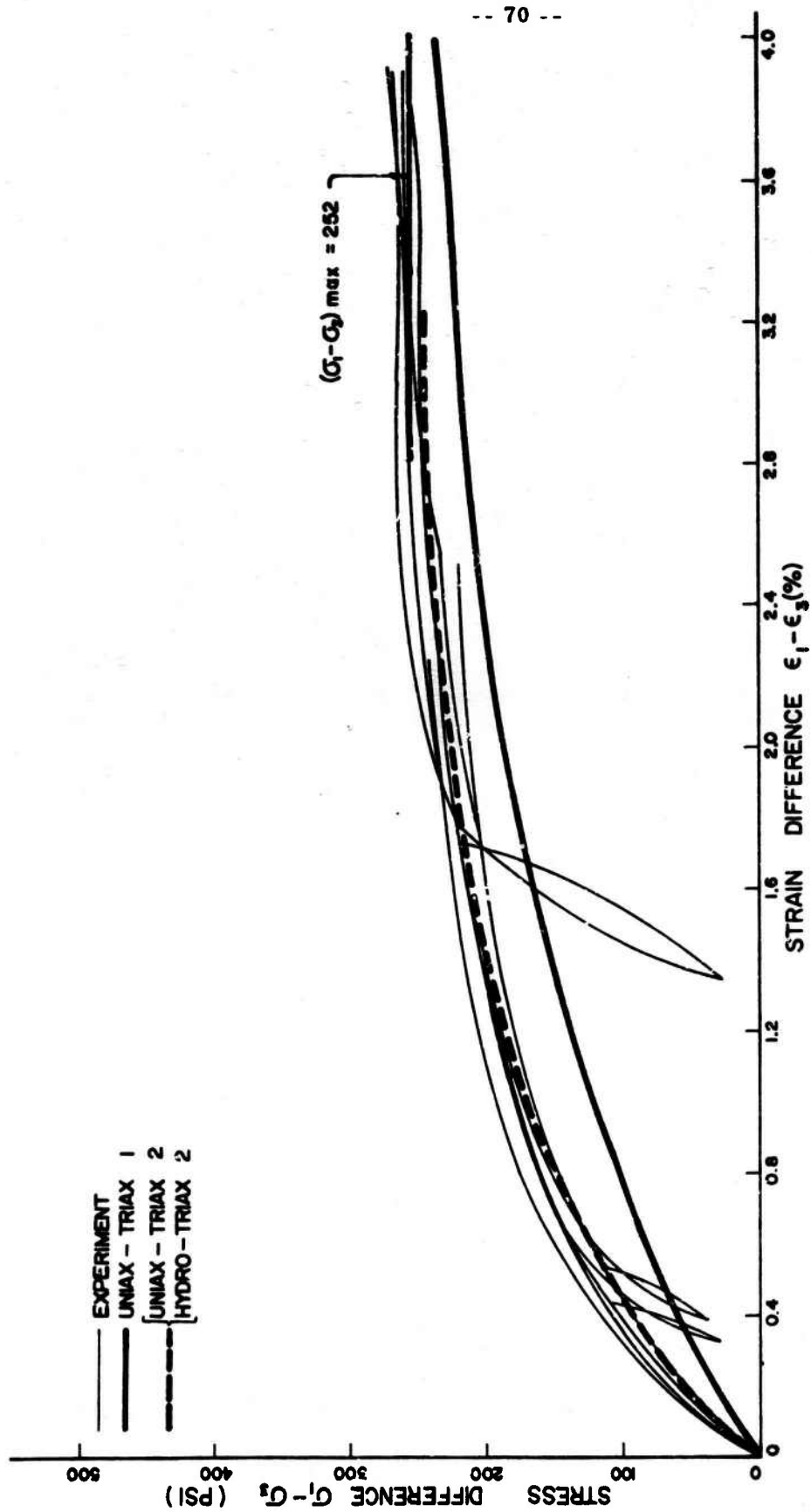
FIG.14   TRIAXIAL   COMPRESSION   TEST
STRESS   DIFFERENCE   VERSUS
STRAIN   DIFFERENCE
$\sigma_3 = 200$ PSI
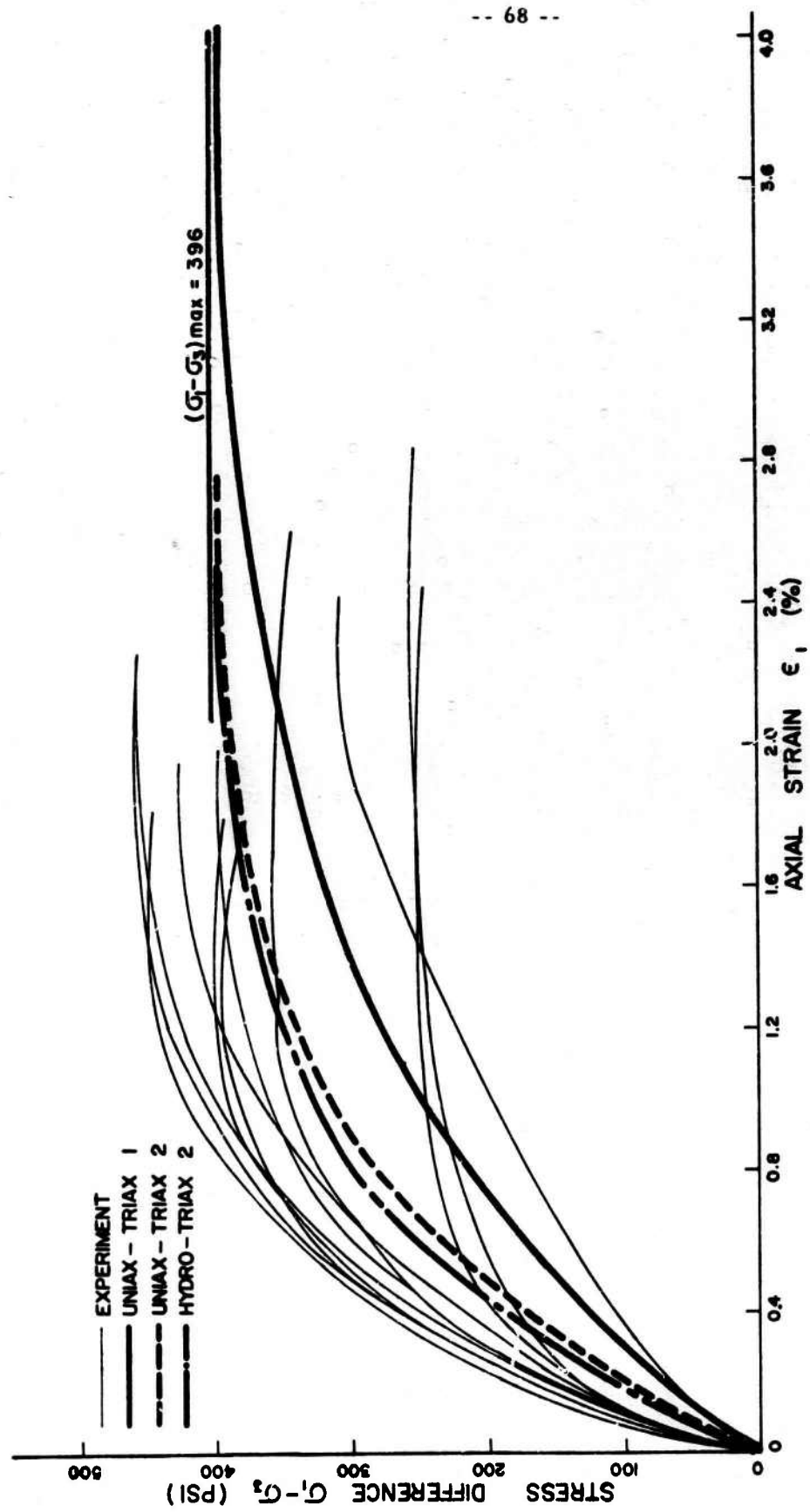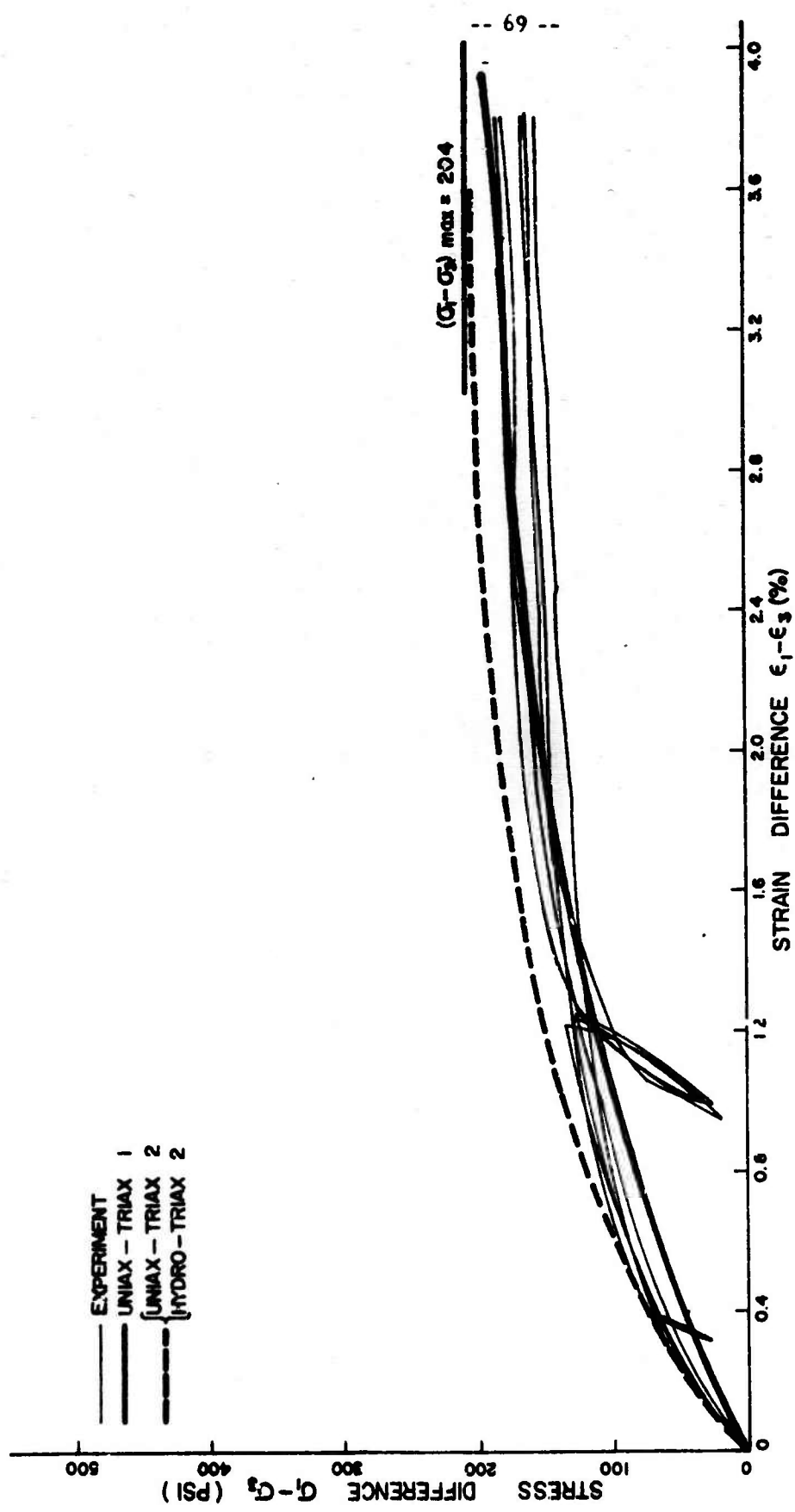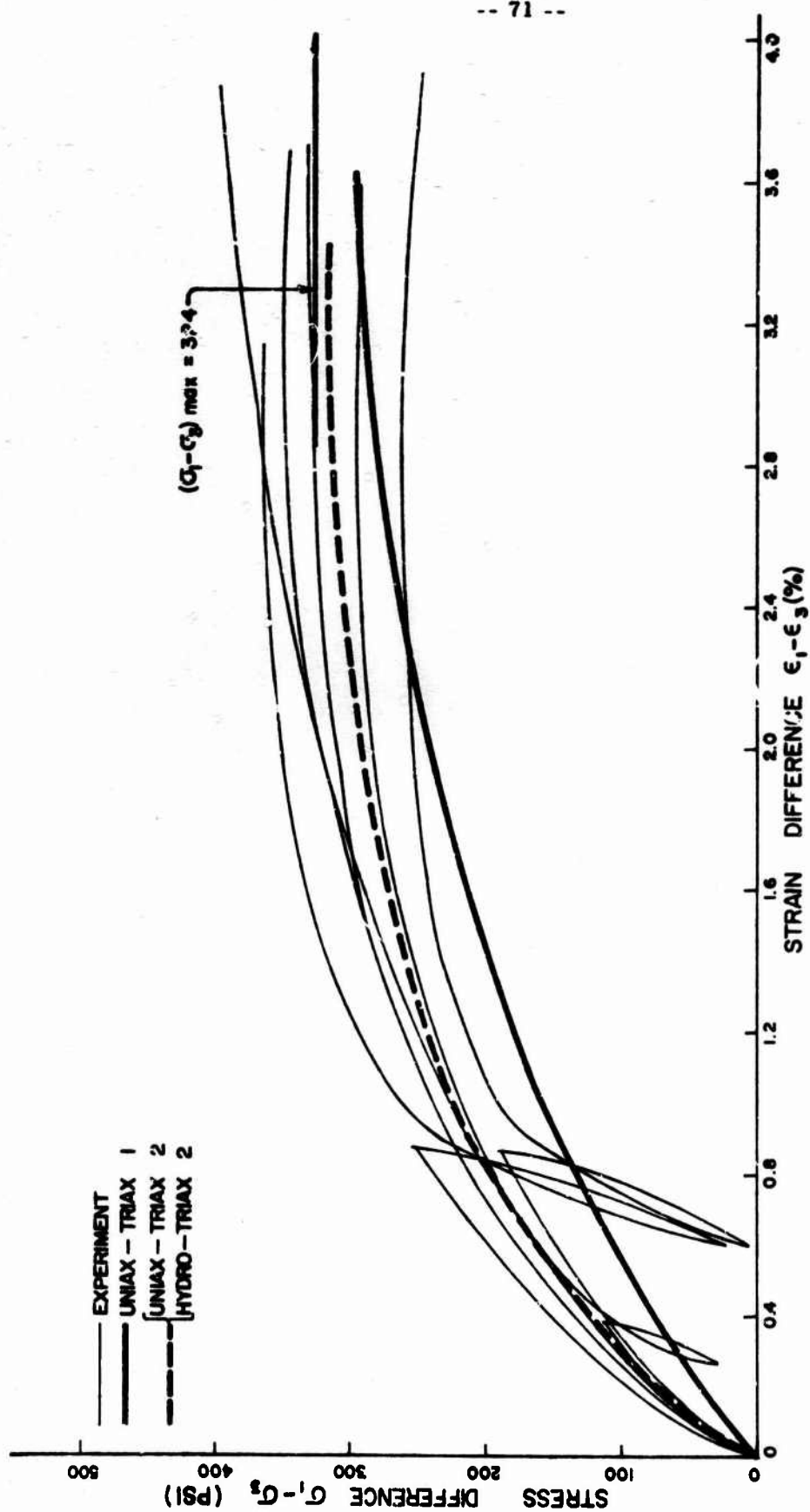
FIG. 15   TRIAXIAL   COMPRESSION   TEST
STRESS   DIFFERENCE   VERSUS
STRAIN   DIFFERENCE
$\sigma_3 = 400$ PSI
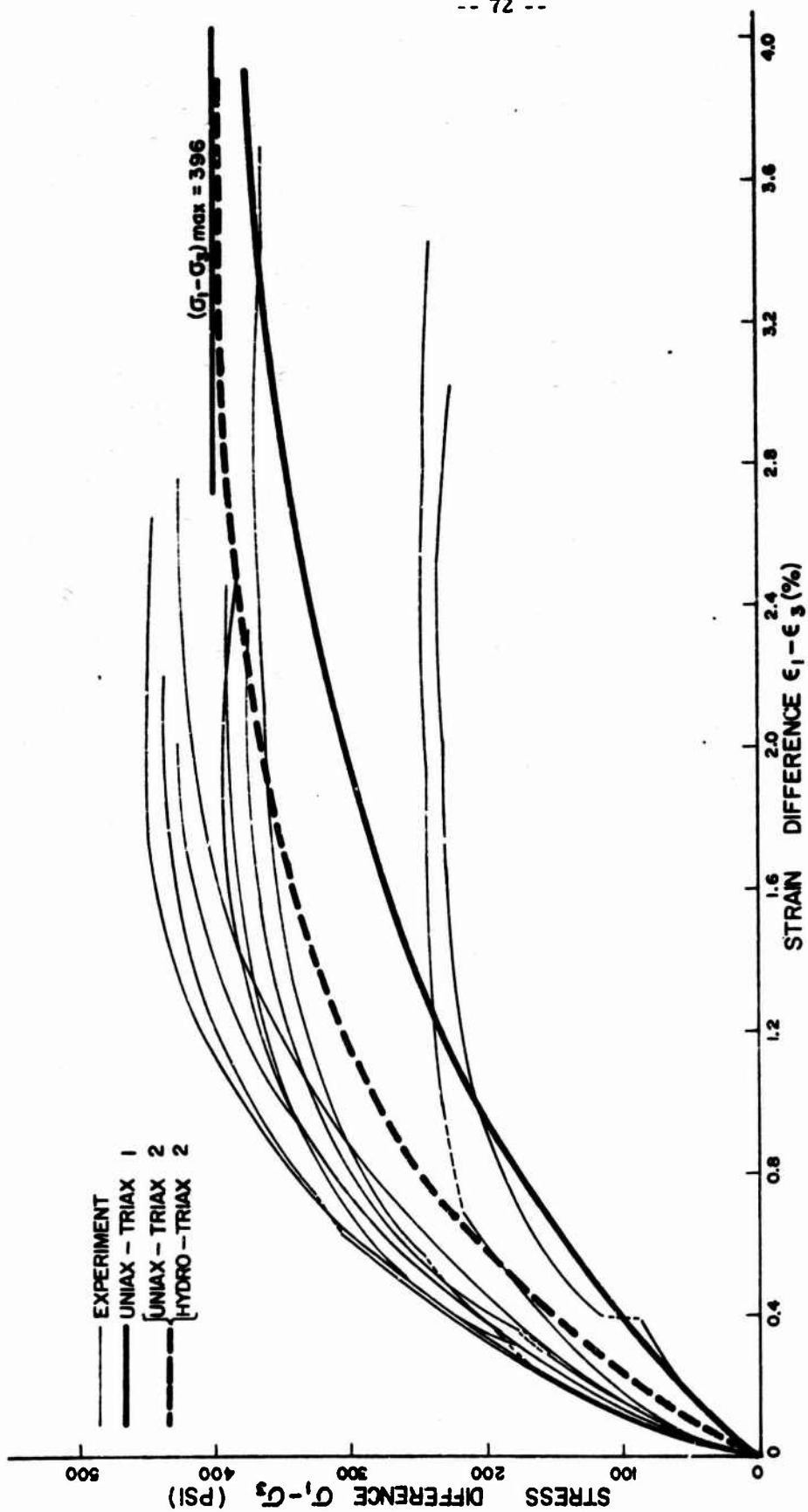
FIG.16   TRIAXIAL   COMPRESSION   TEST
STRESS   DIFFERENCE   VERSUS
STRAIN   DIFFERENCE
$\sigma_3 = 800$ PSI
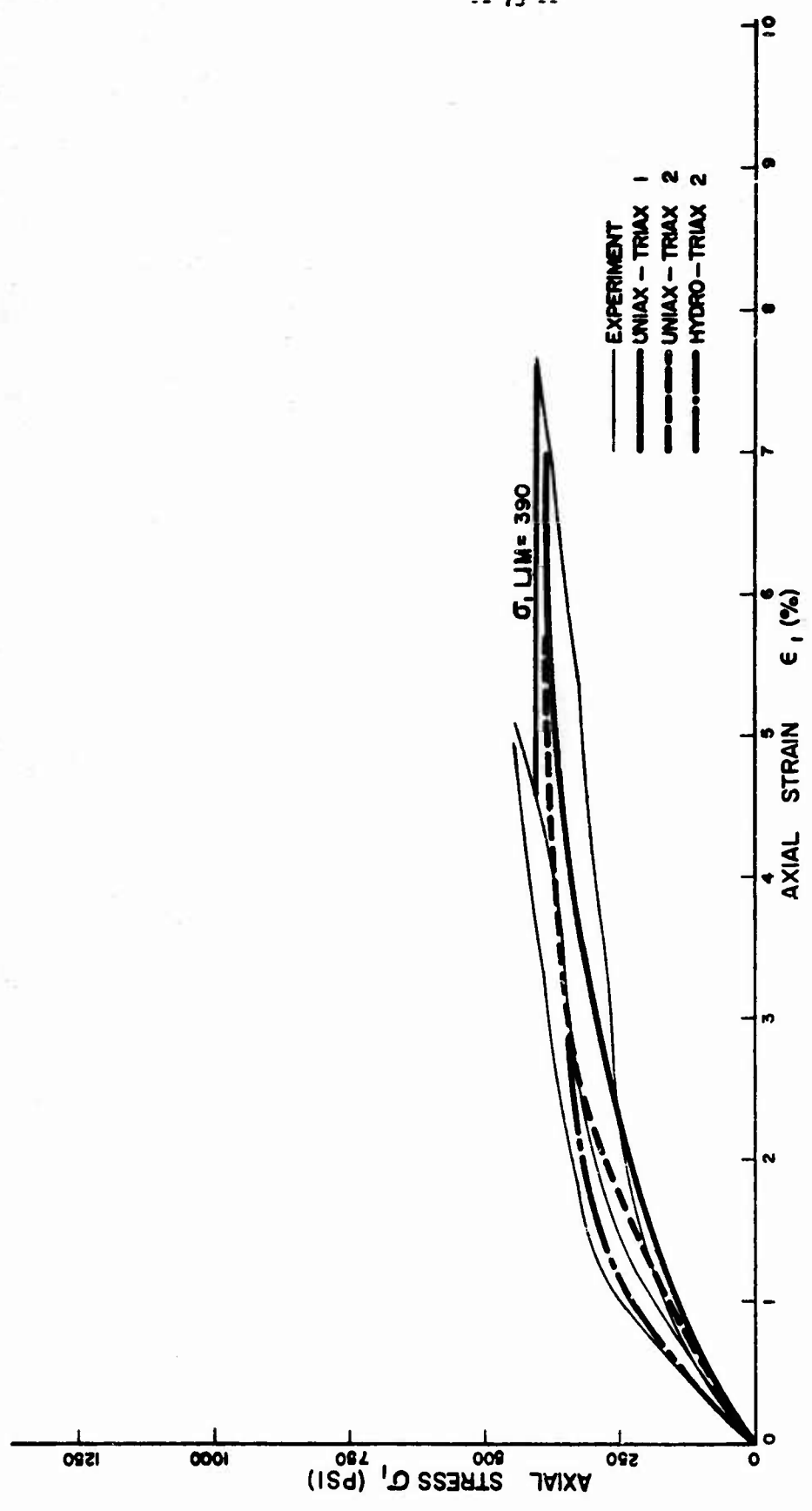
FIG.17   PROPORTIONAL LOADING TEST
AXIAL STRESS VERSUS AXIAL STRAIN
STRESS RATIO $q = \sigma_3/\sigma_1 = 0.4$
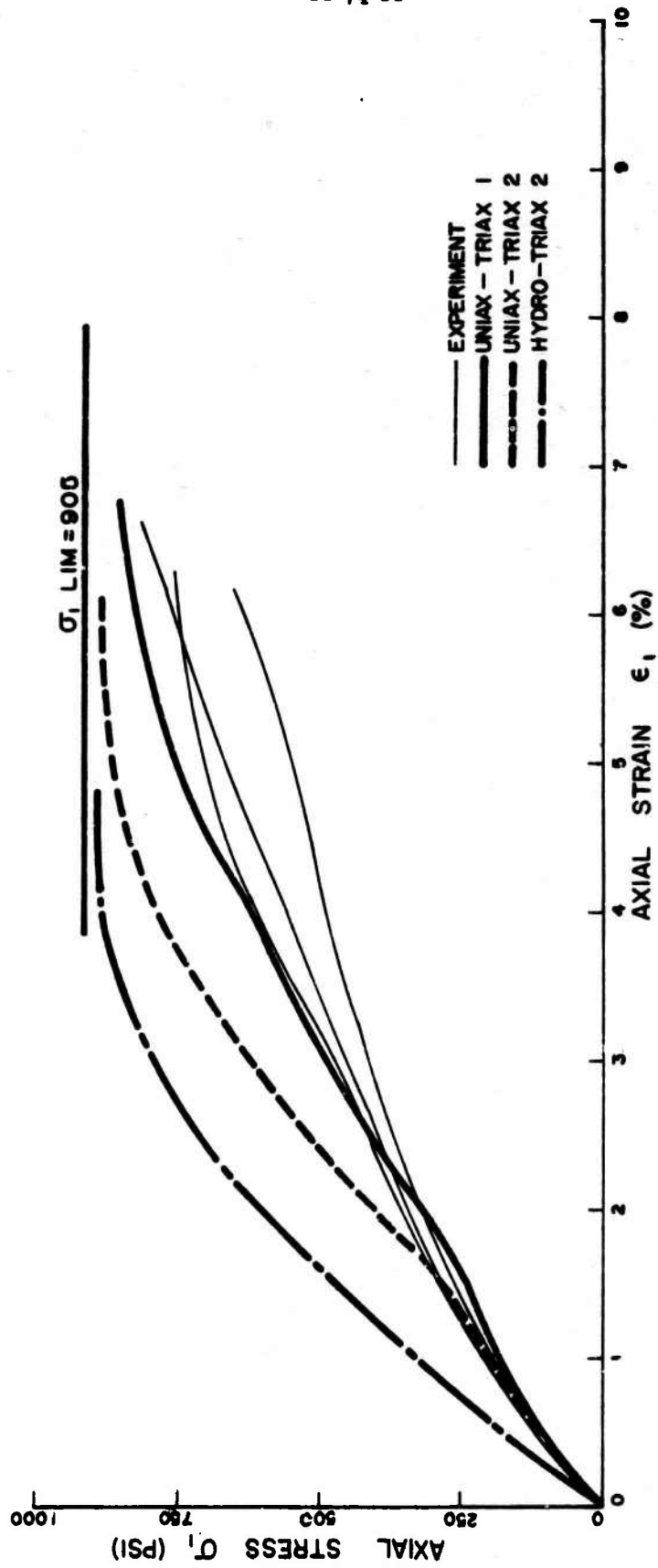
FIG. 18   PROPORTIONAL   LOADING   TEST
AXIAL   STRESS   VERSUS   AXIAL   STRAIN
STRESS   RATIO $q = \sigma_3/\sigma_1 = 0.6$

σ_i LIM = 2013
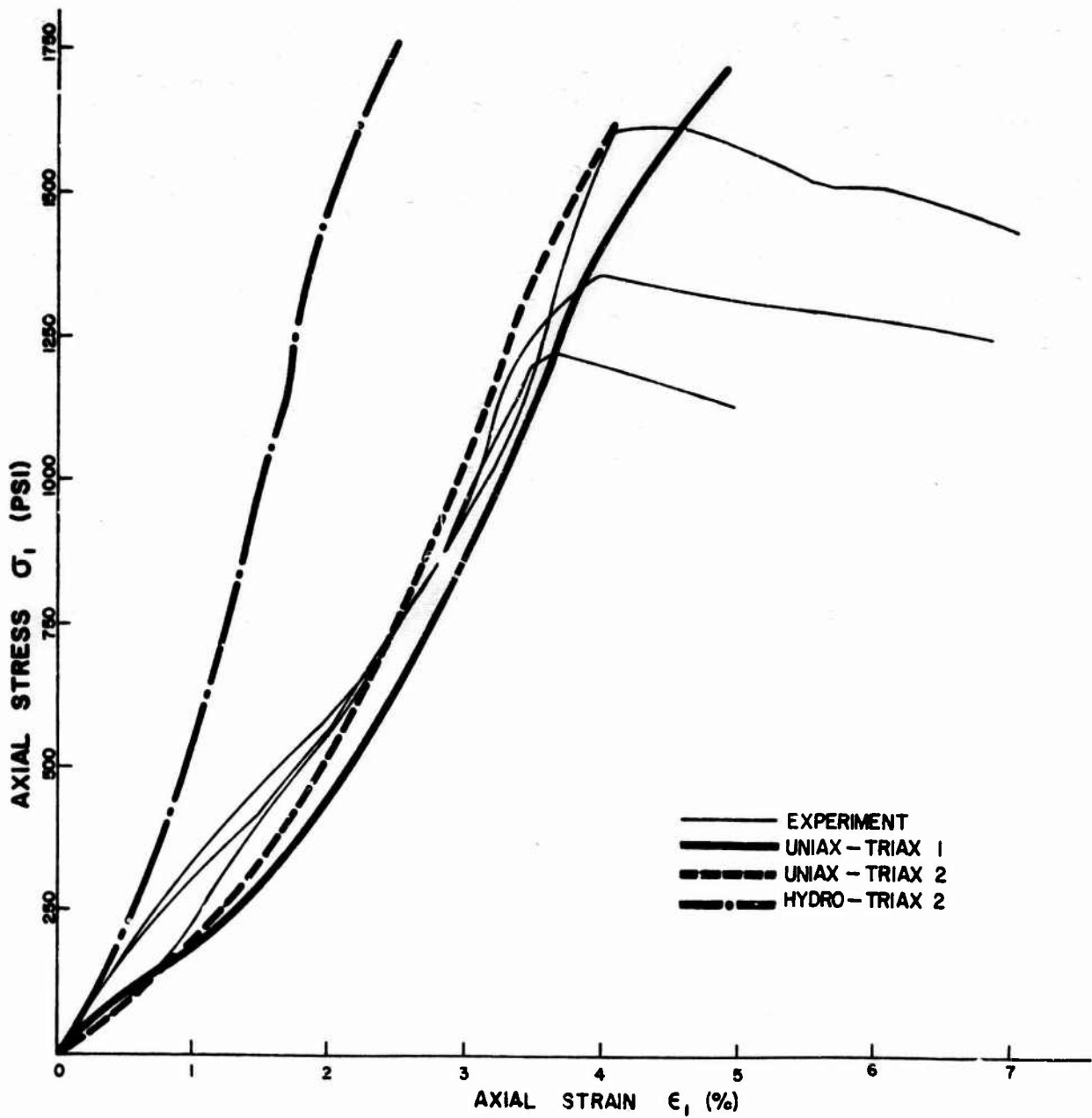
FIG. 19   PROPORTIONAL LOADING TEST
AXIAL STRESS VERSUS AXIAL STRAIN
STRESS RATIO $q = \sigma_3/\sigma_1 = 0.8$
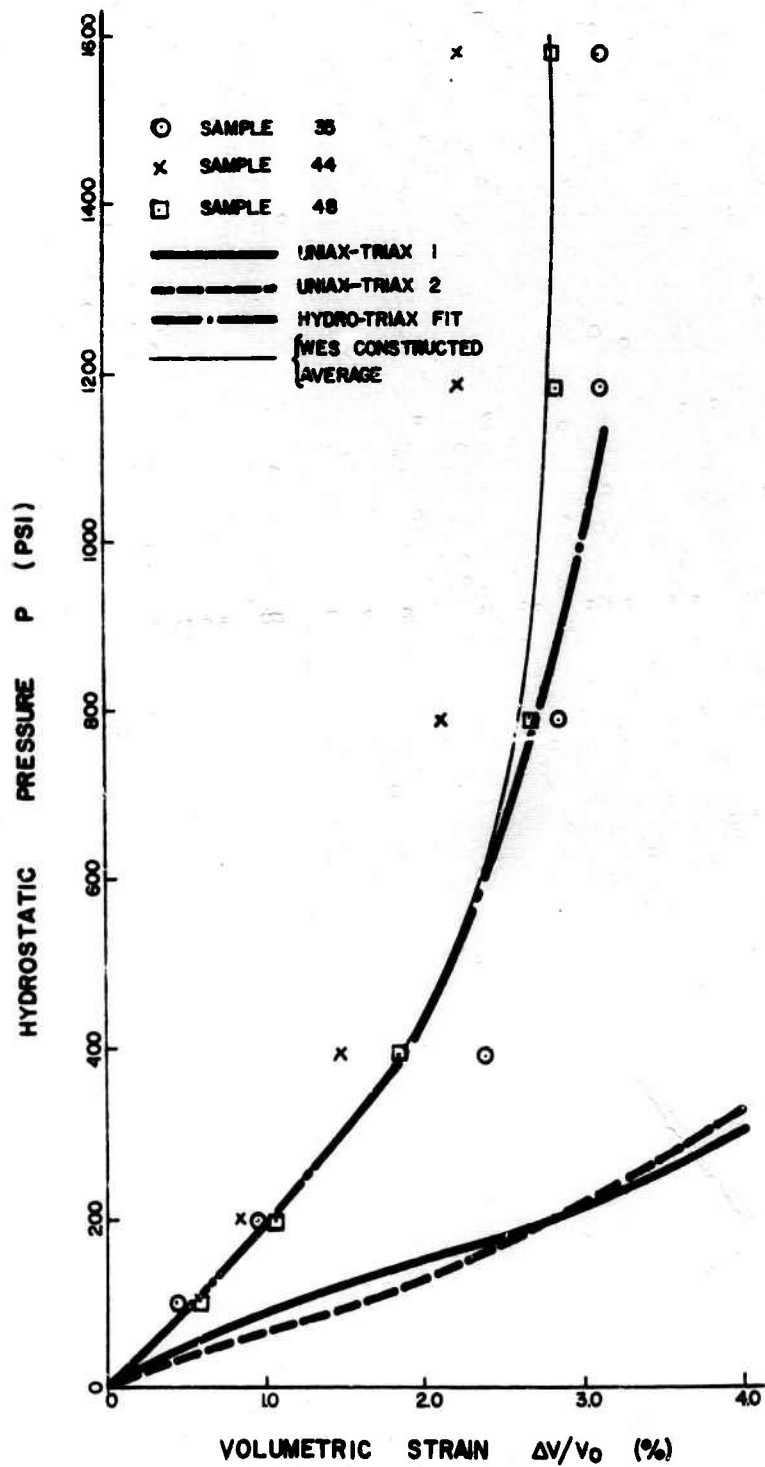
FIG.20   McCORMICK   RANCH   SAND   STATIC
                  HYDROSTAT,   LOADING   ONLY
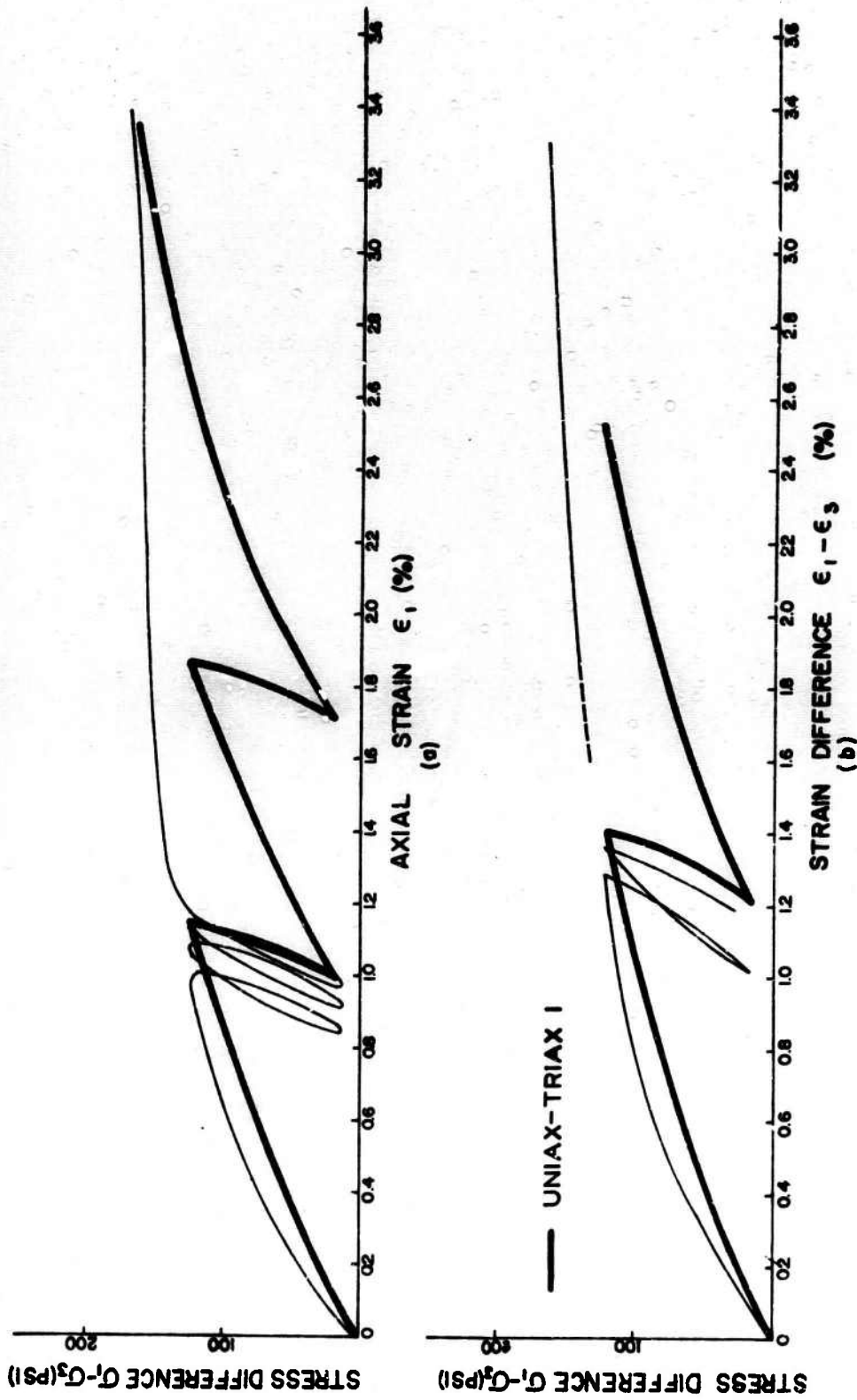
FIG.21   TRIAXIAL COMPRESSION TEST
LOAD CYCLED AT 75% OF FAILURE
$\sigma_3 = 100$ PSI   SAMPLE 113
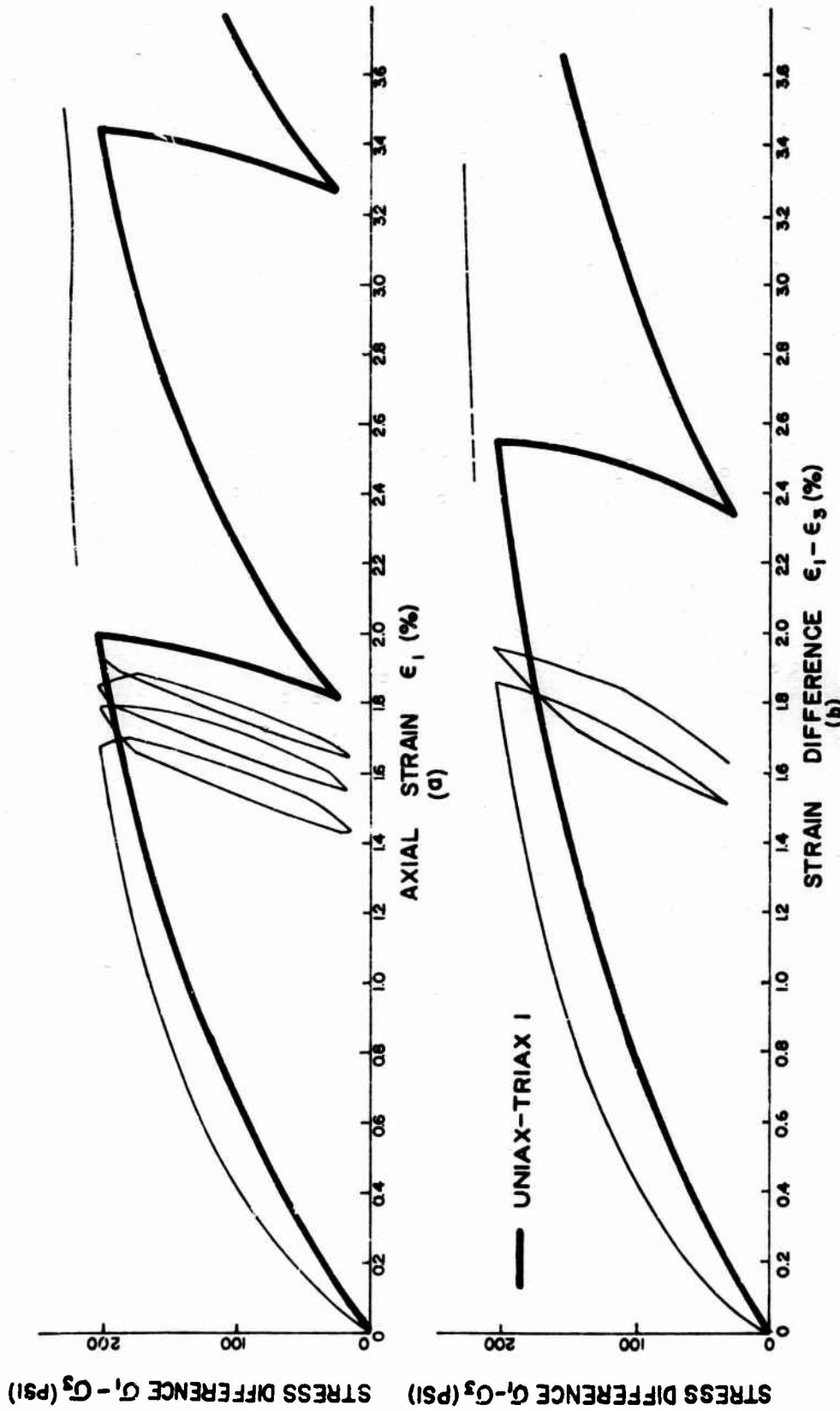
FIG.22 TRIAXIAL COMPRESSION TEST
LOAD CYCLED AT 75% OF FAILURE
σ_3 = 200 PSI   SAMPLE 110
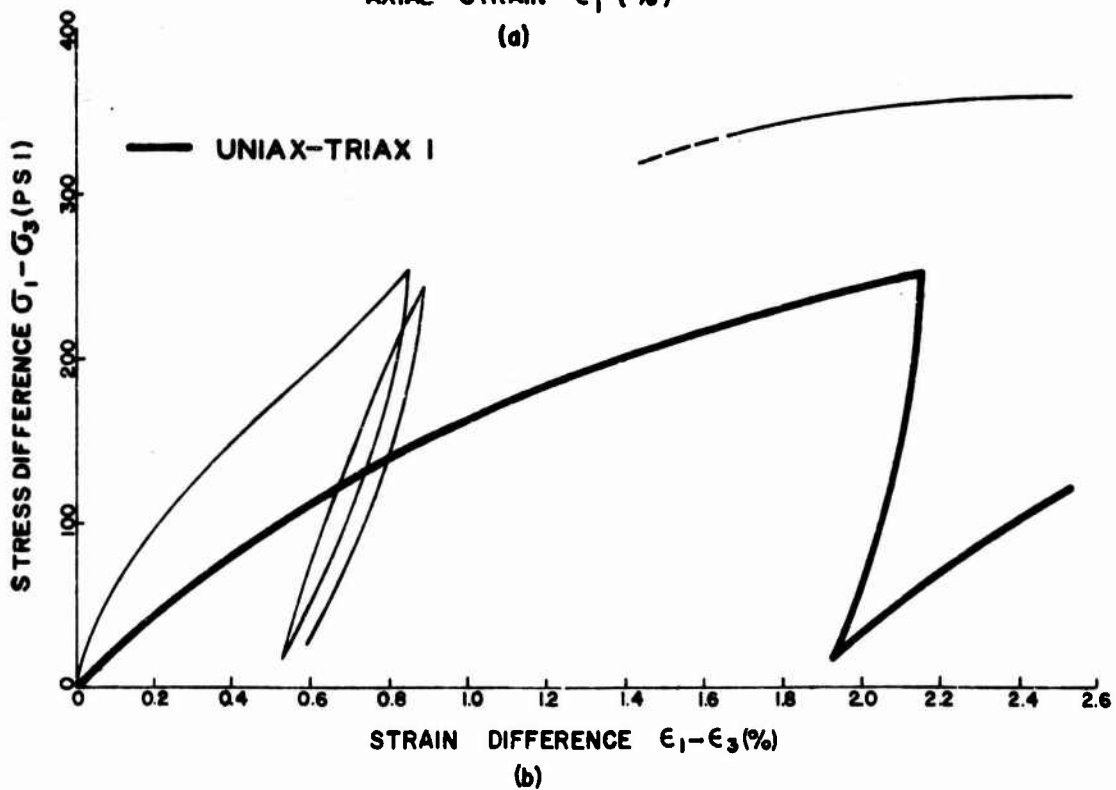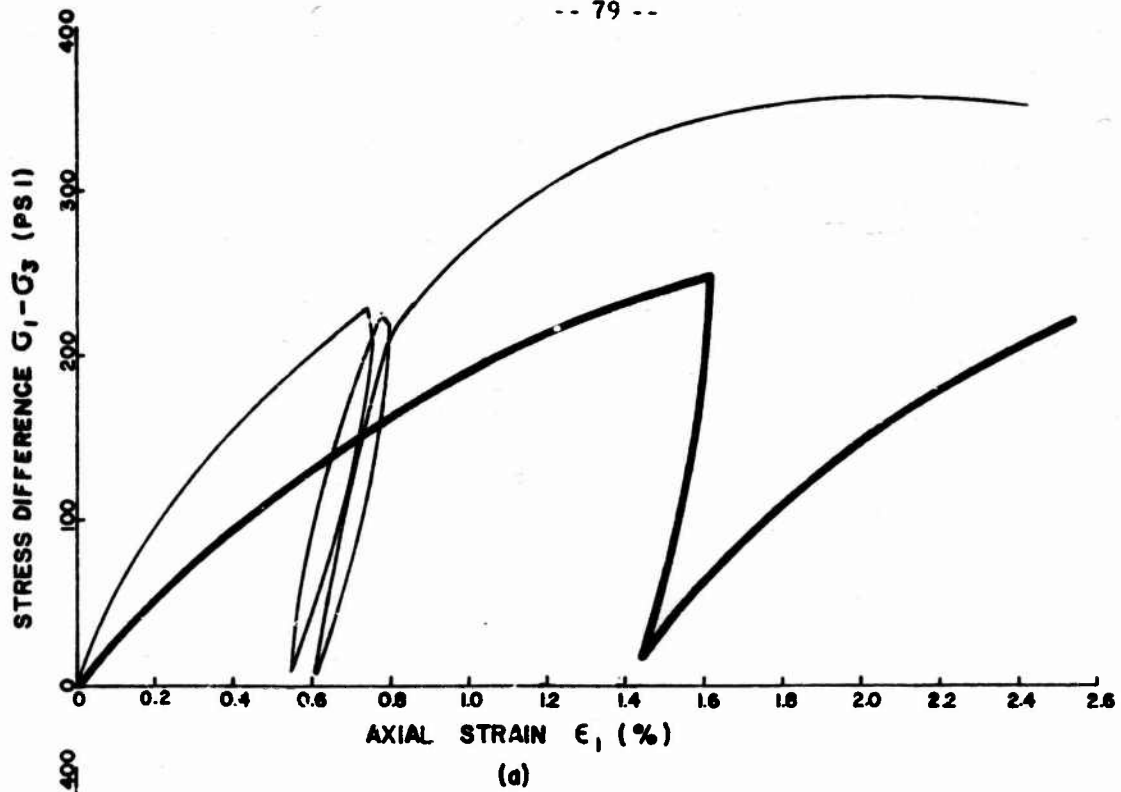
FIG. 23   TRIAXIAL   COMPRESSION   TEST
LOAD   CYCLED   AT   75%   OF   FAILURE

σ_3 = 400 PSI   SAMPLE 121
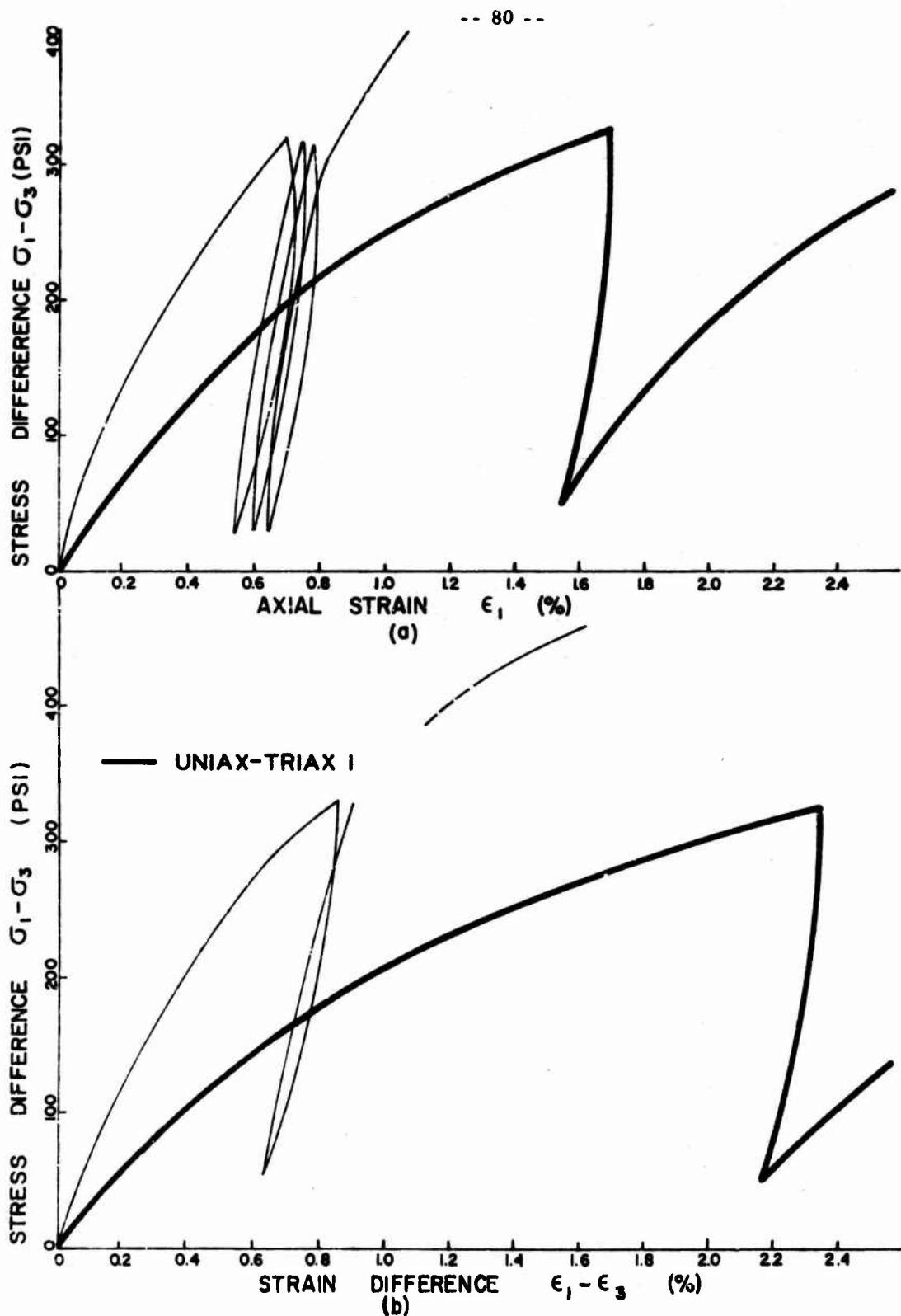
FIG.24 TRIAXIAL COMPRESSION TEST LOAD CYCLED AT 75% OF FAILURE $\sigma_3 = 800$ PSI SAMPLE 131
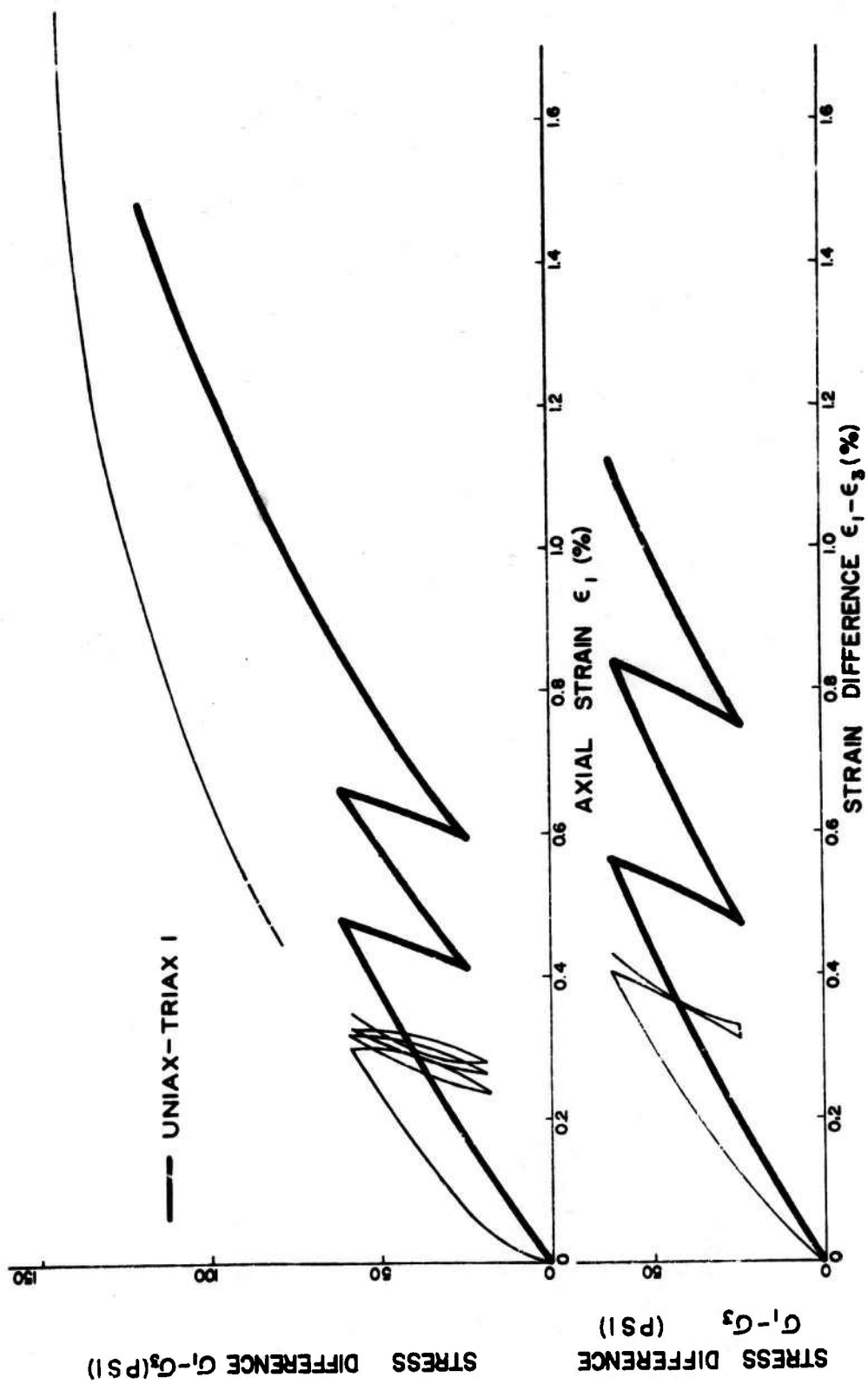
FIG. 25 TRIAXIAL COMPRESSION TEST LOAD CYCLED AT 35% OF FAILURE

$\sigma_3 = 100$ PSI   SAMPLE 115
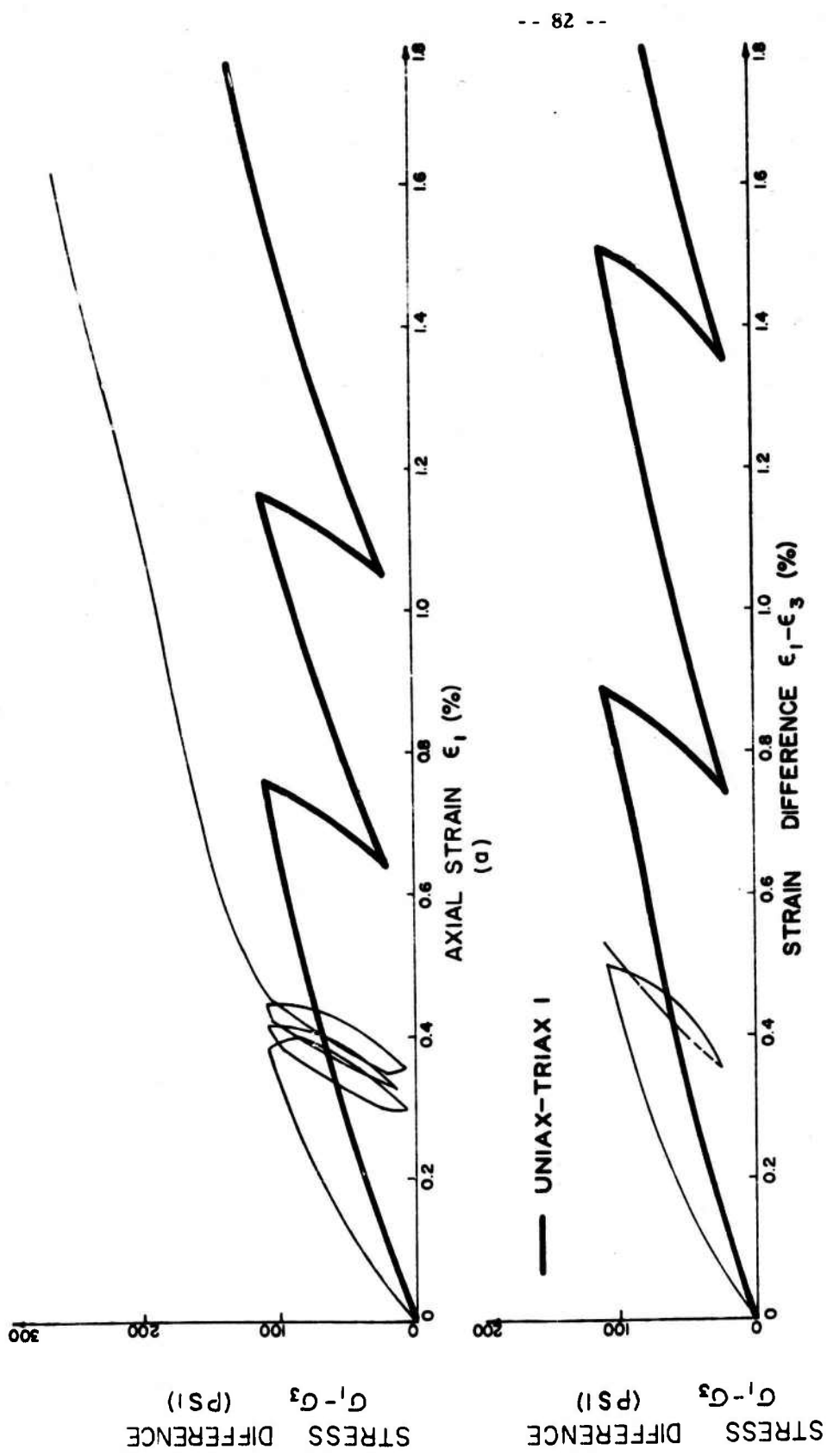
FIG.26 TRIAXIAL COMPRESSION TEST
LOAD CYCLED AT 35% OF FAILURE
$\sigma_3 = 200$ PSI   SAMPLE 132
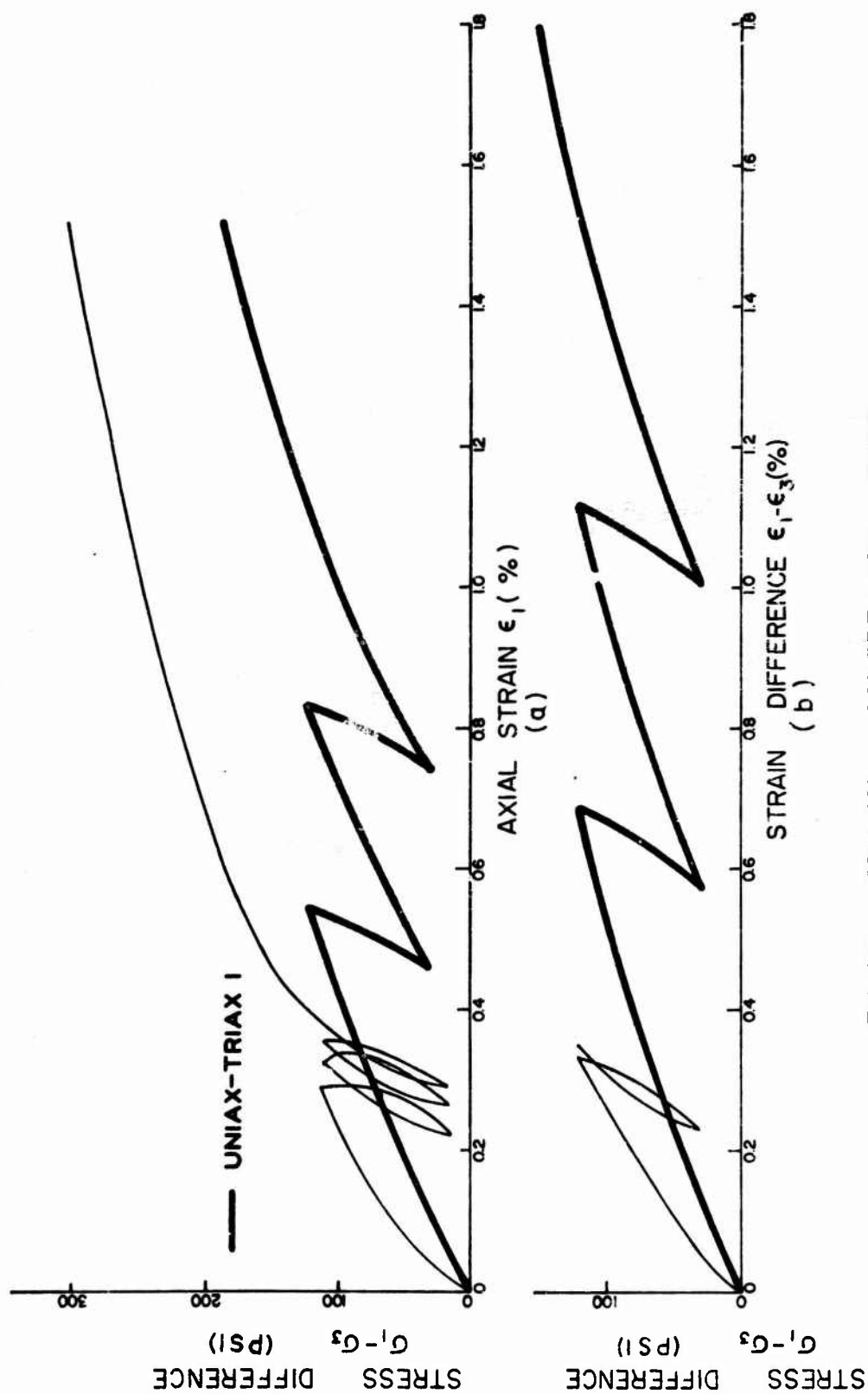
FIG. 27   TRIAXIAL   COMPRESSION   TEST
LOAD CYCLED AT 35% OF FAILURE
σ_3=400 PSI   SAMPLE 136
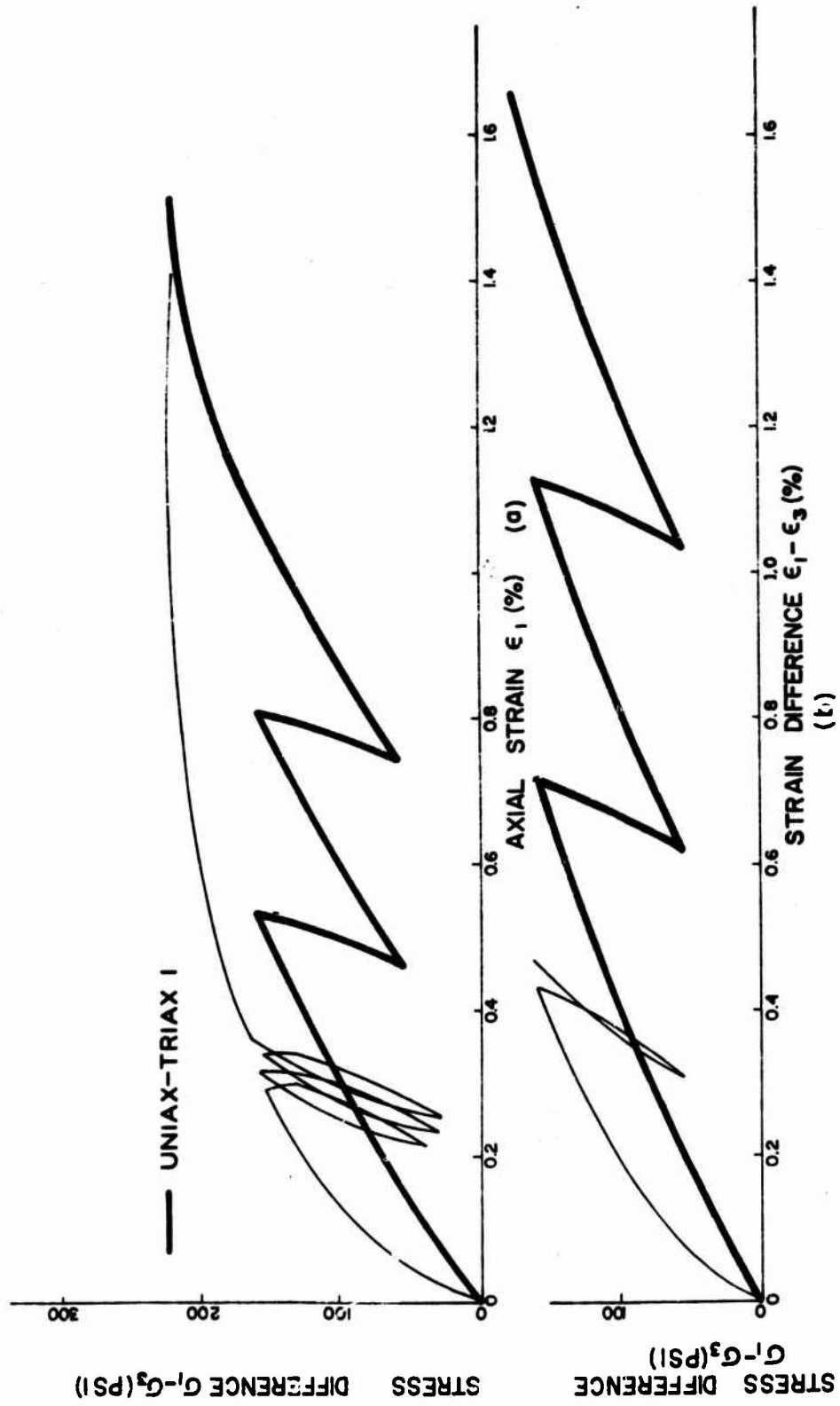
FIG.28 TRIAXIAL COMPRESSION TEST
LOAD CYCLED AT 35% OF FAILURE

σ₃=800 PSI   SAMPLE 138
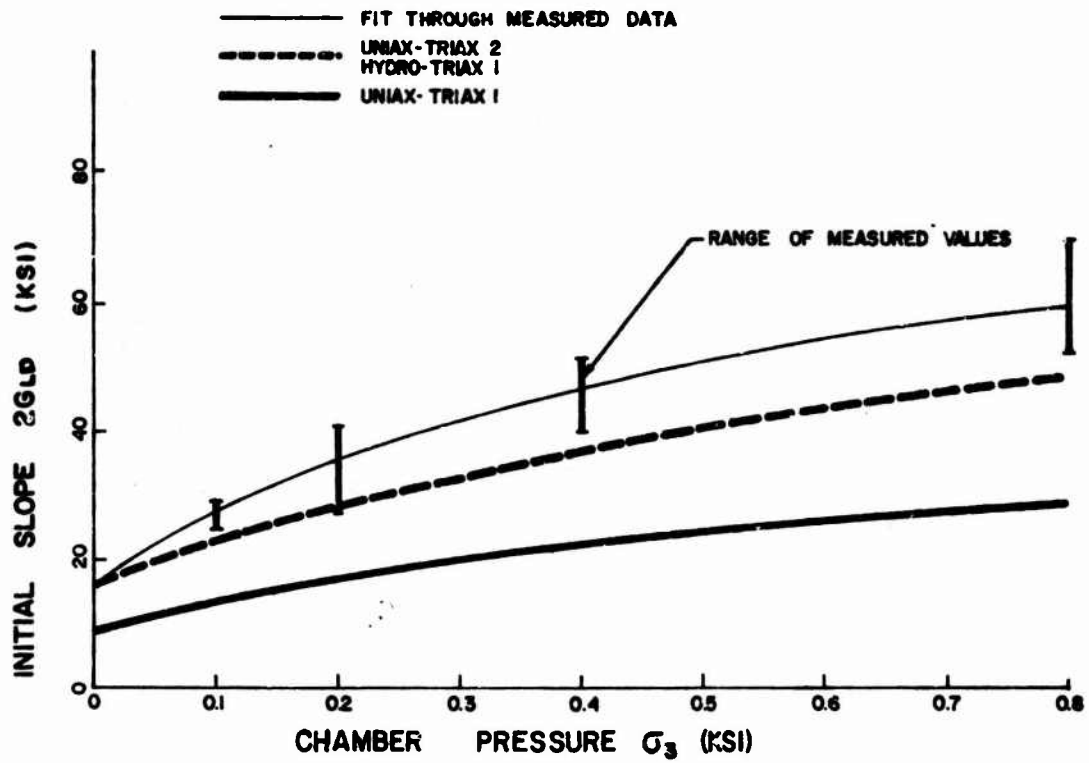
FIG. 29   INITIAL SLOPE OF STRESS-DIFFERENCE VERSUS
STRAIN - DIFFERENCE IN TRIAXIAL COMPRESSION;
MEASURED AND COMPUTED VALUES
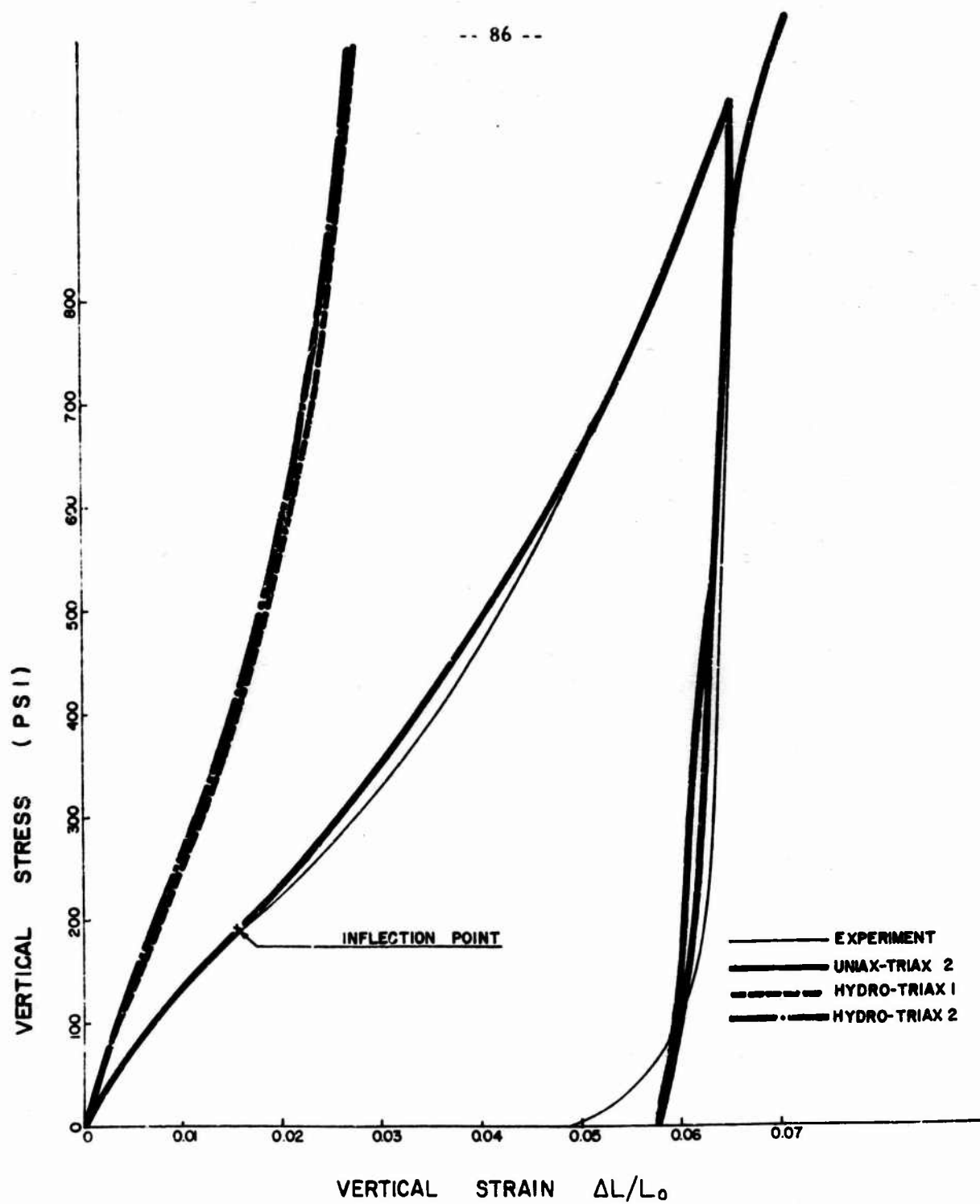
FIG.30 UNIAXIAL STRAIN TEST
UNIAX-TRIAX FIT 2
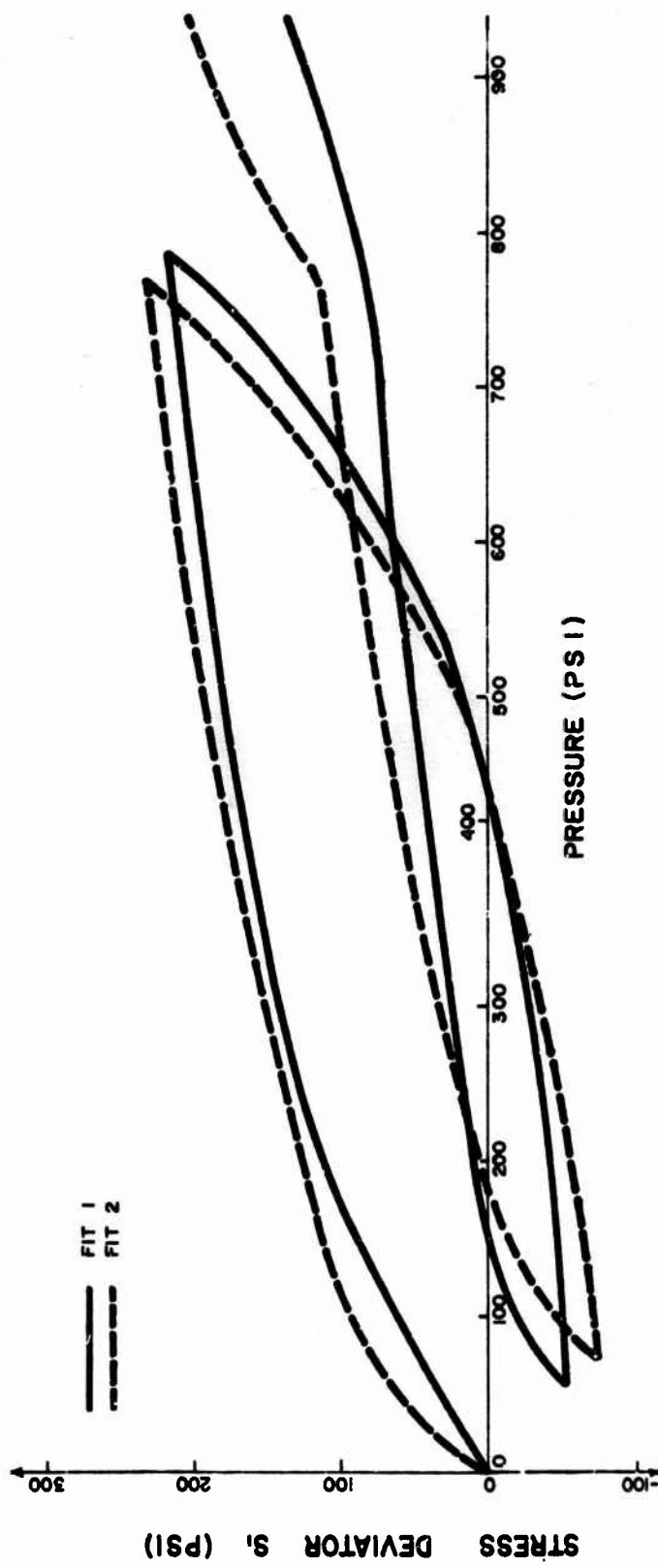
FIG. 31   STRESS   PATH   IN   UNIAXIAL   STRAIN   FOR
UNIAX- TRIAX FITS   I AND 2

APPENDIX

User's Guides and FORTRAN Listings of UNAX2 and PROP.

The two FORTRAN programs, UNAX2 and PROP, which compute
all stress and strain quantities in uniaxial strain and
proportional loading tests, respectively, are listed in this
appendix. A description of the input and output for each
program is given. All the computed results in this report
were obtained by execution of the two programs on the
IBM 1130 computer located in the Weidlinger office.

UNAX2 utilizes four arithmetic statement functions,
CPKLD(EE), CPKUN(P), GLD(SQJ2,P) and GUN(SQJ2,P) which
correspond to Eqs. (3), (4), (5) or (9), and (6) or (10),
respectively, and numerical integration. If the model
description were to change, only these four statements need
be altered. The axial stress SIG is incremented DSIG and a
predictor corrector approach is used to find the strain and
remaining stress quantities SIG3, S1 and P. The bulk and
shear moduli, K and G, are point functions at the new stress
and strain, as are the (constrained) tangent and secant
moduli, EMTAN and EMSEC, which are computed from $K + \frac{4}{3} G$
and SIG/EPS. The local wave velocity V and local Poisson's
ratio NU are also found from K and G. The typical line of
output consists of all the variables mentioned above. In
addition, a complete heading listing all input parameters and
all "useful" constants is given. The program loads, unloads
and then reloads to SIGL, SIGU and SIGR, respectively.

During initial loading the inflection point is recorded and the information is printed at the end of the loading phase. To reduce the amount of output two quantities ISTOR and IPRIN are introduced. The computer stores the complete information each $ISTOR^{th}$ DSIG on the disk for later processing. Of those stored, each $IPRIN^{th}$ is printed on line.

The input is as follows:

TITLE

Cards 1-9   FORMAT (15A4)   Alphanumeric description in columns 1-60 of the particular run and the model. The first, printed in the middle of the page, usually contains identification of the particular run. The remaining 8, printed on alternate sides contain, for example, descriptions of K and G.

Card 10   FORMAT (8E10.0)   Values of the material parameters K_o , K_1 , K_2 , K_{0U} , K_{1U} , ν_0 , $\bar{\gamma}_1$, γ_1 (ν_0 is the initial Poisson's ratio).

Card 11   FORMAT (8E10.0)   Values of the material parameters γ_2 , G_{0U} , $\bar{\gamma}_{1U}$, γ_{1U} , ρ_0 (ρ_0 is the initial density).

Card 12   FORMAT (3A4, E12.0)   Units of stress, density and velocity, and a conversion factor V_{CONV} such that $C_S = \sqrt{G/\rho} * V_{CONV}$ where G, ρ and C_S are in the units given; e.g., KSI, PCF, FPS and 2151.985.

Card 13   FORMAT (4E10.0, 2I5)   Values of program controls SIGL, SIGU, SIGR, DSIG, ISTOR, IPRIN.

Program PROP is written in sections for loading, unloading, reloading of, separately, volumetric and deviatoric stresses. Expressions for stress and strain, Eqs. (15), (42), (43), (48), (49) are evaluated explicitly in the following manner.

On loading, the program computes stresses at discrete volumetric strain points. The strains are incremented by an amount computed in the program as the volumetric strain at SIGLM(1) divided by EENUM - the input number of strain increments. On unloading and reloading the program automatically shifts to stress increments computed as the difference between the pressure at the loading and unloading limits, divided by SGNUM - the input number of stress increments. The reason for switching from strain to stress increments should be apparent from inspection of the formulas in the body of the report appropriate to loading, unloading and reloading.

In the program allowance is made for an initial set
of stresses which may have been applied to the test sample.
The program is capable of handling any number of loading-
unloading-reloading-loading cycles through the input numbers
SIGLM(I) which are values of σ_1 specifying points at which
unloading, reloading, etc., are to occur.

Data is input to PROP according to the following
specifications.

Card #1	TITLE	Alphanumeric title in columns 1-68.
	TITLE (18)	Units of density, i.e., PCF in columns 69-72.
	TITLE (19)	Units of velocity, i.e., FPS in columns 73-76.
	TITLE (20)	Units of stress, i.e., KSI in columns 77-80.
Card #2	ANU	Poisson's ratio ν.
(FORMAT 8E10.0)	RHOZ	Material density ρ_0 in lb/ft^3.
	Q	Proportionality constant (Q=0 gives triaxial test, Q=1 gives Hydrostatic test).
	EENUM	Number of strain increments to be taken on initial loading.
	SGNUM	Number of stress increments to be taken on unloading and re-loading.

	SIG1Z	Initial seating stresses,
	SIG2Z	$\sigma_1^{(o)}$, $\sigma_2^{(o)}$ in KSI.
Card #3	AKO	Loading constants
(FORMAT 8E10.0)	AK1	K_o , K_1 , K_2 for
	AK2	bulk modulus, in KSI.
	GMBR	Loading constants
	GAM1	$\bar{\gamma}_1$, γ_1 , γ_2 for shear
	GAM2	modulus, in KSI.
Card #4	AKOU	Unloading constants K_{OU} , K_{1U}
(FCRMAT 8E10.0)	AK1U	for bulk modulus, in KSI.
	GMBRU	Unloading constants $\bar{\gamma}_{1U}$, γ_{1U} ,
	GM1U	G_{OU} for shear modulus,
	GOU	in KSI.
Card #5	NLIM	Number of limit loads
(FORMAT I5, 7E10.0)		from which unloading
		and reloading is to take place.
	SIGLM(I)	Values of stress σ_1 , in
	I=1, NLIM	KSI, at which unloading and
		reloading occur.

For runs with multiple sets of data, insert a card with a "*"
in column 1 between the data sets.

```
C                    HYSTERETIC  MATERIALS
C                    UNIAXIAL  STRAIN  TEST
C                    LOADING - UNLOADING - RELOADING
C                    COMPILED  ON  JUNE 25, 1968
      REAL KZ,K1,K2,KZU,K1U,NUZ,NUZU,K(31),NU(31)
      DIMENSION SIG3(31),S1(31),P(31),EKK(31),EMTAN(31),G(31),EMSEC(31),
     S    V(31), TITLE(15,9),SAVE(31,10)
      EQUIVALENCE (SAVE(1,1),SIG3(1)),(SAVE(1,2),S1(1)),(SAVE(1,3),P(1))
     1   ,(SAVE(1,4),EKK(1)),(SAVE(1,5),K(1)),(SAVE(1,6),G(1)),(SAVE(1,7)
     2   ,EMTAN(1)),(SAVE(1,8),EMSEC(1)),(SAVE(1,9),V(1)),(SAVE(1,10),
     3    NU(1))
C                    DEFINE  FILES
      DEFINE FILE 60(15,30,U,ITITL )
      DEFINE FILE 61(16,60,U,ISIG3 )
      DEFINE FILE 62(16,60,U,IS1   )
      DEFINE FILE 63(16,60,U,IP    )
      DEFINE FILE 64(16,60,U,IEKK  )
      DEFINE FILE 65(16,60,U,IK    )
      DEFINE FILE 66(16,60,U,IG    )
      DEFINE FILE 67(16,60,U,IMTAN )
      DEFINE FILE 68(16,60,U,IMSEC )
      DEFINE FILE 69(16,60,U,IV    )
      DEFINE FILE 70(16,60,U,INU   )
C                    FUNCTIONS
      CPKLD(EE) = KZ + EE*(K1+K2*EE)
      CPKUN(P) = KZU + K1U*P
      AMIN1(X,Y) = .5*((1.-SIGN(1.,X-Y))*X+(1.+SIGN(1.,X-Y))*Y)
      GLD(SQJ2,P)=GZ+GAMB*SQJ2+AMIN1(P,PC *(GAM1+GAM2*AMIN1(P,PC))
      GUN(SQJ2,P)=GZU+GAMBU*SQJ2+AMIN1(P,PC)*(GAM1U+GAM2U*AMIN1(P,PC))
      MOD(M,N) = M - M/N*N

      READ (2,999) TITLE
C            READ  MATERIAL  PROPERTIES
      READ(2,998) KZ,K1,K2,KZU,K1U,NUZ,GAMB,GAM1,GAM2,GZU,GAMBU,GAM1U
     S   , RHOZ
C      READ  UNITS AND CONVERSION CONSTANT
      READ(2,997) PUNIT,DUNIT,VUNIT,VCONV
C          READ PROGRAM CONTROLS
      READ(2,996) SIGL,SIGU,SIGR,DSIG,ISTOR,IPRIN

C            COMPUTE USEFUL CONSTANTS
      HSQR3 = SQRT(3. )/ 2.
      BETA = 2.*(1.+NUZ)/(1.-2.*NUZ)
      GZ = 3.*KZ/BETA
      PC = -GAM1/2./GAM2
      EZ = 2.*(1.+NUZ)*GZ
      EMZ = KZ + 4./3.*GZ
      CS = SQRT(GZ/RHOZ)*VCONV
      CP = SQRT(EMZ/RHOZ)*VCONV
      GAM2U= GAM2*GAM1U/GAM1
      EMZU = KZU + 4./3.*GZU
      CSU = SQRT( GZU/RHOZ)*VCONV
```

```
      CPU = SQRT(EMZU/RHOZ) *VCONV
      BETAU = 3.*KZU/GZU
      NUZU = 0.5*(BETAU-2.)/(BETAU + 1. )
C        OUTPUT TITLE, INPUT, AND USEFUL CONSTANTS ON DISK
      DO 25 NREC = 1,9
   25 WRITE(60 NREC ) ( TITLE(J,NREC),J=1,15 )
      WRITE(60 10) KZ,K1,K2,KZU,K1U,NUZ,GAMB,GAM1,GAM2,
     S     GZU,GAMBU,GAM1U,RHOZ
      WRITE(60 11) PUNIT,DUNIT,VUNIT,VCONV
      WRITE(60 12) SIGL,SIGU,SIGR,DSIG,ISTOR,IPRIN
      WRITE(60 13) BETA,GZ,PC,EZ,EMZ,CS,CP,GAM2U,EMZU,CSU,CPU,BETAU,NUZU

C         OUTPUT    INPUT
      WRITE(3,995)  TITLE
      WRITE(3,994) KZ,K1,K2,GZ,PUNIT,GAMB,GAM1,GAM2,PUNIT,PC,EZ,EMZ,
     S   PUNIT,RHOZ,DUNIT,CP,CS,VUNIT,NUZ,BETA
      WRITE(3,993) KZU,PUNIT,K1U,GZU,PUNIT,GAMBU,GAM1U,GAM2U,PUNIT,EMZU,
     S   PUNIT,CPU,VUNIT,CSU,VUNIT,BETAU,NUZU
      WRITE(3,992) SIGL,PUNIT,SIGU,PUNIT,SIGR,PUNIT,DSIG,PUNIT,
     S    ISTOR, IPRIN
      WRITE(3,991) PUNIT,VUNIT
      WRITE(3,990 )

C          LOAD   TO  SIGL
      NMAX = SIGL/DSIG/FLOAT(ISTOR) + .001
      NRCMX = (NMAX + 29)/ 30
      SIG  = 0.
      SIG3(1) = 0.
      S1(1) = 0.
      P(1) = 0.
      EKK(1) = 0.
      K(1) = KZ
      G(1) = GZ
      EMTAN(1) = EMZ
      EMSEC(1) = EMZ
      V(1) = CP
      NU(1) = NUZ
      EMIN = EMZ
      AKJ = K(1)
      GJ = G(1)
      PJ = P(1)
      S1J = S1(1)
      EPSJ = EKK(1)
      EMJ = EMTAN(1)
      DO 180 NREC=1,NRCMX
      DO 100 I =1,10
      DO 100 J = 2,31
  100 SAVE(J,I) = 0.0
      N1ST = 30*(NREC-1) + 1
      NLAST = MINO(NMAX,30*NREC )
      DO 150 NN = N1ST , NLAST
      N = NN - N1ST +2
```

```
      DO 130 J=1,ISTOR
      DEPS = DSIG/EMJ
      DP = AKJ /EMJ *DSIG
      DS1 = DSIG - DP
      EPSJ1 = EPSJ + DEPS
      PJP1 = PJ + DP
      S1JP1 = S1J + DS1
      AKJP1 = CPKLD(EPSJ1/3. )
      GJP1 = GLD( HSQR3  *S1JP1, PJP1 )
      EMJP1 = AKJP1 + GJP1/.75
      DEPS = 0.5*(1./EMJ + 1./EMJP1 )*DSIG
      DP = 0.5*(AKJ/EMJ + AKJP1/EMJP1 )*DSIG
      DS1 = DSIG - DP
      SIG = SIG + DSIG
      PJ = PJ + DP
      S1J = S1J + DS1
      EPSJ = EPSJ + DEPS
      AKJ = CPKLD(EPSJ/3. )
      GJ = GLD( HSQR3  *S1J, PJ )
      EMJ = AKJ + GJ/.75
      IF ( EMJ - EMIN) 110,130,130
  110 EMIN = EMJ
      SIGM = SIG
      PMIN = PJ
      EPSM = EPSJ
      VMIN = SQRT(EMIN/RHOZ)*VCONV
  130 CONTINUE
      SIG3(N) = PJ - S1J*0.5
      S1(N) = S1J
      P(N) = PJ
      EKK(N) = EPSJ
      K(N) = AKJ
      G(N) = GJ
      EMTAN(N) = EMJ
      EMSEC(N) = SIG/EPSJ
      V(N) = SQRT(AMIN1(EMSEC(N),EMJ)/RHOZ) * VCONV
      NU(N) = 0.5*(3.*K(N) -2.*G(N))/(3.*K(N)+G(N))
      IF ( MOD(NN,IPRIN)) 150,140,150
  140 WRITE(3,989 ) NN,SIG, ( SAVE(N,J), J= 1,10 )
  150 CONTINUE         .
      JMAX = MINO ( N, 30 )
      DO 160 NFILE = 61,70
  160 WRITE(NFILE NREC)(SAVE(J,NFILE-60),J=1,JMAX)
      DO 170 I =1,10
  170 SAVE(1,I) = SAVE( N , I )
  180 CONTINUE
      WRITE(3,990 )
      WRITE(3,988) SIGM,PUNIT,PMIN,PUNIT,EPSM,EMIN,PUNIT,VMIN,VUNIT

C       UNLOAD  TO  SIGU
      NMAXU = (SIGL - SIGU )/DSIG/FLOAT(ISTOR) + .001
      NRCMU = (NMAXU + 29)/30
```

```
      EPSL = EPSJ
      PMAX = PJ
      K(1) = CPKUN( PJ)
      G(1) = GUN( HSQR3   *S1J, PJ )
      EMTAN(1) = K(1) + G(1)/.75
      EMSEC(1) = EMTAN(1)
      V(1) = SQRT(EMTAN(1)/RHOZ)*VCONV
      NU(1) = 0.5*(3.*K(1)-2.*G(1))/(3.*K(1)+G(1))
      AKJ = K(1)
      GJ = G(1)
      EMJ = EMTAN(1)
      WRITE(3,987 )
      WRITE(3,990 )
      NREC = NRCMX
      NN = NMAX
      WRITE(3,989 ) NN,SIG, ( SAVE(1,J), J= 1,10 )
      DO 280 NR = 1,NRCMU
      NREC = NREC + 1
      DO 200 I =1,10
      DO 200 J =2,31
200   SAVE(J,I) = 0.0
      NLAST = MINO(NMAXU+1-(NR-1)*30,31)
      DO 250 N=2,NLAST
      NN = NN- 1
      DO 230 J = 1,ISTOR
      DEPS = DSIG/EMJ
      DP = AKJ /EMJ *DSIG
      DS1 = DSIG - DP
      EPSJ1 = EPSJ - DEPS
      PJP1 = PJ - DP
      S1JP1 = S1J - DS1
      AKJP1 = CPKUN(PJP1 )
      IF( S1JP1 ) 210,215,215
210   GJP1 = GLD(- HSQR3   *S1JP1, PJP1 )
      GO TO 216
215   GJP1 = GUN( HSQR3   *S1JP1, PJP1 )
216   GJP1 = -AMIN1(0.0, -GJP1 )
      EMJP1 = AKJP1 + GJP1/.75
      DEPS = 0.5*(1./EMJ + 1./EMJP1 )*DSIG
      DP = 0.5*(AKJ/EMJ + AKJP1/EMJP1 )*DSIG
      DS1 = DSIG - DP
      SIG = SIG - DSIG
      PJ = PJ - DP
      S1J = S1J - DS1
      EPSJ = EPSJ - DEPS
      AKJ = CPKUN( PJ )
      IF ( S1J ) 220,220,225
220   GJ = GLD(- HSQR3   *S1J, PJ )
      GO TO 226
225   GJ = GUN( HSQR3   *S1J, PJ )
226   GJ = -AMIN1( 0.0, -GJ )
      EMJ = AKJ + GJ/.75
```

```
    230 CONTINUE
        SIG3(N) = PJ - S1J*0.5
        S1(N) = S1J
        P(N) = PJ
        EKK(N) = EPSJ
        K(N) = AKJ
        G(N) = GJ
        EMTAN(N) = EMJ
        EMSEC(N) = (SIGL -SIG)/(EPSL - EPSJ )
        V(N) = SQRT(EMJ/RHOZ)*VCONV
        NU(N) = 0.5*(3.*K(N) -2.*G(N))/(3.*K(N)+G(N))
        IF ( MOD(NN,IPRIN)) 250,240,250
    240 WRITE(3,989 ) NN,SIG, ( SAVE(N,J), J= 1,10 )
    250 CONTINUE
        JMAX = MINO ( NLAST, 30 )
        DO 260 NFILE = 61,70
    260 WRITE(NFILE NREC)(SAVE(J,NFILE-60),J=1,JMAX)
        DO 270 I = 1,10
    270 SAVE(1,I) = SAVE( NLAST,I )
    280 CONTINUE
        WRITE(3,990 )

C           RELOAD   TO   SIGR
        NMAXR = (SIGR - SIGU )/DSIG/FLOAT(ISTOR) + .001
        NRCMR = (NMAXR + 29)/30
        EPSU = EPSJ
        IF ( S1J ) 300,305,305
    300 G(1) = GUN(- HSQR3  *S1J, PJ )
        GO TO 310
    305 G(1) = GLD( HSQR3  *S1J, PJ )
    310 G(1) = -AMIN1( 0.0, -G(1) )
        EMTAN(1) = K(1) + G(1)/.75
        EMSEC(1) = EMTAN(1)
        V(1) = SQRT(EMTAN(1)/RHOZ)*VCONV
        NU(1) = 0.5*(3.*K(1)-2.*G(1))/(3.*K(1)+G(1))
        GJ = G(1)
        EMJ = EMTAN(1)
        WRITE(3,986 )
        WRITE(3,990 )
        WRITE(3,989 ) NN,SIG, ( SAVE(1,J), J= 1,10 )
        DO 380 NR = 1,NRCMR
        NREC = NREC + 1
        DO 312 I = 1,10
        DO 312 J = 2,31
    312 SAVE(J,I) = 0.0
        NLAST = MINO(NMAXR+1-(NR-1)*30,31)
        DO 350 N=2,NLAST
        NN = NN+ 1
        DO 330 J = 1,ISTOR
        DEPS = DSIG/EMJ
        DP = AKJ /EMJ *DSIG
        DS1 = DSIG - DP
```

```
      EPSJ1 = EPSJ + DEPS
      PJP1 = PJ + DP
      S1JP1 = S1J + DS1
      IF ( PJP) - PMAX ) 315,315,316
315   AKJP1 = CPKUN(PJP1 )
      GO TO 317
316   AKJP1 = CPKLD(EPSJ1/3. )
317   IF ( S1JP1 ) 320,320,321
320   GJP1 = GUN(- HSQR3  *S1JP1, PJP1 )
      GO TO 322
321   GJP1 = GLD( HSQR3  *S1JP1, PJP1 )
322   GJP1 = -AMIN1(0.0, -GJP1 )
      EMJP1 = AKJP1 + GJP1/.75
      DEPS = 0.5*(1./EMJ + 1./EMJP1 )*DSIG
      DP = 0.5*(AKJ/EMJ + AKJP1/EMJP1 )*DSIG
      DS1 = DSIG - DP
      SIG = SIG + DSIG
      PJ = PJ + DP
      S1J = S1J + DS1
      EPSJ = EPSJ + DEPS
      IF ( PJ - PMAX ) 323,324,324
323   AKJ = CPKUN( PJ )
      GO TO 325
324   AKJ = CPKLD( EPSJ/ 3. )
325   IF ( S1J ) 327,328,328
327   GJ = GUN(- HSQR3  *S1J, PJ )
      GO TO 329
328   GJ = GLD( HSQR3  *S1J, PJ )
329   GJ = -AMIN1( 0.0, -GJ )
      EMJ = AKJ + GJ/.75
330   CONTINUE
      SIG3(N) = PJ - S1J*0.5
      S1(N) = S1J
      P(N) = PJ
      EKK(N) = EPSJ
      K(N) = AKJ
      G(N) = GJ
      EMTAN(N) = EMJ
      EMSEC(N) = (SIGU -SIG)/(EPSU - EPSJ )
      V(N) = SQRT(EMJ/RHOZ)*VCONV
      NU(N) = 0.5*(3.*K(N) -2.*G(N))/(3.*K(N)+G(N))
      IF ( MOD(NN,IPRIN)) 350,340,350
340   WRITE(3,989 ) NN,SIG, ( SAVE(N,J), J= 1,10 )
350   CONTINUE
      JMAX = MINO ( NLAST, 30 )
      DO 370 NFILE = 61, 70
      WRITE(NFILE NREC)(SAVE(J,NFILE-60),J=1,JMAX)
370   SAVE(1,NFILE-60) = SAVE(JMAX+1,NFILE-60 )
380   CONTINUE
      WRITE(3,989)  NN ,SIG,(SAVE(NLAST,J), J=1,10 )
      WRITE(3,990 )
      WRITE(60 14 ) NMAX,NRCMX,NMAXU,NRCMU,NMAXR,NRCMR,
```

```
      S    SIGM,PMIN,EPSM,EMIN,VMIN

C               FORMATS
  999 FORMAT( 15A4 )
  998 FORMAT(  8F10.2 )
  997 FORMAT( 3A4, E12.2 )
  996 FORMAT( 4E10.2, 2I5 )
  995 FORMAT( 1H1 30X 15A4/ (1X 90A4 ) )
  994 FORMAT(31H0MATERIAL  PROPERTIES - LOADING / 4H KZ=F10.5,5H, K1=
     1 F10.3, 5H, K2=F10.2,5H, GZ=F10.5,A4,7H, GAMB=F10.4,7H, GAM1=
     2  F10.4, 7H, GAM2= F10.5,2H / A4/ 4H PC=F8.3, 5H, EZ= F10.5,
     3  5H, MZ=F10.5,A4, 7H, RHOZ= F7.3,A4,5H, CP= F8.3, 5H, CS= F8.3,
     4  A4, 6H, NUZ= F7.4, 7H, BETA= F7.3/ )
  993 FORMAT( 33H MATERIAL  PROPERTIES - UNLOADING / 5H KZU= F10.5,A4,
     1  6H, K1U= F10.4, 6H, GZU= F10.5,A4, 8H, GAMBU= F10.4,8H, GAM1U=
     2  F10.4, 8H, GAM2U= F10.5,A4 / 5H MZU= F10.5,A4, 6H, CPU= F8.3,
     3  A4, 6H, CSU= F8.3,A4, 8H, BETAU= F8.3,7H, NUZU= F7.4/ )
  992 FORMAT( 18H PROGRAM  CONTROLS / 6H SIGL=F8.4,A4, 7H, SIGU= F8.4,
     1  A4, 7H, SIGR= F8.4,A4, 7H, DSIG= F9.6,A4, 8H, ISTOR= I3,
     2  8H, IPRIN= I3 / )
  991 FORMAT( 8H LOADING 20X 20HALL STRESSES ARE IN A4,
     S    16H, VELOCITIES IN  A4 )
  990 FORMAT(/3H  N 6X 4HSIG1 6X 4HSIG3 7X 2HS1 9X 1HP 7X 4HEPS1 10X
     S    1HK 10X 1HG 9X 4HMTAN 6X 7HSIG/EPS 5X 1HV 7X 2HNU / )
  989 FORMAT( I4, F10.3, 3F11.4,F10.5, 4F11.3,F10.1,F9.4 )
  988 FORMAT( 20H POINT OF INFLECTION / 7H SIGM = F10.4,A4,5X 6HPMIN =
     1  F10.4,A4, 5X 6HEPSM = F10.6, 5X 6HEMIN = F10.3,A4,5X 6HVMIN =
     2   F10.1, A4/ )
  987 FORMAT( 10H UNLOADING )
  986 FORMAT( 10H RELOADING )
      PAUSE
      CALL EXIT
      END
```

```
C       PROPORTIONAL LOAD TEST
C       SIGMA 2 DOT = Q * SIGMA 1 DOT
C       Q=0 GIVES TRIAXIAL TEST
C       Q=1 GIVES HYDROSTATIC STRESS TEST
C
        DIMENSION SIGLM(6),TITLE(20) ,DP(6)
C
        DATA IASTE/  *  /
        IN=2
        NOUT=3
        SQT3=SQRT(3.)
        SQTO3=SQT3/3.
C
C       INPUT
 1000 CONTINUE
        READ(IN,910) TITLE
    10 READ(IN,901) ANU,RHOZ,Q,EENUM,SGNUM,SIG1Z,SIG2Z
C       LOADING MODULI
        READ(IN,901) AK0,AK1,AK2,GMBR,GAM1,GAM2
C       UNLOADING MODULI
        READ(IN,901) AK0U,AK1U,GMBRU,GM1U,G0U
        READ(IN,902) NLIM,(SIGLM(I),I=1,NLIM)
C
C       NECESSARY CONSTANTS
        LCYCL=1
        LVOL=1
        LDEV=1
        LGOUT=1
        ISAVE=0
        IPC=1
        EM0=0.
        ONTH=1./3.
        ONMIQ=1.-Q
        ONP2Q=1.+2.*Q
        PZERO=(SIG1Z+2.*SIG2Z)*ONTH
        TOGM2=2.*GAM2
        SINIT=Q*SIG1Z-SIG2Z
        CF=1./ONP2Q
        CF1=ONMIQ*CF
        CF2=SQTO3/CF1
        CF3=GMBR*CF2+GAM1
        CF4=GM1U/GAM1*GAM2
        G0=1.5*AK0*(1.-2.*ANU)/(1.+ANU)
        G0BR=G0+GMBR*SQT3*CF*SINIT
         G1BRL=SQT3*CF1*GMBR+GAM1
         G1BRU=SQT3*CF1*GMBRU+GM1U
        G1PCL=SQT3*CF1*GMBR
        G1PCU=SQT3*CF1*GMBRU
         G2BRL=GAM2
        G2BRU=CF4
        RAD=SQRT(G1BRL*G1BRL-4.*G0BR*G2BRL)
        IF(ABS(GAM2)-.1E-3) 11,11,12
```

```
   11 PLIM=-GOBR/G1BRL
      PC=1.E+6
      GO TO 13
   12 PLIM=-(G1BRL+RAD)/TOGM2
      PC=-GAM1/TOGM2
      PC1=.5*PC*GAM1
      IF(PLIM-PC) 13,13,1220
 1220 IF(Q-1.) 1260,1250,1260
 1250 PLIM=1.E+6
      GO TO 13
 1260 PLIM=-(GOBR+PC1)/G1PCL
   13 CS=2153.3*SQRT(GO/RHOZ)
      CP=CS*SQRT(2.*(1.-ANU)/(1.-2.*ANU))
      SLIM1=3.*CF*(PLIM-PZFRO)+SIG1Z
      ELSCO=9.*GO*AKO/(GO+3.*AKO+Q*(2.*GO-3.*AKO))
      DO 14 I=2,NLIM,2
      DP(I)=(SIGLM(I)-SIGLM(I-1))/SGNUM*ONP2Q*ONTH
   14 DP(I+1)=-DP(I)
      DEE=(ONP2Q*ONTH*(SIGLM(1)-SIG1Z)/(3.*AKO))/EENUM
      A=1.5*AK1
      B=3.0*AKO
      C=-PZERO
      TRIAL=PZERO/B
      EO=FQBIC(AK2,A,B,C,TRIAL,.00001,0)
C
C     OUTPUT OF INPUT
      WRITE(NOUT,904) (TITLE(I),I=1,17)
      WRITE(NOUT,914) AKO,AK1,AK2,GO,TITLE(20),GMBR,GAM1,GAM2,TITLE(20),
     1                PC,ELSCO          ,RHOZ,TITLE(18),CP,CS,TITLE(19),
     2                ANU
      WRITE(NOUT,923) AKOU,TITLE(20),AK1U,GOU,TITLE(20),GMBRU,GM1U,CF4,
     1                TITLE(20)
      WRITE(NOUT,913) (SIGLM(I),TITLE(20),I=1,NLIM)
      WRITE(NOUT,915) SIG1Z,TITLE(20),SIG2Z,TITLE(20),PLIM,TITLE(20),EO
      WRITE(NOUT,916)SLIM1
      WRITE(NOUT,941) TITLE(20)
      WRITE(NOUT,950)
C     IS=STEP NUMBER
C     LDEV=1 FOR DEVISTORIC LOAD, 2 FOR DEVIATORIC UNLOAD
C     IPC=1 FOR P LESS THAN PC, 2 FOR P GREATER THAN PC
C
C     LOADING CURVE
      G1BR=G1BRL
      G2BR=G2BRL
      G1PC=G1PCL
      PSAVE=PZERO
      PSG=PZERO
      GINIT=SINIT
      EESAV=EO
      E1SV=0.
      SG1SV=SIG1Z
      S1=SIG1Z-PZERO
```

```
      : P1SV=0.
C        MEASURED LONGITUDINAL STRAIN (FROM SEATING) COMPUTED
C
   15 EE=EESAV-DEE
      PINC=0.
      CF6=2.*G2BR*PSAVE+G1BR
      RAD=SQRT(G1BR*G1BR-4.*G0BR*G2BR)
C
      DO 100 I=1,1000
      IS=ISAVE+1
C        VOLUMETRIC PORTION - LOADING
      EESAV=EE
      EE=EE+DEE
   18 P=EE*(3.*AK0+EE*(1.5*AK1+AK2*EE))
      IF(P-PLIM) 19,19,500
   19 AK=AK0+EE*(AK1+AK2*EE)
      SIG1=CF*(3.*P+2.*SINIT)
C        TEST FOR MAXIMUM VALUE OF STRESS
      DIF=SIG1-SIGLM(LCYCL)
      IF(ABS(DIF)-1.E-4) 20,20,22
   20 LGOUT=2
      GO TO 24
   22 IF(DIF) 24,24,23
   23 P=ONP2G*ONTH*(SIGLM(LCYCL)-SIG1Z)+PZERO
      C=-P
      TRIAL=EE
      EE=FQBIC(AK2,A,B,C,TRIAL,.00001,0)
      GO TO 18
   24 SIG2=Q*(SIG1-SIG1Z)+SIG2Z
C        DEVIATORIC PORTION
      SINEW=SIG1-P
      IF(IS-1) 35,35,2400
 2400 IF(SINEW*(SINEW-S1)) 2415,35,2405
 2405 IF(LDEV-1) 35,35,25
 2415 IF(LDEV-2) 25,35,35
   25 PSG=EESAV*(3.*AK0+EESAV*(1.5*AK1+AK2*EESAV))
      E1SV=E1
   29 GO TO (30,32),LDEV
C        DEVIATORIC UNLOAD
   30 LDEV=2
      G0BR=G0+GMBRU*SQT3*CF*GINIT
      G1BR=G1BRU
      G2BR=G2BRU
      G1PC=G1PCU
      GO TO 34
C        DEVIATORIC LOAD OR RELOAD
   32 LDEV=1
      G0BR=G0+GMBR*SQT3*CF*GINIT
      G1BR=G1BRL
      G2BR=G2BRL
   34 RAD=SQRT(G1BR*G1BR-4.*G0BR*G2BR)
      CF6=2.*G2BR*PSG+G1BR
```

```
      WRITE(NOUT,902) LDEV
   35 IF(P-PC) 36,3500,3500
 3500 GO TO (3505,40),IPC
 3505 IPC=2
      P=PC
      PSG=PC
      SIG1=CF*(3.*PC+2.*SINIT)
      SIG2=0*(SIG1-SIG1Z)+SIG2Z
      S1NEW=SIG1-P
      C=-PC
      TRIAL=EE
      EE=FOBIC(AK2,A,B,C,TRIAL,.00001,0)
      AK=AK0+EE*(AK1+AK2*EE)
      G=G0BR+PC*(G1BR+GAM2*PC)
      CF5=2.*G2BR*PC+G1BR
      E1SV=CF1/RAD*ALOG((CF5-RAD)*(CF6+RAD)/((CF5+RAD)*(CF6-RAD)))+E1SV
      WRITE(NOUT,961)
      GO TO 50
   36 IF(ABS(G2BR)-.1E-3) 39,37,37
   37 CF5=2.*G2BR*P+G1BR
      G=G0BR+P*(G1BR+GAM2*P)
      E1=CF1/RAD*ALOG((CF5-RAD)*(CF6+RAD)/((CF5+RAD)*(CF6-RAD)))+E1SV
      GO TO 50
   39 G=G0BR+G1BR*P
      E1=CF1/G1BR*ALOG(G/(G0BR+G1BR*PSG))+E1SV
      GO TO 50
   40 G=G0BR+PC1+G1PC*P
      E1=CF1/G1PC*ALOG(G/(G0BR+PC1+G1PC*PSG))+E1SV
   50 EPS1=E1+EE-E0
      S1=S1NEW
      ETAN=9.*G*AK/(ONP2Q*G+3.*AK*ONMIQ)
   65 ANU=ONMIQ*ETAN*.5/G-1.
      EPS2=1.5*(EE-E0)-.5*EPS1
      SDIF=SIG1-SIG2
      EDIF=EPS1-EPS2
      WRITE(NOUT,959)IS,SIG1,SIG2,SDIF,P,EE,EDIF,EPS2,EPS1,AK,G,ETAN,ANU
      GO TO (100,110),LGOUT
  100 CONTINUE
C
  110 CONTINUE
      LGOUT=1
  120 IF(LCYCL-NLIM) 125,501,501
C
C     UNLOADING AND RELOADING CYCLES
C
  125 GO TO (130,140,130),LVOL
  130 WRITE(NOUT,957)
      LVOL=2
      AKK0=AK0U
      AKK1=AK1U
      PST=P
      GO TO 160
```

```
  140 WRITE(NOUT,956)
      LVOL=3
  160 SG1SV=SIG1
      SG2SV=SIG2
      EP1SV=EPS1
      E1SV=E1
      LCYCL=LCYCL+1
      ISAVE=IS
      PSG=P
      PSAVE=P
      EESAV=EE
      CF6=2.*G2BR *PSAVE+G1BR
      SINIT=Q*SG1SV-SG2SV
      GINIT=SINIT
      P=PSAVE-PINC
      DP1=DP(LCYCL)
C
      DO 300 I=1,1000
      IS=ISAVE+I
C     VOLUMETRIC PORTION UNLOAD OR RELOAD
      P=P+DP1
      SIG1=CF*(3.*P+2.*SINIT)
      IF(SIG1) 170,180,180
  170 SIG1=0.
      P1=-2.*ONTH*SINIT
      PINC=P1-P
      P=P1
  180 AK=AKOU+AK1U*P
      SIG2=Q*(SIG1-SG1SV)+SG2SV
      IF(AK1U-.1E-3) 185,190,190
  185 EE=ONTH*(P-PSAVE)/AKOU+EESAV
      GO TO 195
  190 EE=ONTH*ALOG(AK/(AKOU+AK1U*PSAVE))/AK1U+EESAV
  195 CONTINUE
C     DEVIATORIC PORTION
  200 S1NEW=SIG1-P
      IF(S1NEW*(S1NEW-S1)) 205,230,202
  202 IF(LDEV-1) 230,230,209
  205 IF(LDEV-2) 209,230,230
  209 PSG=P-DP1
      E1SV=E1
  212 GO TO (215,220),LDEV
C     LDEV=2 FOR DEVIATORIC UNLOAD
  215 LDEV=2
      GOBR=GO+GMBRU*SQT3*CF*GINIT
      G1BR=G1BRU
      G2BR=G2BRU
      G1PC=G1PCU
      GO TO 225
C     LDEV=1 FOR DEVIATORIC LOAD OR RELOAD
  220 LDEV=1
      GOBR=GO+GMBR*SQT3*CF*GINIT
```

```
      G1BR=G1BRL
      G2BR=G2BRL
      G1PC=G1PCL
  225 CF6=2.*G2BR*PSG+G1BR
      RAD=SQRT(G1BR*G1BR-4.*G0BR*G2BR).
      WRITE(NOUT,902) LDEV
  230 IF( P-PC )   231,247,247
  231 GO TO (235,232),IPC
  232 IPC=1
      P=PC
      SIG1=CF*(3.*PC+2.*SINIT)
      SIG2=Q*(SIG1-SIG1Z)+SIG2Z
      S1NEW=SIG1-P
      C=-PC
      TRIAL=EE
      EE=FQBIC(AK2,A,B,C,TRIAL,.00001,0)
      AK=AKC+EE*(AK1+AK2*EE)
      G=G0BR+PC*(G1BR+GAM2*PC)
      CF5=2.*G2BR*PC+G1BR
      PSG=PC
      E1SV=CF1/RAD*ALOG((CF5-RAD)*(CF6+RAD)/((CF5+RAD)*(CF6-RAD)))+E1SV
      WRITE(NOUT,961)
      GO TO 250
  235 IF(ABS(G2BR)-.1E-3) 245,240,240
  240 CF5=2.*G2BR*P+G1BR
      G=G0BR+P*(G1BR+G2BR*P)
      E1=CF1/RAD*ALOG((CF5-RAD)*(CF6+RAD)/((CF5+RAD)*(CF6-RAD)))+E1SV
      GO TO 250
  245 G=G0BR+G1BR*P
      E1=CF1/G1BR*ALOG(G/(G0BR+G1BR*PSG))+E1SV
      GO TO 250
  247 G=G0BR+PC1+G1PC*P
      E1=CF1/G1PC*ALOG(G/(G0BR+PC1+G1PC*PSG))+E1SV
  250 EPS1=E1+EE-E0
      S1=S1NEW
      ETAN=9.*G*AK/(ONP2Q*G+3.*AK*ONMIQ)
      ANU=ONMIQ*ETAN*.5/G-1.
      EPS2=1.5*(EE-E0)-.5*EPS1
      EDIF=EPS1-EPS2
      SDIF=SIG1-SIG2
      WRITE(NOUT,959)IS,SIG1,SIG2,SDIF,P,EE,EDIF,EPS2,EPS1,AK,G,ETAN,ANU
      GO TO (260,260,270),LVOL
C     VOLUMETRIC UNLOAD TEST
  260 IF(ABS(SIG1-SIGLM(LCYCL))-1.E-4) 125,125,300
C     VOLUMETRIC RELOAD TEST
  270 IF(ABS(SIG1-SIGLM(LCYCL))-1.E-4) 125,125,280
  280 IF(ABS(P-PST)-1.E-4) 350,350,300
  300 CONTINUE
C
C
C     VOLUMETRIC RELOADING ON VIRGIN CURVE
  350 WRITE(NOUT,958)
```

```
  360 ISAVE=IS
      E1SV=E1
      EESAV=EE
      PSAVE=P
      PSG=PST
      GO TO 15
  500 WRITE(NOUT,960)
  501 READ(2,900)ICONT
      IF(ICONT-IASTE) 502,1000,502
  502 CALL EXIT
C
C     FORMATS
C
  900 FORMAT(A1)
  901 FORMAT (8E10.0)
  902 FORMAT(I5,7E10.0)
  903 FORMAT(3E20.7)
  904 FORMAT (1H1,//17A4//)
  910 FORMAT (20A4)
  913 FORMAT(/10H SIGMA 1    ,
     1            12HLOAD LIMIT =F10.5,A4,5X,14HUNLOAD LIMIT =F10.5,A4,5X
     1         14HRELOAD LIMIT =F10.5,A4/(50X,F10.5,A4,29X,F10.5,A4/))
  914 FORMAT(31H MATERIAL  PROPERTIES - LOADING / 4H KZ=F10.5,5H, K1=
     1  F10.3, 5H, K2=F10.2,5H, GZ=F10.5,A4,7H, GAMB=F10.4,7H, GAM1=
     2  F10.4, 7H, GAM2= F10.5,2H / A4/ 4H PC=F8.3, 5H, EZ= F10.5,
     3  5H,              7H, RHOZ= F7.3,A4,5H, CP= F8.3, 5H, CS= F8.3,
     4  A4,6H, NUZ= F7.4/)
  915 FORMAT(/1X,14HSIGMA 1 ZERO =F8.5,A4,4X,14HSIGMA 2 ZERO =F8.5,A4,
     1           4X,9HP LIMIT =F8.5,A4,4X,20HMEAN STRAIN E ZERO =F8.5 )
  916 FORMAT(55X,15HSIGMA 1 LIMIT = F8.5,A4//)
  923 FORMAT( 33H MATERIAL  PROPERTIES - UNLOADING / 5H KZU= F10.5,A4,
     1  6H, K1U= F10.4, 6H, GZU= F10.5,A4, 8H, GAMBU= F10.4,8H, GAM1U=
     2  F10.4,8H, GAM2U= F10.5,A4 /)
  941 FORMAT(30X,20HALL STRESSES ARE IN A4/)
  950 FORMAT(/23X,4HSIG1,11X,4HMEAN,5X,4HEPS1,4X,3HLAT,4X,4HLONG,25X,4HT
     1ANG/25X,1H-,11X,6HSTRAIN,6X,1H-,1X,2(2X,6HSTRAIN),24X,3HMOD/3X,1HN
     2,3X,4HSIG1,4X,4HSIG3,4X,4HSIG3,6X,1HP,3X,6HEKK/3.,4X,4HEPS3,3X,4HE
     3PS3,4X,4HEPS1,8X,1HK,8X,1HG,7X,4HMTAN,3X,2HNU//8H LOADING)
  956 FORMAT( 10H RELOADING )
  957 FORMAT( 10H UNLOADING )
  958 FORMAT(28H RELOAD ALONG ORIGINAL CURVE)
  959 FORMAT(I4,4F8.4,4F8.5,3F9.3,F7.4)
  960 FORMAT(4X,38HLIMIT LOAD REACHED, NO FURTHER LOADING)
  961 FORMAT(5X,14HP = P CRITICAL)
      END
```

DOCUMENT CONTROL DATA - R & D

(Security classification of title, body of abstract and indexing annotation must be entered when the overall report is classified)

1. ORIGINATING ACTIVITY *(Corporate author)*	2a. REPORT SECURITY CLASSIFICATION
Paul Weidlinger, Consulting Engineer New York, New York.	Unclassified
	2b. GROUP

3. REPORT TITLE
INVESTIGATION OF GROUND SHOCK EFFECTS IN NONLINEAR HYSTERETIC MEDIA Report 2 - MODELING THE BEHAVIOR OF A REAL SOIL.

4. DESCRIPTIVE NOTES *(Type of report and inclusive dates)*
Report 2 of a series

5. AUTHOR(S) *(First name, middle initial, last name)*
Ivan Nelson

6. REPORT DATE	7a. TOTAL NO. OF PAGES	7b. NO. OF REFS
July 1970	117	4

8a. CONTRACT OR GRANT NO.	9a. ORIGINATOR'S REPORT NUMBER(S)
DACA39-67-C-0048	
b. PROJECT NO.	
c.	9b. OTHER REPORT NO(S) *(Any other numbers that may be assigned this report)*
d.	Contract Report S-68-1

10. DISTRIBUTION STATEMENT
This document has been approved for public release and sale; its distribution is unlimited.

11. SUPPLEMENTARY NOTES	12. SPONSORING MILITARY ACTIVITY
Prepared under contract for U.S. Army Engineer Waterways Experiment Station, Vicksburg, Mississippi	Defense Atomic Support Agency Washington, D.C.

13. ABSTRACT

The present report extends the combined variable moduli model introduced in the previous report, Ref. [1]. This more general model is defined, conditions are set on the various parameters, and the model behavior in uniaxial strain, triaxial compression and proportional loading tests is discussed.

The major portion of the present report deals with the procedures used to fit the current model, including the loading and unloading, to a rather complete set of laboratory data for McCormick Ranch Sand. Actually, four different fits are described, one of them, Uniax-Triax I, in some detail. The theoretical and experimental results are compared and with one fit, Uniax-Triax II, excellent agreement is found for uniaxial strain, triaxial compression and proportional loading tests.

Finally, recommendations are made concerning reloading in shear. User's guides and FORTRAN listings of the two programs, UNAX2 and PROP, used to compute uniaxial strain and proportional loading (including triaxial compression) tests are given in an appendix.

DD FORM **1473** REPLACES DD FORM 1473, 1 JAN 64, WHICH IS OBSOLETE FOR ARMY USE.

KEY WORDS	LINK A		LINK B		LINK C	
	ROLE	WT	ROLE	WT	ROLE	WT
Variable Moduli Material						
Ground Shock						
Hysteretic Material						
Soil Models						
McCormick Ranch Sand						